ISSN 0038-531X

Russian Original Vol. 53, No. 6, December, 1982

June, 1983

SATEAZ 53(6) 807-888 (1982)

SOVIET ATOMIC ENERGY

АТОМНАЯ ЭНЕРГИЯ
(ATOMNAYA ÉNERGIYA)

TRANSLATED FROM RUSSIAN

PEEL HERE

c/b CONSULTANTS BUREAU, NEW YORK

SOVIET ATOMIC ENERGY

Soviet Atomic Energy is abstracted or indexed in *Chemical Abstracts, Chemical Titles, Pollution Abstracts, Science Research Abstracts, Parts A and B, Safety Science Abstracts Journal, Current Contents, Energy Research Abstracts,* and *Engineering Index.*

Mailed in the USA by Publications Expediting, Inc., 200 Meacham Avenue, Elmont, NY 11003.

POSTMASTER: Send address changes to *Soviet Atomic Energy,* Plenum Publishing Corporation, 233 Spring Street, New York, NY 10013.

Soviet Atomic Energy is a translation of *Atomnaya Énergiya,* a publication of the Academy of Sciences of the USSR.

An agreement with the Copyright Agency of the USSR (VAAP) makes available both advance copies of the Russian journal and original glossy photographs and artwork. This serves to decrease the necessary time lag between publication of the original and publication of the translation and helps to improve the quality of the latter. The translation began with the first issue of the Russian journal.

Consultants Bureau journals appear about six months after the publication of the original Russian issue. For bibliographic accuracy, the English issue published by Consultants Bureau carries the same number and date as the original Russian from which it was translated. For example, a Russian issue published in December will appear in a Consultants Bureau English translation about the following June, but the translation issue will carry the December date. When ordering any volume or particular issue of a Consultants Bureau journal, please specify the date and, where applicable, the volume and issue numbers of the original Russian. The material you will receive will be a translation of that Russian volume or issue.

Subscription (2 volumes per year)
Vols. 52 & 53: $440 (domestic); $489 (foreign)
Vols. 54 & 55: $500 (domestic); $555 (foreign)

Single Issue: $100
Single Article: $7.50

CONSULTANTS BUREAU, NEW YORK AND LONDON

c/b
233 Spring Street
New York, New York 10013

Published monthly. Second-class postage paid at Jamaica, New York 11431.

SOVIET ATOMIC ENERGY

A translation of *Atomnaya Énergiya*

June, 1983

Volume 53, Number 6 **December, 1982**

CONTENTS

	Engl.	Russ.
Comparison of the Technicoeconomic Characteristics of Nuclear Power Stations with Modern Thermal and Fast Reactors — A. A. Rineiskii	807	360
Physical Characteristics of an RBMK Reactor in the Transitional Period — V. S. Romanenko and A. V. Krayushkin	816	367
Radiation Environment during the Commissioning and Power Runup in the Fifth Unit at the Novyi Voronezh Nuclear Power Station — N. A. Verkhovetskii, V. P. Ivannikov, V. F. Kozlov, V. P. Kruglov, L. M. Luzanova, A. T. Pocevin, P. D. Slavyagin, and L. P. Kham'yanov	825	373
A New Method of Monitoring Radioactive Aerosols from Nuclear Power Stations with RBMK Reactors — L. N. Moskvin, G. G. Leont'ev, S. N. Nekrest'yanov, A. P. Eperin, V. G. Shcherbina, and A. G. Mokhnachev	828	376
Gas Desorption during Irradiation of Metals with Molybdenum Ions — N. P. Katrich and V. N. Kanishchev	832	379
Simulation of Reactor Conditions in Investigations of Radiation Damage of the Surface of Materials — B. A. Kalin	837	382
Analysis and Estimate of Neutron Cross Sections of Curium Isotopes — T. S. Belanova	841	386
Neutron-Transmission Function for the Region of Unresolved Resonances — A. V. Komarov and A. A. Luk'yanov	849	392
LETTERS TO THE DITOR		
Analysis of the Surface and Erosion of the Graphite Diaphragm of the T-3M Tokamak in the Tearing Mode — D. G. Baratov, G. V. Gordeeva, M. I. Guseva, V. N. Dem'yanenko, A. N. Mansurova, S. V. Mirnov, V. A. Stepanchikov, and V. P. Fokin	854	396
Photoneutrons from Thick D_2O, Be, and Pb Converters at E_{max} = 15 MeV — A. V. Drobinin, M. Leonard, and Yu. M. Tsipenyuk	858	398
Direct Charged-Particle Energy Conversion in a System Composed of a Magnetic Expander and Planar Collector — S. K. Dimitrov and A. V. Makhin	861	400
Currents Generated in Pyroelectrics by γ Irradiation — B. A. Levin	863	401
Reactor Tests of Two Thermoemission Electric Power Generating Elements in a Single Loop Channel — V. P. Baril'chenko, V. P. Berzhatyi, A. S. Karnaukhov, V. P. Kirienko, V. A. Maevskii, V. K. Morozov, A. V. Nikonov, N. N. Parkhomenko, V. S. Pastukhov, V. V. Sinyavskii, and Yu. A. Sobolev	866	402
INDEX		
Author Index, Volumes 52-53, 1982	871	
Tables of Contents, Volumes 52-53, 1982	877	

The Russian press date (podpisano k pechati) of this issue was 11/24/1982. Publication therefore did not occur prior to this date, but must be assumed to have taken place reasonably soon thereafter.

COMPARISON OF THE TECHNICOECONOMIC CHARACTERISTICS OF NUCLEAR POWER STATIONS WITH MODERN THERMAL AND FAST REACTORS

A. A. Rineiskii

UDC 621.039.526

The positive experience of operating nuclear power stations with fast reactors in the Soviet Union (BN-350, BN-600) and abroad ("Phoenix," PFR) confirms that at the present time the theoretical principles and technology have been developed, and design-construction experience has been built up, allowing powerful energy units to be constructed with breeder reactors. It is obvious that in the next decade the real structure of nuclear power generation will be formed, including thermal and fast reactors. It is well known that the main purpose of the extensive introduction into nuclear power generation of fast breeder reactors consists in the considerable expansion of the fuel-energy base due to the use of all uranium (and not only the fissile ^{235}U isotope as in thermal reactors) and possibly thorium. As calculations show, the economic advantages of fast reactors clearly are manifested in the conditions of limited reserves of cheap natural uranium. At the present time, there is no other such-assimilated source of the production of fuel and electric power as fast reactors.

The designated nuclear power generation development program in the Soviet Union, incorporating fast reactors, has been achieved. In accordance with the Principal Directive for the Development of the National Economy of the country [1], the problem in the current Five-Year Plan is the development of reliable and economical power generating units with fast reactors with a capacity of 800 and 1600 MW. One of the important economic indexes of nuclear power stations is the installed kW cost. The absolute and relative values of this quantity for nuclear power stations of different types can have a corresponding influence on their contribution to the general structure of nuclear power generation, and also on the choice of the physical and other most-important reactor characteristics.

In the published papers, contradictory expressions are encountered in connection with how much more expensive a fast reactor is than a thermal reactor. One of the reasons for these differences is the comparison of reactors with a different capacity and degree of technology development, and that were constructed at a different time. For example, in certain foreign publications the economic characteristics of demonstration fast reactors, recently introduced into operation, or of constructed commercial fast reactors, are composed with those of standard thermal water-cooled/water-moderated reactors (1000-1300 MW), introduced by the development of commercial technology. It is obvious that the comparison turns out to be far from favorable for fast reactors. Therefore, the choice of subjects for comparison, in order to establish the ratio of the specific costs, and also to answer the question of how much more expensive a fast reactor is than a thermal reactor, is of fundamental importance.

As it is well known, in 1980 nuclear power stations with BN-600 and VVÉR-1000 reactors were completed and brought on stream. But although the degree of development and the solution of the safety problems of these reactors are significantly different (the first semiindustrial fast integrated BN-600 reactor and, representing the third generation of water-cooled/water-moderated reactors, the pilot power unit VVÉR-1000), in view of the absence of more comparable analogs a comparison was made of the specific natural and cost indexes of thermal and fast reactors, by the example of these installations. It should be mentioned that the absolute values of the cost characteristics of comparable power units, due to their development and different design organizations, are nonindicative and therefore no emphasis can be placed on them.

In addition to the analysis of the technicoeconomic characteristics of the BN-600 and VVÉR-1000, certain specific indexes and design solutions of RBMK channel reactors and organic fueled thermoelectric power stations were derived for comparison. The inclusion of other types for the analysis of power installations should promote an understanding of the specific features of the nuclear power stations compared.

Translated from Atomnaya Énergiya, Vol. 53, No. 6, pp. 360-367, December, 1982. Original article submitted March 15, 1982.

0038-531X/82/5306-0807$07.50

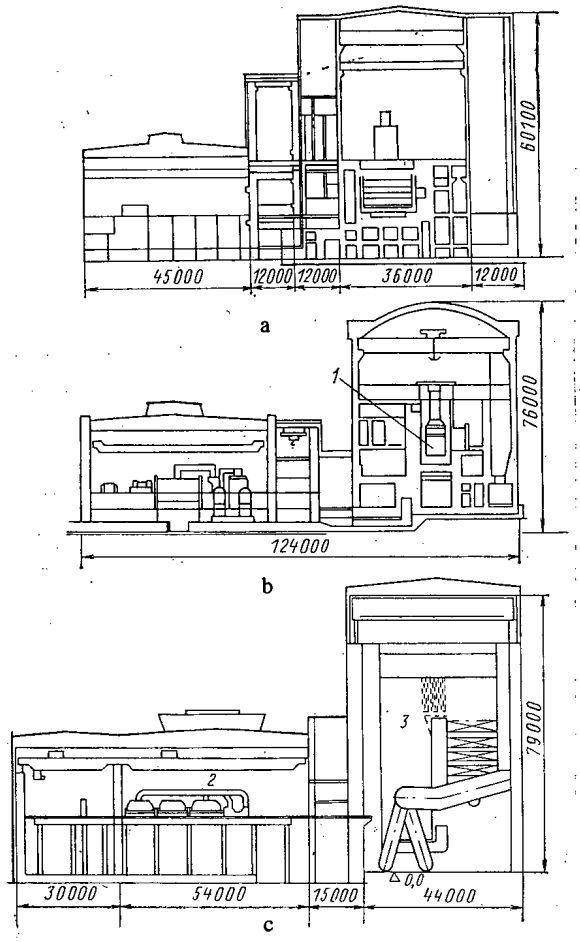

Fig. 1. Grouped schemes: BN-600 (a), VVÉR-1000 (b), and a 1200 MW thermal power station (c). 1) Reactor, 2) turbogenerator, 3) steam boiler.

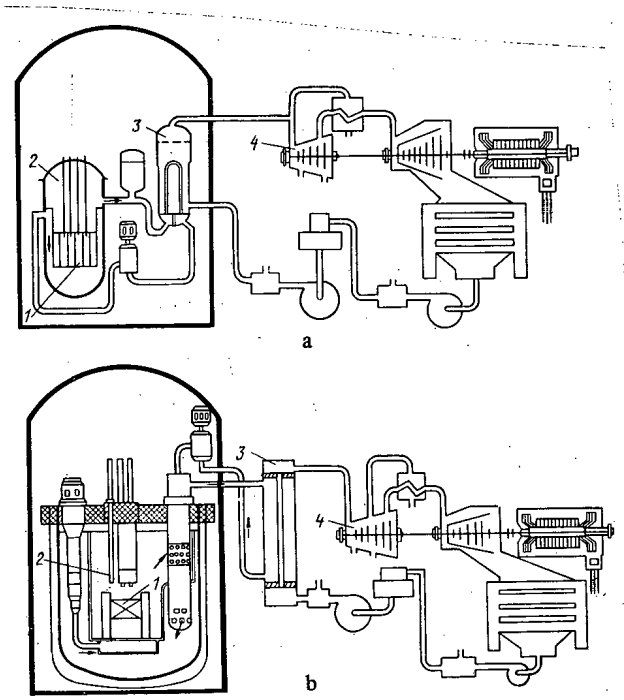

Fig. 2. Schematic diagram of a thermal (a) and fast (b) reactors: 1) core; 2) reactor; 3) steam generator; 4) turbine.

TABLE 1. Technicoeconomic Characteristics of Reactors

Parameters	RBMK-1000 [2,4]	VVÉR-1000 [2,3]	BN-600
Electrical capacity, MW	1000	940	600
Nucl. power sta. eff., %	31,3	31,3	40,6
Mass of plant, pipelines, and shielding metal, tons/MW (elec.)	49	38	58
Volume of ferroconcrete structures, m^3/MW (elec.)·10^3	0,23	0,18	0,17
Labor costs on carrying out construction-repair work on industrial installations man-d/kW (elec.)	3—3,5	2,8—3,2	3,5
Specific capital costs on the structural part (by comparison with the VVÉR-1000), %	—	100	96
Total specific capital costs (by comparison with the VVÉR-1000) at the middle of 1981, %	—	100	140

Comparison of Grouped and Schematized Solutions

Figure 1 shows simplified layouts of the BN-600 and VVÉR-1000 reactors and a 1200 MW gas—oil thermal power station. The role of the steam generating plant in the thermal power station is fulfilled by a single unit — the steam boiler. The nuclear steam generating plant (NSGP) represents a system of components: the reactor and the circulatory system with the coolant, pipelines, pumps, and intermediate heat exchangers for transferring heat from the reactor to the steam generator. From safety conditions, several parallel heat removal units (loops) (2-4) are required, which complicates the layout and makes the plant expensive. In the machine hall equipment of a fast reactor, either turbine installations and an auxiliary plant, identical with the thermal power station (possibly with small modifications), are used, or, just as for thermal reactors, new turbine installations with reduced steam parameters. Thus, from the point of view of grouping solutions and the composition of the plant for conversion from organic to nuclear fuel, the steam boiler is replaced by the nuclear reactor with a more extensive list of thermomechanical plants and a system which serves for cooling the core and transporting heat from the reactor to the steam generator. All this, obviously, has affected the cost characteristics of nuclear power stations.

Fast reactors, by comparison with thermal reactors, have additional intermediate circuits, including heat exchangers, circulatory pumps and pipelines. However, in integrated versions of fast reactor designs (Fig. 2), outside the reactor vessel, just as in a thermal reactor, there is also a single coolant circuit, which also connects the reactor with the generator (SG). Owing to the disposition of all of the plant of the primary circuit in the reactor vessel, structural volumes are reduced and the solution of problems of the leak tightness of the radioactive sodium compartment is simplified.

Comparison of the Technicoeconomic Characteristics of Fast and Thermal Reactors

Natural and Cost Characteristics of Power Stations. Table 1 shows the most important natural cost indexes and certain relative cost indexes of modern power stations with thermal and fast reactors. It can be seen from Table 1 that the difference in the specific natural and cost indexes of thermal and fast reactors is not so significant if we consider that the fast reactor being compared has a considerably lower capacity. As shown in [2], with increase of the capacity of the power unit by a factor of 2, up to 10% of the capital costs are saved. Therefore, if the BN-600 is to have an electrical capacity identical with the thermal reactor, the specific capital costs in the fast reactor can be reduced by 8-9%. The region of construction of the nuclear power station has a definite effect on the installed kW cost. Based on the analysis conducted, the following conclusion can be drawn about the cost of the BN-600

TABLE 2. Specific Indexes of Material Content and Costs of Plants and Systems of Nuclear Power Stations with BN-600 and VVÉR-1000 Reactors

	Specific metal content, tons/MW		Percentage of total cost of plant	
	BN-600	VVÉR-1000	BN-600	VVÉR-1000
Reactor				
Vessel with intra-vessel equipment: main circulatory pump-1 (MCP) intermediate heat exchanger, primary circuit pipelines (for BN-600); auxiliary reactor systems	7,7	1,8	29,5	11,1
Technological Plant				
Steam generators, main circulatory pump (secondary circuit of the BN-600), pipelines from reactor to steam generator, auxiliary systems	6,2	5,7	26,1	31,7
Machine hall plant				
Turbines with main and auxiliary plant, pipelines from accessory and other equipment	16	14,5	5,8	21,5
Electrotechnical equipment	—	—	10,3	7,5
Automatic equipment, control and measuring equipment (CME), dose monit.	—	—	7,1	12,7
Plant of ancillary buildings and structures	7,5	5,0	10	10,8
Plant of fuel recharging system	1,3	2,2	5,8	3,1
Shielding slabs: upper fixed shield (BN-600); doors, covers of manholes; bottom plates in floor of compartments (BN-600).	19,3	8,8	5,4	1,6

(third unit of the Beloyarsk nuclear power station) and the VVÉR-1000 (fifth unit of the Novovoronezh nuclear power station): in comparable conditions (identical electrical capacity, region, and period of construction), the difference in the specific capital costs amounts to 30-50%. This cost difference of electric power should be compensated by the efficient fuel production by fast reactors.

The data given in Table 1 about labor costs on carrying out constructional repair work, and also constructional experience of the BN-600, indicate that the processes of constructing nuclear power stations with fast and thermal reactors are not so significant. The somewhat increased specific capital costs for fast reactors by comparison with VVÉR are explained by the higher total cost of the plant. It is interesting to note that the specific costs on construction are almost equal. The increased cost of a fast reactor plant, as can be seen

from Table 1, is explained by the larger inventory and increased metal content. Therefore, a reduction of the metal content of the plant, and a reduction of the use of expensive stainless steel because of this, is one of the most important problems when constructing and designing fast reactors. Definite successes in this direction have been achieved in a high-capacity reactor design (1600 MW), and also because of the increase of capacity of the BN-600 up to 800 MW (BN-800) as a result of certain improvements and changes in design. The capacity of 800 MW has been obtained without increasing the metal content of the BN-600.

Natural and Cost Characteristics of the Plant of the BN-600 and VVÉR-1000. In order to clarify the reasons for increasing the material capacity and the cost of fast reactors by comparison with thermal reactors, all the equipment of the facilities was divided into functional groups, with an apportionment for each of the natural and cost indexes (Table 2). In the constitution of the BN-600 nuclear steam generating plant, the greatest material content and the most expensive is the integral reactor itself: its specific material content is a factor of four greater than for the VVÉR-1000 reactor. Further, for the BN-600 the components are arranged according to cost in this order: equipment of the secondary circuit (steam generator, sodium pumps and pipelines, and auxiliary systems), electrotechnical equipment, equipment of ancillary buildings and structures, control and measuring equipment (CME) and automatic equipment, and recharging plant and systems. The greatest material content and the most expensive in the constitution of the nuclear steam generating plant of the VVÉR-1000 is the thermomechanical plant (steam generators, coolant circulation system).

It should be mentioned that the specific cost of the machine hall plant of the BN-600 is considerably lower than the cost of the VVÉR-1000, despite the use of turbines in the BN-600 with a lower unit capacity (by a factor of 2.5). The latter is explained by the use of three K-200-130 commercial turbines with a capacity of 200 MW each in the BN-600 whereas for the VVÉR-1000 two special silent-running turbines were developed, with a capacity of up to 500 MW. The electrotechnical equipment is somewhat more expensive for fast reactors, which is explained by the presence of systems for electrically heating the pipelines and the sodium plant. The use of a considerable amount of so-called "shielding metal" is characteristic for the BN-600, due to the necessity of protection from radiation (upper fixed reactor shield, doors of compartments, manhole covers) and from combustion of sodium (bottom plates in the floor of compartments, linings, etc.).

It should be recognized that the possibilities of reducing the metal by the use, where this is possible, of concrete and other substitute steels, and also the possibilities of structures with a reduced metal content, are not yet completely exhausted

Analysis of the Natural and Cost Indexes of the Plant in the Nuclear Steam Generating Plant of the BN-600.

Reactor and Primary Circuit Plant and Systems. All the plant of the BN-600 primary circuit is mainly located inside the reactor vessel. Outside the vessel there are auxiliary systems for coolant and inert gas, and also equipment of the transfer-technological section. The specific natural and relative cost characteristics of the plant and systems of the primary circuit are shown in Table 3.

The largest metal content and the most expensive component of the primary circuit is the reactor with its complete equipment. It can be seen from Table 3 that there is a direct relationship between the metal content and the cost. The reactor components with the largest metal content are the intravessel thermal and neutron shields (steel shells, rods and tubes with graphite) — 35% of the total metal content and 20% of the cost of the reactor. The considerable volume of mechanical assembly work on the construction platform, in addition to the large metal content, contributes to the somewhat greater cost of the BN-600. It is well known that the reactor vessel and the majority of the intravessel components of the reactor have been prepared, welded, and assembled on the construction platform, These operations, as we can see from Table 4 by the example of the greatest metal-containing components of the reactor, have significantly increased their cost.

By comparison with the factory delivery, the cost of the above-mentioned manufactured articles, because of the mechanical assembly operations on the construction platform, have increased by approximately a factor of two. The latter shows the necessity for improvement of the technology and mechanization of these operations on the construction platform. However, it would be incorrect to assume that fast reactors must be more expensive than thermal reactors because many of their components are welded and assembled on the construction platform.

TABLE 3. Primary Circuit Plant and Systems of the BN-600

Type of plant, coolant	Metal coolant		Percentage of total plant cost
	tons/MW	percentage of total metal content	
Reactor with intratank elements and equipment	6,07	79	81
Auxiliary primary circuit systems	1,23	16	8
Other plants, including standby [main circulatory pumps, intermediate heat-exchangers (IHE)] and appliances	0,4	5	9
Sodium (700 tons)	—	—	2

TABLE 4. Components of the Total Cost of Operations on Preparation of the BN-600, %

Preparatory operation	Reactor vessel with thermal shields and shell	Intratank neutron shield
Factory delivery	56	53
Consolidated assembly on the platform	34	27
Installation	10	20

TABLE 5. Plant and Systems of the Secondary Circuit

Type of plant, coolant	Metal content		Percentage of tot. cost of plant of the secondary circuit
	tons/MW	percentage of total metal content of secondary circuit	
Steam generator with framework	4,0	65	73
Secondary circuit's electric pumps with main pipelines and thermal insulation	0,9	5	12
Auxiliary sodium and gas systems	1,3	20	11
Sodium (1155 tons)	—	—	4

Analysis showed that the specific cost of the VVÉR-1000 (total cost of reactor divided by its mass) was high (15 ruble/kg by comparison with 13.8 ruble/kg for the BN-600), although the VVÉR was manufactured almost entirely in factory conditions. The latter obviously means that the thin-walled vessel structures of the fast reactor (e.g., the thickness of the vessel 30-50 mm) are less labor consuming in the case of welding and other mechanical operations, by comparison with vessel and other components of the VVÉR with a wall thickness of up to 200 mm. In order to reduce the cost and accelerate the construction of fast reactors, structural and technological developments must be accomplished by taking account of the use of assembly units of the vessel and other reactor components with the maximum degree of factory preparation.

Plant and Systems of the Secondary Circuit. Data about the specific metal content and cost of these plant and systems are given in Table 5. Both the reactor in the primary circuit

and also the steam generator in the secondary circuit have the greatest metal content and are the most expensive. The main attention must be paid to these components of fast reactors in construction and design development.

Paths for Reducing the Metal Content of Fast Reactors

Fast breeder reactors with sodium cooling have a number of positive engineering characteristics: high efficiency — higher by one-third than for existing thermal reactors; compact core; minimum heat-exchange surface area of the steam generators and intermediate heat exchangers; and low pressure in the reactor vessels and heat exchange plant (0.15-0.2 MPa) and delivery pipelines (0.6-0.8 MPa). By considering the most general discussions, it might have supposed that the difference in efficiency alone must mainly compensate the difference in cost per kW because of the introduction of a third circuit, although, as practice shows, a reduction of the number of circuits does not necessarily reduce cost. As an example we can quote the single-circuit RBMK reactors, which are more expensive than the dual-circuit VVÉR [4]. With a reduction of the number of heat transfer circuits, the requirements on leak tightness, choice of materials, and maintenance and repair of the relatively massive branched steam-power generating part of the nuclear power station are made more stringent, which significantly reduces the gain from the exclusion of compact reactor circuits.

The insignificant pressure in the reactor vessel and plant, and compact core and heat exchange surface area [$S^{BR}_{SG+IHE} = S^{VVER}_{SG} = 35\ m^2/MW\ (elec.)$] make it possible to locate the core and heat exhange plant in thin-walled small-sized vessels, which must lead to a reduction of the metal content.

It is customary to assume, as the qualitative characteristic of the thermomechanical plant the ratio of the mass of the main metal used for the circulation circuit to the total mass of the manufactured articles. In the BN-600, the reactor vessel, intermediate heat exchanger (IHE), main circulatory pump (MCP), pressure collector, pipelines can be related to this metal category, i.e., the plant which ensures the circulation of the coolant and heat transfer. The ratio of the main metal mass to the total mass of the BN-600 amounts to 1/4, whereas in the VVÉR-1000 this ratio is close to unity and in the steam boiler it amounts to 1/2. In the integral reactor there is a relatively large expenditure of metal on the so-called shielding structures: neutron, thermal and biological shields, and supporting structures (bearing collar, MCP and IHE mountings). Since these structures are disposed inside the reactor vessel in the coolant, it is essential to use quality materials (at the present time this is stainless austenite steel) with high demands on the purity of the surface treatment. As a result, their cost approximates to the cost of the plant. Therefore, the urgent problem for the development engineers of fast reactors is the reduction of the expenditure on metal, at the expense of reducing its mass and the use of low-grade steels or their substitutes, and also the development of successful grouping solutions, e.g., increasing the distance between the core and the plant, which is required in maintenance and repair. In certain foreign reactor designs ("Superphoenix," CDFR), because of the increased distance between the core and the IHE, the layer of sodium between them fulfills an important role, from the point of view of shielding from the activation of the intermediate circuit. This role, although it leads to an increase of the diameter of the reactor vessel, allows the thickness and mass of the intravessel steel shield to be reduced. As a result, the total mass of the reactor is reduced. Definite successes in reducing the intravessel shielding were achieved with the development of integral groupings with a horizontal reactor vessel [5]. In these versions, without increasing the diameter of the reactor vessel, the distance between the core and IHE can be made so that the sodium layer completely fulfills the function of the neutron shield.

The use of loop grouping allows a number of intravessel structures to be given up. The developments on variations of these groupings are being carried out in the Federal Republic of Germany (SNR-2 reactor) [6], and in Japan and the USA [7]. It is reckoned that with a positive solution of some of the principal grouping problems, the specific metal content of the primary circuit can be reduced in the loop grouping. It is reckoned also that the block generator will have large reserves from the point of view of metal content.

Integral and Loop Grouping of the Reactor. The technicoeconomic characteristics of the loop version of a reactor of the BN-600 type are determined by taking account of the data on the BN-350 and of developments on the loop version in the initial planning of the BN-600.

Data are given below on the metal content and cost of the BN-600 in the integral (I) and loop (L) feasibilities, respectively:

	I	L
Reactor vessel with thermal shields, casing, thermal insulation, neutron shield, bearing collar, tons/MW (elec.)	3.9	0.7
Plant: IHE, MCP, rotatable plug, pressure chamber with collectors and neutron support, tons/MW (elec.)	2.2	2.5
Pipelines with casings, accessories, thermal insulators, tons/MW (elec.)	–	1.67
Total metal content of main plant of primary circuit: tons/MW (elec.)	6.1	4.85
%	100	80
Cost of main plant of the primary circuit (in relation to the integral version), %	100	85

Because the cost of the reactor itself comprises 25% of the total cost of the nuclear power station, a reduction by 15% of the cost of the reactor leads to a reduction of the total cost of the plant by 3-4%. With respect to the nuclear power station as a whole, if it is further assumed that the cost of the structural part remains unchanged, the saving will amount to not more than 2-3%. In the loop grouping, the extended pipelines of radioactive sodium, with accessories, insurance casings, and electrical heating, increase the metal content of the primary circuit. Based on the **estimates** made, the following provisional conclusions can be drawn: loop groupings, in the case of the use of conventional methods of compensation for the thermal expansions of the pipelines (due to space bends), obviously will not have an appreciable gain in the costs of metal and materials. Taking account of the necessary increase of structural volumes with this method of compensation, and approximately identical cost per installed kW can be expected for both types of grouping. For loop groupings it will be necessary to find new methods, in principle, of separation and compensation of the pipelines for the purpose of reducing their length significantly. There are definite reserves for increasing the coolant velocity in noncorroding pipelines up to 4-6 m/sec, which is significantly less than in water-cooled/water-moderated reactors. This measure would allow the diameter of the pipelines to be reduced. Problems of safety and, in particular, assurance of leaktightness of the radioactive circuit and reliable cooling of the reactor core have a large effect on the choice of the type of compensation. As experience in designing shows, these problems are resolved most simply in integral groupings. However, even in loop groupings with a successful solution of the problems of pipeline compensation and leak tightness of compartments, the metal costs can be reduced and an appreciable economic effect can be obtained. A number of suggestions for solving the problem of the thermal expansion of the pipelines can be found in the studies on the SNR-2 [6] and LMFBR reactors, with a capacity of 1200 MW [7]. In these versions, preference is given to closed loop groupings in their core, and the intermediate heat exchangers are located at a small distance, separated by a concrete wall (which serves as the neutron shield) and joined by short pipelines with movable connections (bellows or lens compensators). The designers of the loop structures accept that not all routes for improving them have been used, which obviously is a stimulus for continuing work on loop groupings, e.g., in the SNR-2 reactor with a capacity of 1300 MW [8].

Sectional-Modular and Block Construction of the Steam Generator are used at present in the BN-600 and "Phoenix," and in the "Superphoenix" reactor under construction, respectively. Sectional-modular construction of the steam generator has great flexibility in operation: There is the possibility, by means of an attachment, of taking a section with a defective module out of operation without shutting down the whole heat transfer loop. With the appropriate choice of the number of sections, disconnection of one of them has almost no effect on the output of the nuclear power station. All this ensures a high load factor of the nuclear power station, even in the case of depressurization of individual modules. However, these operational advantages are achieved at the expense of a higher metal content and cost, and of complication of the steam generator layout. Block construction does not have these advantages and it also does not have flexibility in operation, inherent with sectional constructions. It can be supposed that in the future, after perfecting the technology for ensuring a high quality of manufacture of the steam generator, and after studies in actual conditions of the problems of thermohydraulics, corrosion, etc., which will allow the reliable operation of the heat exchange surface to be predicted, conversion to block construction can be effected. In

TABLE 6. Technicoeconomic Characteristics of Steam Generator

Parameter	Block, VVÉR-1000 [9]	Sectional, BN-600	Block "Superphoenix" [10]
Capacity (thermal/electric), MW	750/210	490/200	750/300
Mass of steam generator, tons	320	600	180
Specific metal content, tons/MW (elec.)	1,5	3,0	0,6
Specific cost (by comparison with VVÉR-1000)	1,0	2,9	—

this case, the metal content of the steam generator is reduced significantly by comparison with the existing sectional construction and the block steam generators of thermal reactors (Table 6).

The optimistic approach shown with the choice of the block construction of the "Superphoenix" steam generator is reinforced by the relatively reliable operation of the "Phoenix" steam generator, with an extensive program of experimental tests on a heavy-duty (50 MW) steam generator test rig, and also by the significant large reserves of power in the power system. In the French power system [11], there is a considerable reserve of installed capacity even during the annual load peaks, which facilitates operating conditions, reduces the problem of withdrawing the block for maintenance, and reduces losses from idling periods.

CONCLUSIONS

Design—construction solutions will be improved in proportion with the buildup of experience of operation and improvement of technology. Several alternatives to these solutions, ensuring a reduction of the metal content, were considered above, and others are in the stage of development. Problems of reducing the cost and metal content were not essential for the development of experimental industrial and demonstration reactors. In the development of high-capacity power reactors, problems of economics and competitiveness will be very important. For the complete realization of potentially feasible fast reactors, from the point of view of metal content and cost, it is possible that new design solutions will be required, differing from those being used at the present time.

The author sincerely thanks O. D. Kazachkovskii and M. F. Troyanov for cooperation in carrying out the work and for fruitful discussion of the results.

LITERATURE CITED

1. Principle Trends of Economic and Social Development of the Soviet Union in 1981-1985 and the Period up to 1990 [in Russian], Politizdat, Moscow (1981), p. 340.
2. L. M. Voronin, Special Features of Designing and construction of Nuclear Power Stations [in Russian], Atomizdat, Moscow (1980), pp. 96, 98.
3. V. M. Berkovich et al., Teploenergetika, No. 4, 18 (1974).
4. V. S. Konviz and L. P. Mikhailov, in: Nuclear Power Stations [in Russian], No. 2, Énergiya Moscow (1979), p. 34.
5. O. D. Kazachkovskii et al., in: Nuclear Power and Its Fuel Cycle, IAEA, Vienna, Vol. 1, (1977), p. 293.
6. M. Kochler et al., in: Proceedings of an International Conference on Optimization of Sodium-Cooled Fast Reactors, BNES, London (1977), p. 317.
7. A. Amorosi et al., in: Proceedings of an International Conference on Optimization of Sodium-Cooled Fast Reactors, BNES, London (1977), p. 201.
8. R. Huper, in: Fourteenth Annual Meeting of the International Working Group on Fast Reactors, Vienna, March 31-April 3 (1981), p. 45.
9. T. Kh. Margulova, Nuclear Power Stations [in Russian], Vysshaya Shkola, Moscow (1978), p. 11.
10. G. Cuttica, Nucl. Eng. Int., No. 6, p. 5 (1978).
11. Thermal Power Generation of France [in Russian], Minénergo SSR, Moscow (1977), p. 40.

PHYSICAL CHARACTERISTICS OF AN RBMK REACTOR IN THE TRANSITIONAL PERIOD

V. S. Romanenko and A. V. Krayushkin

UDC 621.039.539.1

The transitional period of RBMK operation is understood to mean the time interval from the instant of reactor startup to the arrival at steady conditions of fuel reloading. The latter stage is characterized by a constant (over time) frequency of fuel-element reloading and depth of burnup of the loaded fuel. Certain other quantities indicating the state of the active zone — e.g., the reactivity coefficients — are also constant. More rigorous consideration shows that in steady conditions these characteristics oscillate about a mean value which is constant over time. The length of the transitional period depends on the composition of the initial load and on what fuel is used for reloading. With the fuel characteristics typical for RBMK reactors, the length of the transitional period is 5-6 years.

The transitional period may also be understood to mean a time interval in which a reactor operating in steady conditions is reloading with fuel of another type, different from the original load.

A property of the RBMK is the considerable change in the reactivity coefficients determining the dynamic properties of the energy-liberation field in the course of the transitional period. The determination of these dependences is an important problem in the neutron-physics calculation of an RBMK. Calculation of the time dependence of the fuel-element loading frequency is necessary for the prediction of the fuel consumption at an atomic power plant and also for the choice of optical conditions of organizing the transitional period.

In the present work, a rational method of neutron-physics calculation of transitional-period characteristics for an RBMK is described, the basic physical processes occurring in the reactor in this period are analyzed, and certain reserves of the fuel cycle are pointed out.

Choice of Mathematical Model of the Reactor. The problem of calculating the transitional period is solved by mathematical modeling of the burnup and reloading of the fuel on a computer. The basic block of programs realizing the algorithm for the calculation of the fuel burnup and reloading is the block for the calculation of the energy-liberation field. Calculation of the transitional period consists in the successive calculation of critical states of the reactor, separated by a certain time step. The energy-liberation field obtained in the initial step is used to calculate the fuel burnup in the course of the whole step. The fall in reactivity due to fuel burnup in the given step is estimated. From the condition of maintaining constant reactivity, the number of additional absorbers requiring substitution in order to compensate for the excess reactivity of the initial load or the burned-up fuel elements is determined. At the end of each time step, the following condition must be satisfied:

$$\Delta K_{\text{R}} - \Delta K_{\text{B}} = 0, \tag{1}$$

where ΔK_{R} is the increase in reactivity due to reloading, and ΔK_{B} is the fall in reactivity due to fuel burnup. In the numerical calculation, the condition in Eq. (1) is usually replaced by the approximation

$$|\Delta K_{\text{R}} - \Delta K_{\text{B}}| \leqslant \varepsilon, \tag{2}$$

where ε is some sufficiently small number.

Let Δt be the time step; $R(t)$, desired mean fuel-element reloading frequency over the interval Δt; ΔR, error in determining $R(t)$; and $E(t)$, rise in reactivity due to a single substitution. Then Eq. (2) may be rewritten in the form

Translated from Atomnaya Énergiya, Vol. 53, No. 6, pp. 367-373, December, 1982. Original article submitted January 29, 1982.

 0038-531X/82/5306-0816$07.50

from which it follows that, if ε is specified, the corresponding choice of time step is necessary for the calculation of R(t) with a definite error. In particular, with decrease in Δt, decrease in ε is necessary to maintain the error in calculating R(t) at previous level, and this leads unavoidably to increase in the machine time required for the calculation of the transitional period. Since conditions of continuous reloading are being discussed, the time step separating the given critical states must be sufficiently small. This indicates the need for high speed in the block for the calculation of the energy-liberation field, since with decrease in time step the number of operations involving it increases.

As the block for calculation of the energy-liberation field, any of the available programs for calculating the channel-by-channel energy-liberation field may be used. For example programs of QUAM type [1] may be used; these are the fastest for two-dimensional RBMK calculation. However, the large number of active-zone channels (∿ 2000) means that the time to calculate the energy-liberation field even when these programs are used is ∿ 1.5 min on a BÉSM-6 computer. In this case, the time required to calculate the transitional period exceeds 20 h. Three-dimensional calculations in such a situation are impossible, since the time necessary for the calculation would increase by a minimum of ten times. The requirement for multivariant calculations of the transitional period leads to the necessity of using simpler models of the reactor.

Homogenization of the Active Zone. The neutron field of the RBMK may be written in the form of some macroscopic field, which reflects the smooth variations in the neutron flux due to leakage and properties of the individual zones of the reactor, and a microscopic field describing the fine structure of the neutron flux inside the given zone, which arises because of the different properties of the fuel elements having different burnup depths and also because of the presence of absorber in the zone (additional rods of the control and safety system).

The problem of calculating the neutron field in the reactor may be divided into two parts: calculation of the macroscopic field giving a mean neutron flux over the chosen reactor zone, and of the microscopic field inside each zone. The consideration will be for two energy groups (superthermal and thermal neutrons); all the absorption will be regarded as being concentrated in the thermal group. The simplest approximation is obtained if it is assumed that the mean neutron flux over the microcell is the same in all microcells with a fuel element present in the given zone. This assumption is justified by the considerable neutron diffusion length in both energy groups (L^2 ∿ 150–200 cm^2), the burnup-independent leakage cross section in the superthermal group, and the largely burnup-independent absorption cross section in the thermal group (in the range 0-20 MW • day/kg uranium, the mean absorption cross section over the microcell in the thermal group varies by 10%).

The equations of two-group theory will be used to calculate the macrofluxes; for a purely thermal reactor, they take the form

$$\begin{aligned} \nabla D_1 \nabla \Phi_1 - \Sigma_{12}\Phi_1 + K_\infty \Sigma_2 \Phi_2 = 0; \\ \nabla D_2 \nabla \Phi_2 - \Sigma_2 \Phi_2 + \Sigma_{12}\Phi_1 = 0, \end{aligned} \tag{3}$$

where D_1, D_2 are diffusion coefficients; Σ_{12}, cross section for transition from the fast to the thermal group; Φ_1, Φ_2, fluxes of fast and thermal neutrons; K_∞ and Σ_2, multiplication coefficient of the medium and the effective neutron-absorption cross section in the thermal region, which also includes absorption in the superthermal energy range. The two-group parameters of the system in Eq. (3) are determined as follows: In each zone, D_1, D_2, and Σ_{12} are taken to be equal to the corresponding quantities for a microcell with fresh fuel elements, since according to the calculation they do not depend on the enrichment and depth of burnup of the fuel. The only parameter by which they are significantly influenced is the heat-carrier density. For microcells with absorber, D_1, D_2, and Σ_{12} are close to the corresponding values for microcells with fuel elements, which allows them to be regarded as equal.

Suppose, further, that S(P, t) is a function describing the fuel-element distribution with respect to the burnup depth at time t in the given zone, such that

$$\int_0^{P_M} S(P, t)\, dP = 1,$$

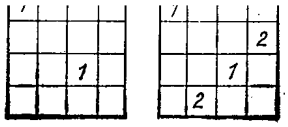

Fig. 1. Cell of periodicity of the active zone of an RBMK with and without additional absorber: 1) control; 2) additional absorber.

where P_M is the maximum burnup depth in the zone. In this case, $S(P, t)dP$ is the proportion of fuel elements with a burnup depth of between P and P + dP. The function $S(P, t)$ is calculated taking account of the specific loading and unloading of the fuel. For the initial load, it may be represented by the delta function $\delta(P)$. In steady conditions, the constant distribution $S(P) \sim 1/\Sigma_f(P)$ is established, where $\Sigma_f(P)$ is the mean fission cross section over the cell. In the transitional period, $S(P, t)$ changes from a delta function to a smooth steady distribution.

The mean absorption and multiplication coefficients of the microcells with a fuel element may be calculated as

$$\bar{\Sigma}_a(t) = \int_0^{P_M} \Sigma_a^c(P)\, S(P, t)\, dP;$$

$$\bar{K}_\infty(t) = \int_0^{P_M} K_\infty^c(P)\, \Sigma_a^c(P)\, S(P, t)\, dP/\bar{\Sigma}_a(t). \qquad (4)$$

The functions $\Sigma_a^c(P)$ and $K_\infty^c(P)$ — the absorption cross section and multiplication coefficient of a microcell with a fuel element as a function of the burnup depth — are obtained from a preliminary detailed calculation using special "cell" programs.

The next step is to consider how $\bar{K}_\infty$ and $\bar{\Sigma}_a$ vary in the presence of absorber in the reactor. In RBMK reactors, absorber is usually placed in regular lattices, so that a large part of the active zone represents a fragment of an infinite polylattice. The cell of periodicity of the latter is called the polycell (Fig. 1).

Following the homogenization method described above, the polylattice is replaced by a homogeneous multiplication medium, in which periodically positioned cells with absorber are placed. The constants of the multiplication medium are determined from Eq. (4). Each cell with absorber is surrounded by an external multiplication medium, and the active zone is represented in the form of a set of cells with absorber at the center. Continuing the homogenization, an expression is obtained for the parameters of Eq. (3)

$$K_\infty = \bar{K}_\infty Q_k;$$
$$\Sigma_2 = \bar{\Sigma}_a Q_\Sigma. \qquad (5)$$

To obtain the factors Q_k and Q_Σ, a multiplication medium in which a regular lattice of cells with absorber is "inserted" is assumed. The expanded cells in which the cell with absorber is surrounded by an external multiplication zone are separated. This expanded cell is "cylinderized," and the mean flux density of thermal neutrons over its zone is calculated analytically under the assumption of a plane superthermal flux. At the outer boundary of the expanded cell, the condition $d\Phi/dr = 0$ is imposed. An expression of the type in Eq. (5) is obtained if there is a single lattice of absorber. In reality, there are several lattices of absorber in the active zone (lattices of additional absorber, of control rods, etc.). In this case, applying Eq. (5) successively, the following approximate expressions may be obtained:

$$K_\infty = \bar{K}_\infty \prod_{i=1}^{N} Q_k^i;$$
$$\Sigma_2 = \bar{\Sigma}_a \prod_{i=1}^{N} Q_\Sigma^i, \qquad (6)$$

where N is the number of absorber lattices.

The multiplication coefficient of the polycell shown at the left in Fig. 1 is 1.0200, while for a polycell with two types of absorber (at the right in Fig. 1) the corresponding figure is 0.8890. For comparison, note that the calculation of the given polycells using programs solving the Galanin–Feinberg equations gives 1.0186 and 0.8697, respectively. Thus, the agreement between the homogenized and "accurate" calculations of a heterogeneous system is satisfactory if a single absorber lattice is considered, and less satisfactory for more complex systems. In the latter case, a small correction is required to the factors Q_k^i and Q_Σ^i in Eq. (6). It is expedient to use Eq. (6) for the multiplication coefficient of the polylattice in determining the reactivity coefficients, since this allows the components from cells with multiplying and nonmultiplying channels to be distinguished. In calculating the reactivity coefficients, it is first necessary to determine the change in the multiplication coefficient of each spatial zone with change in the corresponding parameter (heat-carrier density, fuel or moderator temperature). Differentiation of Eq. (6) gives the two components

$$d_x(\mathbf{r}, t) = \frac{1}{k_\infty(\mathbf{r}, t)} \frac{\partial k_\infty(\mathbf{r}, t)}{\partial x} = \frac{1}{\bar{k}_\infty(\mathbf{r}, t)} \frac{\partial \bar{k}_\infty(\mathbf{r}, t)}{\partial x} + \sum_i \frac{1}{Q_i^h(\mathbf{r}, t)} \frac{\partial Q_i^h(\mathbf{r}, t)}{\partial x}. \quad (7)$$

The first component of the local reactivity coefficient corresponds to the multiplication properties of cells with a fuel element, while the second describes the leakage of neutrons into cells with absorber, and also the properties of the absorber with change in x. The total reactivity coefficient in this case is determined by the expression

$$\alpha_x(t) = \frac{1}{\overline{\Delta x}} \int_V \alpha_x(\mathbf{r}, t)\, \Delta x(\mathbf{r})\, \Phi^2(\mathbf{r}, t)\, dV, \quad (8)$$

where V is the reactor volume; Δx (r), increment in x; Φ(r, t), thermal-neutron flux; and $\overline{\Delta x}$ mean increment in x over the reactor volume.*

On the basis of the given method, the programs REF-Z and REF-R, intended for the calculation of the RBMK transitional period, have been written. The first is a point approximation in the radial direction, but describes in detail the change in reactor properties in the axial direction, including the feedback between the neutron flux and the heat-carrier density. Using the programs, the reloading frequency, burnup depth vapor coefficient of reactivity, and reactivity coefficients with respect to the fuel and moderator temperatures may be calculated as a function of the time. The fuel component of the electrical energy cost has also been calculated by the method outlined in [2]. The time constant for the development of the first azimuthal harmonic (τ_{01}) of the neutron flux is a very important quantity characterizing the stability of the radial–azimuthal distribution of the energy liberation. In the REF-Z program, there is a block for the calculation of the time constant of the development of the first azimuthal harmonic τ_{01} as a function of the time from the instant of reactor startup. The calculation is performed by a method similar to that described in [3]. The REF-R program is a point approximation in the axial direction, but allows a reactor consisting of several radial zones, in each of which loading occurs in a definite manner, to be investigated. In particular, it offers the possibility of determining the reloading frequency in each of the zones as a function of the time, which ensures constancy over time or variation according to a definite law of the form of the radial neutron field. In the case of a single zone, with conditions of reflection at the boundary, the REF-R program models the "burnup sublattice" in a homogeneous approximation. The given programs require inconsiderable use of computation time (~15 min on a BESM-6 computer per variant) for the calculation of reactor characteristics in the transitional period (~2000 effective days) and are used for multivariant calculations.

Some results of calculational investigations are given below.

Burnup and Reloading of Fuel. Results of calculation by the REF-R program, using a heterogeneous program of the burnup depth and reloading frequency of the fuel as a function of the time, for design conditions of occurrence of the RBMK transitional period, are shown in Fig. 2. The heterogeneous program considers some mean polycell of the active zone of the type shown in Fig. 1. The results are normalized so that the reloading frequency and burnup depth in steady conditions are equal to unity.

The curves obtained by the REF-R program are smooth, since in the homogeneous approximation no account is taken of the scatter over the burnup depth between fuel elements of the same age, which is a consequence of neglecting the microstructure of the neutron flux. The microstructure is taken into account in the heterogeneous method, which results in more com-

*In obtaining Eq. (8), the condition K (r) ≈ 1 is satisfied in the reactor volume.

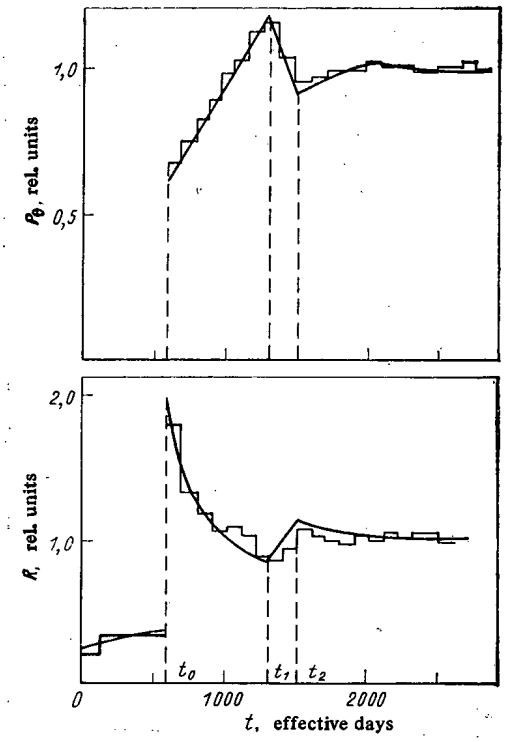

Fig. 2. The dependence of the burnup depth of the unloading fuel (P_B) and the frequency of fuel-element reloading (R) on the time t, counted from the instant of reactor startup (point approximation).

plex dependences. In Fig. 2, the mean values of the reloading frequency and burnup depth over a period of 100 effective days obtained from the heterogeneous calculation are shown. The agreement between the heterogeneous and homogeneous calculation with respect to the burnup depth, an integral characteristic, is satisfactory. There is a different appearance to the curve of the reloading frequency, which relates to local characteristics and depends significantly on the neutron flux at the fuel element reloaded at a given moment. Therefore, instead of a smooth curve, heterogeneous calculation gives a more complex dependence, which, however, basically repeats the trend of the "homogeneous" curve. The difference in the mean values over an interval of ∿100 effective days given by the two methods is ∿8% for the reloading frequency and ∿5% for the burnup depth.

Using the given heterogeneous program, the transitional period of the reactor at the Leningrad atomic power station has been calculated. Such calculations, using polylattices as models of the active zone, may be regarded as calculations in a certain "improved point" approximation. They show that the current value of the burnup depth of the fuel is predicted with an error of 10%. The yearly mean fuel-element reloading frequency is predicted with the same error. Note that with description of the process of fuel burnup and reloading in the maximum possible detail, the error in calculating the burnup depth and the reloading frequency will be determined by the error in calculating K_∞ using "cell" programs. If the latter is found at a level of 1%, then the burnup depth may be obtained with an accuracy of ∿5%. Taking this into account, it may be concluded that the given homogeneous approach to the calculation of the above-noted characteristics has a similar "order of accuracy." The difference in the results of the homogeneous and heterogeneous calculations also allows the influence of all the simplifications and assumptions employed on the final result to be estimated.

The given period (Fig. 2) may be arbitrarily divided into four intervals. In the interval from 0 to t_0, the additional absorbers are unloading and replaced by fresh fuel elements. Since the increment in reactivity in this case is relatively large, the effect of replacing the additional absorbers by fuel elements is small. At time t_0, the replacement of burned-up fuel elements by fresh ones begins. The effect of the substitution is considerably less, and therefore the reloading frequency increases discontinuously by a small factor. With increase in burnup depth of the unloaded fuel elements, the effect of their replacement by fresh ones increases, and the reloading frequency falls. At time t_1, the last fuel element of the initial load, which has the maximum burnup depth, is unloaded. Correspondingly, the

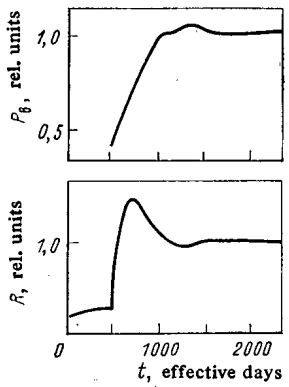

Fig. 3. Dependence of the burnup depth of unloaded fuel and the frequency of fuel-element reloading on the time, counted from the instant of reactor startup (a reactor of finite radius).

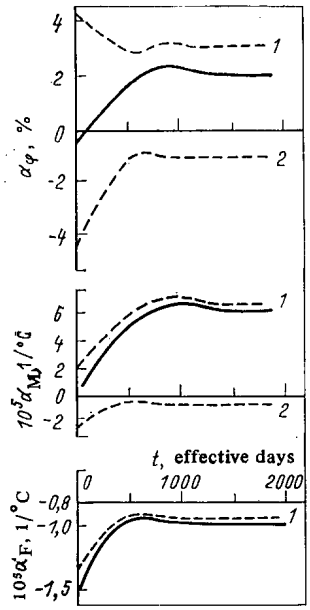

Fig. 4. Dependence of the pair coefficient of reactivity (α_φ) and the reactivity coefficient with respect to the moderator and fuel temperature (α_M and α_F) on the time, counted from the instant of reactor startup. Dashed curves 1 and 2 correspond, respectively, to the first and second components of the reactivity coefficients, and the continous curves correspond to the resulting value.

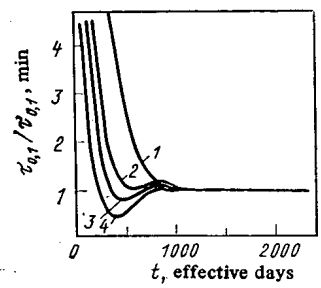

Fig. 5. Time dependence of the time constant of the development of the first azimuthal harmonic (τ_{a1}) for initial loading by fuel of enrichment 2 (1), 1.75 (2), 1.65 (3), 1.55% (4).

reloading frequency reaches a minimum at this moment. In the interval t_1-t_2, the fuel elements loaded in the interval 0-t_1 in place of additional absorbers are unloaded. After time t_2, the burnup depth and reloading frequency change inconsiderably over a certain interval, and reach steady values. Note that this form of the curves is well traced in the homogeneous calculation. Heterogeneous effects lead to "blurring" of the maxima and minima on the curves (step dependences).

If a reactor of finite radius is considered, taking account of the real form of the field, then the times t_0, t_1, and t_2 in each radial zone may be shifted with respect to each other (Fig. 3). However, in this case, too, the mean values of the reloading frequency and burnup depth over intervals of 100 effective days will not differ from those calculated in the point approximation by more than 8-10%.

Reactivity Coefficients. The dependences plotted in Fig. 4 are calculated from the REF-Z program. As already noted, the reactivity coefficient may be written in the form

$$\alpha_x = \alpha_x^1 + \alpha_x^2,$$

where α_x^1 is the first component in Fig. 4, taking account of the change in properties of cells with fuel elements, and α_x^2 is the second component, taking account of the change in neutron leakage into cells with absorbers and also the properties with change in x.

The component α_x^2 depends on the number of absorbers in the active zone, and is negative for the initial load. With reduction in the number of absorbers (unloading of the additional absorbers), this component reduces in absolute magnitude, which is the reason for the increase in the pair coefficient of reactivity.

The basic reasons for the change in the component α_x^1 of the pair coefficient are the decrease in effective lattice step of the working channels and the change in isotopic composition of the fuel over time. The component α_x^1 of the temperature coefficients increases over time, on account of the change in isotopic composition of the fuel, and stabilizes when the isotopic composition is steady.

Reduction in Enrichment of the Initial Load. The advantage of using fuel of enrichment higher than 1.8-2% in RBMK reactors was described, e.g., in [4]. However, high enrichment in the initial load leads to difficulties in compensating the excess reactivity and is economically disadvantageous. For this reason, when increasing the enrichment of the fuel used for reloading, it is expedient to reduce the enrichment of the initial load, which may be done, e.g., as a result of loading some of the fuel elements with natural uranium. As shown by calculation, the gain in the total fuel consumption over the transitional period due to reduction in enrichment of the initial load increases with reduction in enrichment (up to an enrichment of $\sim$1.4%). However, reduction in enrichment of the initial load entails an increase in the reactivity coefficients, and primarily in the pair coefficient, which impair the control of the reactor. If the situation is favorable from the viewpoint of reactor controllability at the initial moment, significant worsening in the dynamic properties of the active zone may occur in the course of the transitional period.

The results of calculating τ_{01} as a function of the time, counted from the instant of reactor startup, are shown in Fig. 5 for several variants of initial loading (calculation by REF-Z). The initial variant chosen is that in which fuel of 2% enrichment is used both for the first load and for reloading. Defining $\tau_{01\min}$ as the minimum achievable value, determined on the basis of experience of reactor use, τ_{01} considerably exceeds $\tau_{01\min}$ at the initial instant. With increase in the reactivity coefficients, τ_{01} decreases. Its minimum value is attained in steady conditions. Curves 2-4 in Fig. 5 correspond to initial loading by fuel of reduced enrichment, with reloading, as before, by fuel of 2% enrichment. At a certain enrichment of the initial load, there appear time intervals in which $\tau_{01} < \tau_{01\min}$. There are methods of increasing τ_{01} in the given intervals — e.g., by retaining a certain number of additional absorbers in the active zone and then unloading them at a later time — but in this case the advantages of reducing the enrichment are partially or even completely lost. Thus, the lower limit of enrichment of the initial load should be determined from considerations of the dynamic characteristics of reactor operation in the transitional period.

Profiling the Enrichment Over the Fuel-Element Height. The dependence shown in Fig. 6 is characteristic of operating RBMK reactors. With increase in fuel enrichment, there is a depression of the height field over the first 200-300 effective days, after which the form of the field is unchanged. Also in Fig. 6, the initial form of the height field (dashed) and

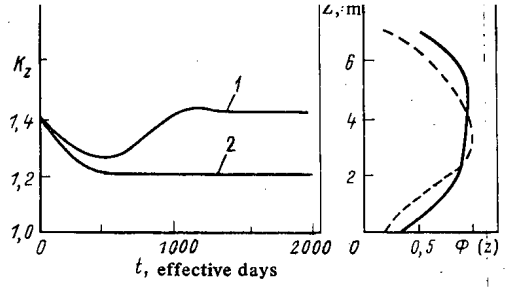

Fig. 6. Time dependence of the nonuniformity coefficient of the density of the thermal flux of neutrons over the height of the active zone (K_Z) for the cases in which profiled (1) and homogeneous (2) fuel elements are used.

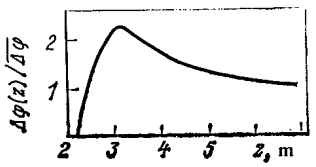

Fig. 7. Change in vapor content $\Delta\varphi$ (Z) over the height of the active zone ($\overline{\Delta\varphi}$ is the change in vapor content over the height).

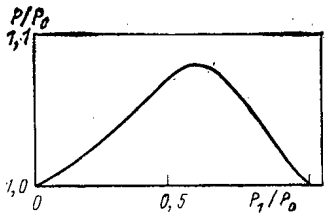

Fig. 8. Dependence of the burnup depth of unloaded fuel elements in steady conditions on the burnup depth (P_1) at which the upper and lower parts of the fuel element are interchanged.

the form of the steady field (continuous curve) are shown. Leakage of neutrons over the height, due to depression of the field, increases by ∿1%, which leads to reduction in burnup depth of the fuel. As shown by calculations, the limiting fuel-element power depends very little on the relative distribution of the energy liberation over the height of the active zone [5]. Taking this into account, and also that there exists a margin with respect to the maximum temperature of the fuel elements, the height field may be maintained close to its initial form in the course of reactor operations, or may be even more convex. This may be accomplished by profiling the fuel-element enrichment over the height. Reloading with fuel elements which have an elevated enrichment of the fuel in the central region and, correspondingly, lower enrichment at the upper and lower ends allows the convex form of the field to be maintained and allows increase in leakage due to the depression effect to be avoided (curve 1). Profiling the enrichment without change in the mean fuel-element enrichment leads to increase in the fuel burnup depth by ∿ 3-7%; channel-by-channel nonuniformity of the power increases inconsiderably here (∿ 3-5%) in comparison with the case in which homogeneous fuel elements are used.

One further important advantage of profiled fuel elements is the possibility of reducing the pair coefficient of reactivity without increasing the mean enrichment. Calculation shows that the creation of a section of length 200 cm in the central region of a fuel element in which the enrichment is 2.4%, while retaining a mean enrichment over the height of 1.8%, allows the pair coefficient to be reduced by $\sim 1/\beta$ in comparison with the case in which a fuel element homogeneous over the height with an enrichment of 1.8% is used. This may be understood from the condition in Eq. (8). The central region of the active zone has the greatest statistical weight. In addition, a typical form of variation in the vapor content over the height takes the form in Fig. 7, with a maximum in the central region. Therefore, reduction

in the local vapor coefficient in the central region is found to be most effective.

The effect of height-field depression in burnup may also be eliminated by interchanging the upper and lower ends of the fuel element and then completing burnup (Fig. 8). It is obvious that there must exist an optimum in this dependence, since reversing the fuel element at the beginning or end of the fuel-element lifetime would lead to no gain in burnup depth. If the fuel-element burnup depth attained without reversal (P_0) is taken as unity, the maximum gain will be at $P_1/P_0 \simeq 0.6$, and is 9%. This value also corresponds to a maximum of K_z.

Thus, the physical characteristics of RBMK reactors undergo significant changes in the course of the transitional period. The character of these changes depends on the specific operating conditions and must be determined in each case taking these conditions into account.

LITERATURE CITED

1. S. S. Gorodkov, "New method of calculating heterogeneous reactions," Preprint IAE-2251, Moscow (1973).
2. S. V. Bryunin et al., At. Energ., 46, No. 4, 219 (1979).
3. V. I. Budnikov et al., At. Energ., 45, No. 5, 331 (1978).
4. I. Ya. Emel'yanov et al., At. Energ., 46, No. 3, 139 (1979).
5. N. A. Dollezhal' and I. Ya. Emel'yanov, Channel Nuclear Power Reactor [in Russian], Atomizdat, Moscow (1980).

RADIATION ENVIROMENT DURING THE COMMISSIONING AND POWER RUNUP IN THE FIFTH UNIT AT THE NOVYI VORONEZH NUCLEAR POWER STATION

N. A. Verkhovetskii, V. P. Ivannikov, V. F. Kozlov,
V. P. Kruglov, L. M. Luzanova, A. T. Pocevin,
P. D. Slavyagin, and L. P. Kham'yanov

UDC 621.039.584

The fifth unit at Novyi Voronezh nuclear power station is the first in a large series of stations fitted with VVÉR-1000 nuclear reactors. The physical commissioning of the unit was performed on April 30, 1980. In May of that year, it was connected to the power network and began to be run up to power. The nominal reactor power was attained on February 20, 1981. The design features of the fifth unit have been described along with the startup and the lines of subsequent improvement in [1].

To provide radiation safety in the case of a maximum design accident MDA, the entire principal circulation loop is enclosed in a shield made of prestressed reinforced concrete designed to withstand a pressure of 0.55 MPa. The MDA was taken as an accident involving loss of the primary coolant by instantaneous failure of a pipeline of maximum diameter (Du-850) coinciding in time with complete loss of load.

Passive and active emergency-cooling systems for the core are provided for the case of MDA, along with a system for reducing the pressure inside the containment. All the active systems providing safety in the station have 100% threefold backup. If the control panel fails there is a reserve panel, from which the safety systems can be controlled and the unit shut down and cooled.

The design of the station divides the areas into ones that cannot be entered (e.g., within the sealed part of the containment, where staff are not admitted with the equipment working), areas periodically visited, and permanently staffed areas. Staff are admitted to the first two of these by special permission under dosimetric control, e.g., for equipment repair.

During the commissioning and runup periods, the biological shield of the reactor was examined, along with the other spaces in the power station, to determine the penetrating radiation levels; radiochemical analysis were also performed on the water in the first loop and estimates were made of the state of the fuel-rod sheathes, and measurements were made of the removal of water (in an organized fashion and from leaks) from the loop. In addition, gas and aerosol measurements were made on the air inside the containment, in the various ventilating systems, and in the gas-cleaning units, with estimates of the rates of release of gases and aerosols to the atmosphere and of liquid wastes to the drains. All of this was accompanied by monitoring of the radiation doses to the staff during commissioning and runup, and also during regular shutdowns.

The biological shield was examined when the reactor power was 20, 40, 75, and 100% of nominal. At 100% power, the levels of n and γ rays did not exceed the permissible values of 0.008 and 0.004 μSv/sec (1 Sv = 100 rem , correspondingly, for spaces temporarily and permanently staffed, as laid down by the health rules for design and operation (SPAES-79).

The radioactivity of the air inside the containment and the gas and aerosol releases are determined by the activity and radionuclide composition of the coolant in the first loop when there are unorganized leaks. Activated corrosion products deposited in the first loop determine the radiation enviroment during regular prophylactic repair and fuel changing. Therefore, particular attention was given to the radionuclide composition of the coolant and deposits during the commissioning and runup periods (Table 1).

Table 1 shows that after 50% power was reached, the specific activities of ^{131}I and gaseous fission products (^{133}, ^{135}Xe, ^{85m}, ^{88}Kr, etc.) were less than the design level by two orders of magnitude, this level corresponding to 1% of fuel pins with gas leaks in the sheathes. When 95% power was reached in February 1981, the contents of these radionuclides increased by

Translated from Atomnaya Énergiya, Vol. 53, No. 6, pp. 373-375, December, 1982. Original article submitted June 16, 1982.

0038-531X/82/5306-0825$07.50

TABLE 1. Design Contents at 100% Reactor Power and Actual Contents of Some Fission and Corrosion Products in the Coolant and Deposits in the VVÉR-100

Radionuclide	Coolant, kBq/liter				Deposits in loop and contribution to dose rate	
		date of measurement, reactor power, %				
	theory	21.07.80, 57	11.09.80, 49	07.04.81, 95	kBq/cm^2	%
^{133}Xe	$5,2\cdot10^5$	7,0	122,1	1295	—	—
^{135}Xe	$4,4\cdot10^5$	1,8	222,0	1295	—	—
^{85m}Kr	$6,6\cdot10^3$	2,4	41,0	410	—	—
^{88}Kr	$5,2\cdot10^4$	3,7	55,5	610	—	—
^{3}H	$5,2\cdot10^3$	—	—	3,2+3	—	—
^{131}I	$18,8\cdot10^3$	5,2	444	740	0,0	0,0
^{133}I	$4,8\cdot10^5$	14,0	$1,9\cdot10^3$	$1,0\cdot10^3$	0,0	0,0
^{135}I	$22,2\cdot10^4$	8,1	925	$1,3\cdot10^3$	0,0	0,0
^{60}Co	10,0	—	—	0,18	19,0	17,6
^{58}Co	9,2	0,09	0,9	1,1	151,7	62,5
^{54}Mn	13,3	—	—	1,1	37,5	13,0
^{59}Fe	1,48	—	—	0,74	6,8	3,1
^{41}Ar	—	9,6	555	$1,6\cdot10^3$	—	—
Total	$1,0\cdot10^5$ (gases) $1,8\cdot10^4$ (^{131}I)	14,9 (gases) 5,2 (^{131}I)	440,6 (gases) 444 (^{131}I)	$3,6\cdot10^3$ (gases) 740 (^{131}I)	315,0	96,2

Notes: 1. 1 kBq = (1/3.7) · 10^{-7} Ci. 2. The sum value for the gases does not include ^{41}Ar arising from activation. 3. The deposits in the principal circulation pump were measured on the working ring and on the body. 4. There was 3.8% contribution to the dose rate from the deposits due to ^{51}Cr, ^{110m}Ag, ^{95}Zr, ^{124}Sb, ^{134}Cs.

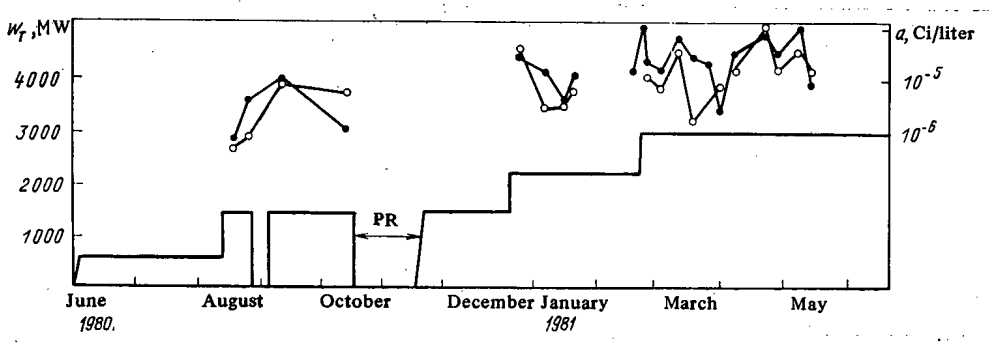

Fig. 1. Graph for the thermal power of the reactor W_T and the specific activity a of ^{131}I (●) and ^{134}I (○) in the coolant (1 Ci = $3.700 \cdot 10^{10}$ Bq)

a substantial factor. Fission products occur in the coolant because of failure of fuel-rod sheathes at 50% power and additional failure after 95%.

The design value of the specific activity was based on the design flow rates of the coolant for purification and outgassing (flushing) together with leakage, along with the purification factors assumed. We give below the design D and actual A values of these flow rates in tons/h:

	D	A
Purification flow rate (SVO-1)	40.0	9.5±2
Outgassing flow rate (flushing) (SVO-2)	27.2	10±2
Organized tapoff	2.5	2.5
Unorganized leaks	0.2	0.08—1.0

The number of leaking rods was determined by the standard method using the ratio of the reference isotpes ^{131},^{134}I in the coolant (Fig. 1) and on the basis of flow data. It was found that the number of leaking (not gas-tight) rods after attaining 50% power was only 20-30, i.e., was 0.04-0.06 of the permissible value. When 100% power was reached, the number of leaking rods stabilized at the 0.16 level, which corresponds to the usual values for Soviet and foreign nuclear power stations [2].

The leakage and specific activity of the coolant affected the gas and aerosol concentrations inside the containment and the rate of release to the atmosphere. In March and April 1981, e.g., the concentrations of radioactive gases were $2.6 \cdot 10^2 - 1.8 \cdot 10^4$ Bq/liter, and ^{131}I $(4.8 - 28.8) \cdot 10^{-3}$ Bq/liter, while the long-lived ($T_{1/2}$ > 3 days) β-active aerosols accounted for 4.5×10^{-4} Bq/liter.

The measured released rates for gases and ^{131}I from the containment to the atmosphere (through the ventilation stack) in this period on average for a month were $(15.5 - 18.8) \cdot 10^{10}$ and 3×10^7 Bq/day, correspondingly. This gas release rate is less than the design value (7.4×10^{12} Bq/day) by a factor 40, and it is less by two orders of magnitude than the permissible value laid down by SPAES-79 as 1.85×10^{13} Bq/day. This very slight release of radioactive gases and ^{131}I occurs because there were only a few leaking rods (0.16 of the permissible value) and also because of the continuous outgassing of the coolant by flushing with a flow rate of 10 tons/h and adsorption of the gases by carbon filters. The specific activity of the gases released in the atmosphere after purification on these filters was not more than 7.5×10^5 Bq/liter, while the release rate was 3.7×10^{10} Bq/day.

During the commissioning operations in 1980, about 11×10^3 m^3 of unbalanced water (on average about 100 m^3/day) was released to check tanks and the drains. The specific activity of this water never exceeded 7.4 Bq/liter, i.e., it was less than the permissible level for drinking water (1.0 Bq/liter). The total activity of the water discarded to the drains was not more than about 1.6×10^8 Bq. This release of unbalanced water virtually ceased after commissioning and runup to nominal power.

During these operations, the collective dose from external γ radiation to the staff, from the time of physical commissioning up to October 21, was about 0.5 man • cSv = 1 rem). On October 21, 1980, the unit was shut down for prophylactic repair (without fuel reloading), which took 25 days, and the collective dose increased by 1.4 man • cSv. The subsequent operation at 75% power increased the dose up to the end of 1980 to 3.1 man • cSv.

On the whole, for 1980, the average individual dose was 0.025 cSv, while the collective dose was 5 man • cSv, or in terms of unit electrical energy produced during the startup period, 0.05 man • cSv/GW • h (0.43 man • cSv/MW • yr).

During the first half of 1981 and the subsequent three months, the unit was operated mainly at nominal power, and the doses to the staff were, correspondingly, 20 and 50 cSv. The average individual dose in this period was not more than 0.35 cSv, while the collective dose was 0.17 man • cSv/MW • yr.

On October 12, 1981, the unit was shut down again for a second prophylactic repair and first fuel change. The collective dose for 1981, including the dose during PR, was about 200 man • cSv or 0.4 man • cSv/MW • yr. These values are half those previously encountered with Soviet nuclear power stations containing the VVÉR-440, and they are virtually equal to the best value attained at the Bruno Leuschner nuclear power station in the German Democratic Republic [3].

The basic design features were thus confirmed during the commissioning and runup, particularly as regards radiation safety of the staff and population near a nuclear power station containing VVÉR-1000 reactors. Further operation of the fifth unit will provide additional data on the radiation environment of a nuclear power station of this type and on the use of standard VVÉR-1000 units.

LITERATURE CITED

1. Yu. V. Vikhorev et al., At. Energ., 50, No. 2, 87 (1981).
2. V. I. Solyanyi and O. A. Nechaeva, At. Tekh. Rubezhom, No. 3, 3 (1981).
3. G. Dichev et al., At. Energ., 50, No. 2, 99 (1981).

A NEW METHOD OF MONITORING RADIOACTIVE AEROSOLS FROM NUCLEAR POWER STATIONS WITH RBMK REACTORS

L. N. Moskvin, G. G. Leont'ev,
S. N. Nekrest'yanov, A. P. Eperin,
V. G. Shcherbina, and A. G. Mokhnachev

UDC 621.039.76

Highly informative methods have been developed for monitoring radioactive aerosols in releases from nuclear power stations, because of the need for quantitative consideration of local radioactive contamination [1]. Existing methods are designed for prolonged or continuous monitoring of the dispersed phase, using filters at each point of release, with subsequent laboratory analysis of the samples.

A new method has been proposed [2] for monitoring radioactive aerosols in the gases from nuclear power stations. It is possible to determine the activity a_{ji} of nuclide i at point j by multiplying the activity in the coolant a_{oi} by the dilution factor R_j, is found from the activity ratio for a base reference nuclide (B reference) at the given point of release and in the coolant in the first loop. When this scheme is realized, the monitoring sensitivity under normal operating conditions is increased by a factor 10^2-10^4, while the analysis times for the individual nuclides are reduced by factors of 10-100.

Here we report some experiments on the use of the new method used with a steady working state in a nuclear power station with RBMK reactors. Figure 1 shows a simplified scheme for the power station and the production of the releases. There are four types of release channel: 1) coolant—steam—air pipe—gas holder—purification filter—release; 2) coolant—air pipe—gas holder—filter—release; 3) coolant—air pipe—filter—release; and 4) coolant—air pipe—release. During the experiments we examined the ratios of the activity of radionuclides in the air in the blower systems to the activities of the same nuclides in the coolant in the multiple forced circulation MFC loop. We also examined the passage of the nuclides through the filters in the release channels 1-3.

The radionuclide activities in the MFC coolant were determined by γ spectrometry and group chromatographic isolation of the radio elements with selective sorbents using the URAN apparatus [3, 4]. The aerosol samples were taken by an aspiration method and used in γ spectrometry. Figure 2 shows the design of the aspiration device and its connection to the sampling line. The columns contained standard AFA-RMP-20 aerosol filters and specific sorbents that remove all forms of iodine, including the organic component [5]. In the first series of experiments, we used two columns in parallel, each of which was filled with a double batch of the iodine sorbent. This showed that the spread of the values about the mean of the two independent determinations was not more than 11%, while the radioiodine that passed through the aerosol filter was collected to over 95% by the first layer of sorbent. In the subsequent experiments we used a single column filled with half the amount of iodine sorbent. The activities of the aerosols were very low (the release rate was well below the maximum permissible value [1]), so the concentration times range from 1 to 50 days. The air flow rates through the filters were monitored with rotameters and were maintained at 10 or 20 liter/min. The relative standard deviation was ±20%. We used a spectrometer based on a TGDK-63A semiconductor detector fitted with a lead shield of thickness 5 cm, together with an LP-4840 multichannel analyzer made by Nokia. The energy resolution of the spectrometer was 6 keV for the 1332 keV line of ^{60}Co. The spectrometry information was processed by a BESM-6 computer using the SIMP program [6].

During these studies, series of experiments were performed on all the ventilation systems representing a radiation hazard and on the stack. Special experiments were performed on the lines containing filters to determine the breakthrough coefficients for the various nuclides. For this purpose, aspiration devices were connected simultaneously to the line before and after the filter cell. In order to obtain reliable values, the radionuclide activities in the

Translated from Atomnaya Énergiya, Vol. 53, No. 6, pp. 376-378, December, 1982. Original article submitted March 1, 1982.

 0038-531X/82/5306-0828$07.50

TABLE 1. Statistical Results for Individual Ventilation Systems

Parameter	B-1	B-2	B-3	B-4	B-5	B-6	B-7	B-8	B-9	B-10	B-11	B-12	Stack
No. of observations for system n_j	7	10	2	1	8	1	1	1	5	1	3	1	3
No. of determinations of R factor from all observations N	45	61	9	5	44	7	5	6	46	11	11	6	15
Weighted mean deviation $\bar{\delta}_j^R$, %	19	23	23	15	25	13	33	21	48	32	22	17	26
Weighted mean value of deviation $\bar{\beta}_j^R$, %	7	16	14	16	12	13	—	—	21	13	27	08	13

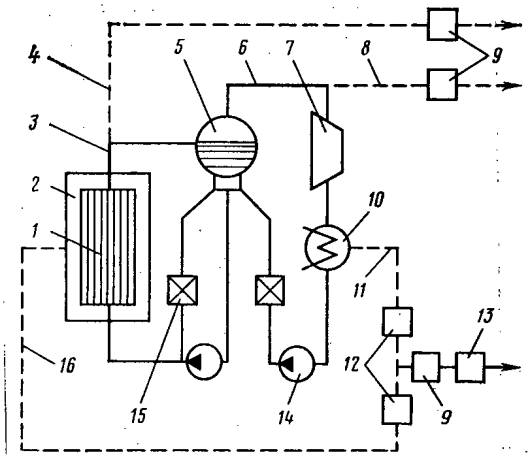

Fig. 1. Simplified hydraulic scheme for the RBMK and radionuclide release channels from spaces around the reactor linked to the coolant loop: 1) core; 2) reactor space; 3) multiple forced circulation MFC loop; 4) release channel from MFC loop spaces; 5) separator drum; 6) steam tract; 7) turbine; 8) release channel from spaces containing steam pipes; 9) aerosol filters; 10) turbine condenser; 11) ejector release; 12) delay gas holders; 13) carbon filters; 14) pumps; 15) water filters; 16) extraction from reactor space.

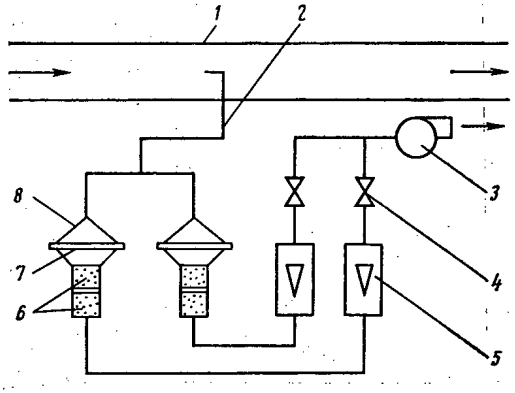

Fig. 2. Scheme for sampling aerosols from air pipes: 1) air pipe; 2) sampling tube; 3) blower; 4) valve; 5) rotameter; 6) sorbents for removing other forms of iodine; 7) AFA-RMP-20 aerosol filter; 8) column.

coolant were determined not less than three times during the aerosol concentration period.

To estimate the spread in the dilution factors $R_{ji} = a_{ji}/a_{oi}$ for the various nuclides, the data were processed for each ventilation system. We calculated the relative standard deviations of the R factors δ_l^R [7], then the values of the δ_l^R were averaged over the series of ex-

TABLE 2. Statistical Results for All Ventilation Systems

Parameter	For nuclide i		For B reference	
	$(\bar{\delta}\pm S_{\bar{\delta}})$, relative	Confidence range for $\mathcal{P}=0,95$	$(\bar{\beta}\pm S_{\bar{\beta}})$, relative	Confidence range for $\mathcal{P}=0,95$
R-factor	0,27±0,02	(0,23; 0,30)	0,15±0,02	(0,12; 0,18)
K_{br}	0,32±0,02	(0,28; 0,37)	0,34±0,08	(0,13; 0,56)

periments performed with the same accuracy but with different numbers of determinations. Then the values for the δ_l^R can be taken as the numbers of determination of the R factor in experiment m_l, which gives the weighted mean deviation for ventilation system j:

$$\bar{\delta}_j^R = \frac{1}{N}\sum_{l=1}^{n_j} m_l \delta_l^R, \tag{1}$$

where $N = \sum_{l=1}^{n_j} m_l$ is the number of determinations of R in all the experiments and n_j is the number of experiments for ventilation system j. Similarly, we calculated the weighted mean relative deviation in the dilution factor from the B reference (^{24}Na [2]) relative to the arithmetic mean:

$$\bar{\beta}_j^R = \frac{1}{N}\sum_{l=1}^{n_j} m_l \beta_l^R, \tag{2}$$

where

$$\beta_l^R = \frac{|R_l^B - \bar{R}_l|}{\bar{R}_l}.$$

The results (Table 1) indicate that the values of $\bar{\delta}_j^R$ for all 12 ventilation systems and the stack are small (from 13 to 33%), apart from one branch, where the spread was 48%. The weighted mean values $\bar{\beta}_j^R$ for the dilution factor for the B reference were less in value (from 7 to 21%). The data from systems B-1, B-2, and B-5 are more reliable, where the activities were higher and the numbers of experiments were larger. For these systems $\bar{\delta}_j^R$ = 19-25%, while $\bar{\beta}_j^R$ = 7-16%.

The complete set of data was used in calculating the weighted mean deviations $\bar{\delta}^R$, $\bar{\beta}^R$, the standard deviations in the determining these $S_{\bar{\delta}}$, $S_{\bar{\beta}}$, and the confidence bounds for the true value. It was assumed that the measurements contained only random errors. Student's t distribution [7] was used to define the confidence range for measurements differing in accuracy. Table 2 gives the results, as well as the data from statistical processing, for the breakthrough coefficients for the various nuclides:

$$K_{br,i} = a_i^{\varepsilon}/a_i,$$

where a_i, a_i^{ε}, are the specific activities of nuclide i before and after the filter.

The number of radionuclides for which K_{br} could be calculated varied from 4 to 17 in accordance with the working conditions, the performance of the filter, and the power-station mode. The values of K_{br} for the sum of the aerosol and gas forms of iodine were higher by about an order of magnitude than those for other nuclides; K_{br} for the aerosol component of the iodine was close to the average. The relative standard deviations of the K_{br} for the individual radionuclides constituted from 0.22 to 0.36 and were due mainly to errors in measuring the activity in the air after the filters. The range in the relative deviations with respect to the base reference was 0.03-0.51 in modulus. The weighted means $\bar{\delta}^K$, $\bar{\beta}^K$, the standard deviations, and the confidence ranges were calculated via a scheme analogous to that used for the R factors.

Activity ratios were found for the MFC coolant and the air in the ventilation system for the various release channels, which differed in volume of the spaces around the reactors, the amount of equipment in them, and the length of the air pipes. The values of the effective coolant leaks range from 0.3 to 30 kg/h. Under these conditions, the standard deviations of the R factors for the individual nuclides were 23-30% of the mean with $\mathcal{P} = 0.95$ probability. In 1.5 years of examination, there was only one case of a marked shift in the balance for certain long-lived nuclides in the aerosol samples by comparison with the coolant, which was due to brief repair operations, which as a rule are usually known in advance. The effects of these can be allowed for. The data indicate that the radionuclides are sorbed on aerosol particles when the coolant evaporates and lose their chemical individuality (an exception is represented by volatile nuclides, in particular iodine). The trends in aerosol passage through the filters correspond to this mechanism. During the experiments we observed no systematic deviation of the breakthrough coefficients for any radionuclide present in aerosol form. The relative mean-square deviation in the breakthrough coefficients about the mean was 28-37% for $\mathcal{P} = 0.95$ probability.

These data confirm that one can organize reference monitoring of radionuclides in aerosols from nuclear power stations containing RBMK reactors, because the main source of aerosol activity is the MFC coolant when the station is operating normally, while loss of part of the aerosol in the air pipes and samplers does not alter the ratios between the long-lived nuclides found in the coolant. The methods used in this monitoring are simple and involve analyzing the radionuclide composition of the coolant, together with the determination of the dilution factors for one nuclide that is readily identifiable at the exit points, so it is possible to set up automatic on-line monitoring systems for the passage of radionuclides to the environment.

We are indebted to V. A. Mel'nikov, V. S. Miroshnikov, E. V. Sosnovskaya, and V. V. Chetverikov for assistance in developing the methods and to G. N. Morozov and S. K. Kaputin for assistance in the experiments.

LITERATURE CITED

1. L. A. Buldakov et al., in: Radiation Safety in Nuclear Power [in Russian], Atomizdat, Moscow (1981), p. 34.
2. L. N. Moskvin, G. G. Leont'ev, and S. N. Nekrest'yanov, At. Energ., 51, No. 4, 232 (1981).
3. L. N. Moskvin et al., ibid., 35, No. 2, 83 (1973).
4. L. N. Moskvin et al., Byull. Izobret., No. 47, 225 (1978).
5. L. N. Moskvin et al., At. Energ., 47, No. 5, 303 (1979).
6. S. R. Avramov, E. V. Sosnovskaya, and V. M. Tsupko-Sitnikov, Preprint P10-9741, JINR, Dubna (1976).
7. L. Z. Rumshinskii, Mathematical Processing of Experimental Results [in Russian], Nauka, Moscow (1971).

GAS DESORPTION DURING IRRADIATION OF METALS WITH MOLYBDENUM IONS

N. P. Katrich and V. N. Kanishchev

UDC 548:539.12.04

Investigations of the mechanism of gassing during bombardment of a solid with accelerated ions make a contribution to the understanding of processes associated with the formation of radiation defects, and extend our knowledge of gas–solid systems. The practical value of these investigations is obvious, if only in relation to the first wall of a thermonuclear reactor, subjected to the action of intense fluxes of fast particles. The quantitative characteristics of desorption under the interaction of light ions with a solid have already been determined [1]. Such investigations with heavy ions, to which the present paper is devoted, have been carried out for the first time.

The experiments were conducted on a setup (Fig. 1) in which, apart from the diffusion pump and the traps, all of the parts of the vacuum system were made of stainless steel and assembled with copper seals. This design allows the apparatus to be heated to 300-400°C for degassing. The main devices used for evacuation are low-temperature titanium pumps 1, 2, 3, 4 installed directly in the chamber of the ion source and in the measuring chamber. This arrangement of the pump, together with prolonged degassing of the chambers, allows a maximum vacuum of $\sim 1.33 \cdot 10^{-8}$ Pa to be achieved in the enclosed volume. In this case the high-vacuum valve 5 is closed and oil vapor from the diffusion pump is completely prevented from entering the operating volume. The hydrogen pumping rate is $\sim 10^4$ and 10^3 liter/sec for the first and second pumps.

In the work described here we used a source that we had developed earlier for producing thermal ions of high-melting-point metals. It constitutes an axial Pierce gun. The distance between the focusing electrode 6 and the extracting electrode 7 of the gun is 30 mm. The diameter of the holes in both electrodes is 10 mm. The ion emitter 8 of diameter 8-9 mm and length up to 15 mm is mounted in a molybdenum holder 9 so that it can be moved vertically by an electrically insulated push-rod 10. The emitter is heated by the spot of ribbon electron beams formed by an axial electron gun in a plane perpendicular to the emitter axis. The cathode slits of the focusing electrode 11 of the electron gun are arranged on a 110 mm circle. The power supply to the emitter can be adjusted by varying both the potential difference (up to 15 kV) that accelerates the electrons and the electron-beam current (up to 1 A). A detailed description of the ion source was given in [2].

The axially symmetric ion beam formed by the gun passes through a single electrostatic lens 12 and enters a drift chamber that connects the chamber of the source and the measuring chamber. At the exit of the drift tube is an 8-mm-diameter limiting diaphragm, and behind it are the plates of the capacitor 14, whose electric field deflects the ion beam 3° from the axis of formation. The vacuum conductivity of the drift tube, determined by the conductivity of the apertures in the diaphragm holder, is calculated for hydrogen (170 liters/sec). Through a 3.5-mm-diameter diaphragm and a 4 mm calibrated aperture in the bottom of the chamber 15, the ions reach the target 16, which is pressed to a copper holder by a disk. The holder is connected to a tube, through which it can be cooled during the experiment. The emitter-target distance is ~ 650 mm.

The investigations were carried out as follows: The ion source is made of single-crystal molybdenum. The target, 10 mm in diameter and 2 mm thick, was cut from a massive metal single crystal, and then ground mechanically, polished chemically, and washed in alcohol. Once the apparatus had been pumped down to a vacuum of $\sim 1.33 \cdot 10^{-3}$ Pa, a furnace (not shown in Fig. 1) was switched on to heat the apparatus. Heating for the purpose of degassing was continued for 4 h with the chamber walls at 300°C. After this the small tank 1 of the low-temperature titanium pump, including the titanium-sputtering device 2 of this pump, was filled with liquid nitrogen.

The ion emitter was heated by an electron beam to the operating temperature, an indicator

Translated from Atomnaya Énergiya, Vol. 53, No. 6, pp. 379-382, December, 1982. Original article submitted February 5, 1982.

 0038-531X/82/5306-0832$07.50

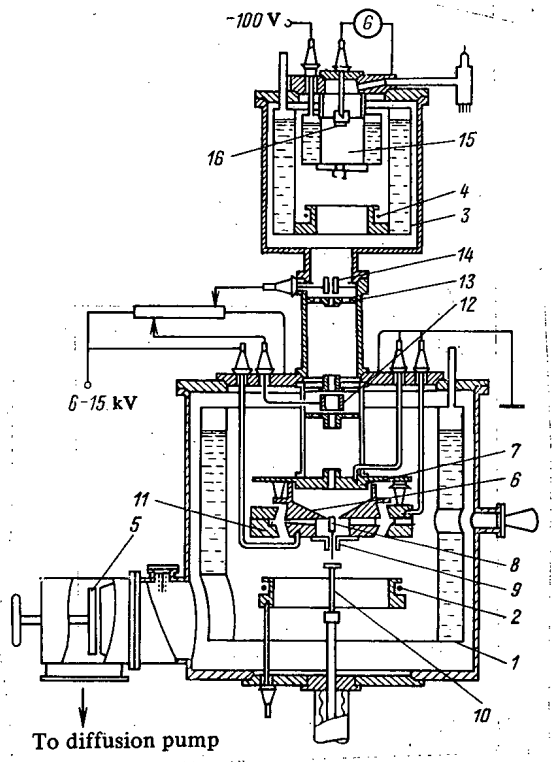

Fig. 1. Experimental setup.

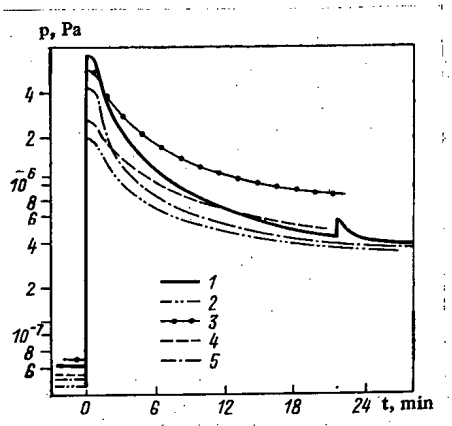

Fig. 2. Partial pressure p vs time; t = 0 at beginning of target bombardment with ions; 1,2) desorption of nitrogen and hydrogen from niobium at 78°K; 3,4) desorption of nitrogen and hydrogen from niobium at 293°K; 5) desorption of hydrogen from copper at 293°K.

of which was the ion current falling on the electrically insulated target chamber. When the vacuum in the chamber of the source reached $\sim 1.33 \cdot 10^{-5}$ Pa, liquid nitrogen was poured into the small tank and the titanium-sputtering device 4 was switched on. Titanium was sputtered in the source chamber continuously throughout the experiment, while in the measuring chamber it was sufficient to have several three-minute sputterings until the onset of ion bombardment of the target. At a pressure of $\sim 1.33 \cdot 10^{-7}$ Pa in the measuring chamber, the high-vacuum valve 5 opened and liquid nitrogen filled the tank of the target chamber. The partial gas pressure in chamber 15 was measured with an IPDO-4 instrument with an RMO-4 transducer; this pressure was $\sim 1.33 \cdot 10^{-8}$ Pa prior to the onset of ion bombardment of the target.

In our work we used a beam of 8 keV molybdenum ions with $i^+ = 0.04$ μA ($j^+ = 0.2$ μA $\cdot$ cm^{-2}). Bombardment of the target was started with the application of voltage to the deflecting plates of the capacitor. Gases liberated from the target during and after irradiation under the conditions of dynamic pumping [3] increased the partial pressure in the target chamber. The desorption rate (sec^{-1}) was calculated from the formula

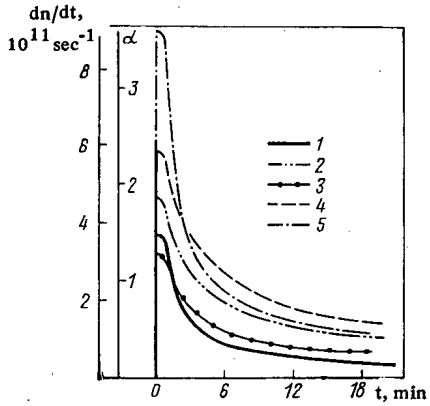

Fig. 3. Desorption rate dn/dt and desorption coefficient α vs time, calculated from the data of Fig. 2.

$$\frac{dn}{dt} = \frac{n_L [p(t) - p_0] w}{10^4}; \quad (1)$$

the desorption coefficient was found from the formula

$$\alpha = \frac{dn}{dt} \frac{q}{i^+}, \quad (2)$$

where n_L is the Loschmidt number; P_o, initial partial gas pressure (Pa); p(t), partial gas pressure at the time t of the measurement; w, rate of evacuation from the target chamber through a calibrated aperture ($2.9 \cdot 10^{-3}$ cm$^3 \cdot$ sec^{-1} for hydrogen at room temperature); i^+, ion beam current (A); and q, ion charge (C).

The results of the measurements of the partial gas pressure in the target chamber during molybdenum-ion bombardment of a niobium single crystal target cooled with liquid nitrogen (T_M = 78°K) and flowing water (T_M = 293°K) are given in Fig. 2. Curves 1 (T_M = 78°K) and 2 (T_M = 293°K) correspond to measurements of the pressure of gas with a mass number of 28; curves 3 and 4 correspond to measurements of hydrogen pressure. By the well-known procedure [4] we identified the gas with mass number 28. Analysis of the relation between the signals from particles with mass numbers 12, 14, and 16 showed that the gas with mass number 28 which is released in the target chamber during bombardment of niobium is primarily nitrogen. Figure 2 also shows how the hydrogen pressure in the target chamber depends on time (curve 5) during bombardment of single-crystal copper (T_M = 293°K) with molybdenum ions. Within the limits of sensitivity, no variations were observed in the nitrogen pressure during bombardment of the copper. Since hydrogen and nitrogen dissolve well in niobium, while nitrogen dissolves much more poorly in niobium than hydrogen does [5], we can conclude that the increase in pressure in the target chamber with the introduction of an ion beam is due to the interaction of the ions with the target; the influence of secondary effects (e.g., gas desorption from the chamber walls owing to scattered ions) on the measurements can be neglected.

The large desorption coefficients (Fig. 3) calculated from the data of the curves in Fig. 2 cannot be explained on the basis of reasonable values of the coefficients of niobium and copper sputtering by molybdenum ions. If the pressure in the target chamber were determined by the effect of sputtering, the desorption curves would have reached saturation. This was not observed to occur at radiation doses of up to $\sim 5 \cdot 10^{15}$ cm^{-2}. Gas liberation from the target cooled to liquid-nitrogen temperature also cannot be explained by ordinary diffusion of substitutional impurities; the activation energy is too high for migration. Gas desorption from the ion-bombarded target can be represented as the diffusion of impurity atoms as part of radiation defect-impurity complexes, with subsequent disintegration of these complexes on the surface of the target [1].

The initial spike on the curves in Fig. 2 can be attributed to the desorption of gas adsorbed on the target surface. The curves for the desorption of nitrogen from niobium cooled to liquid-nitrogen temperature when ion bombardment is resumed after a pause of several minutes (curve 1 in Fig. 4) also begin with a spike, whose amplitude increases with the length of the pause, but with a pause of the same duration the amplitude decreases as the irradiation dose increases. The curves of hydrogen desorption from niobium (T_M = 78°K) with the resumption of bombardment (see Fig. 4, curve 2) do not have such a singularity. Apparently, during the pause nitrogen accumulates on the surface of the niobium target cooled to 78°K, primarily

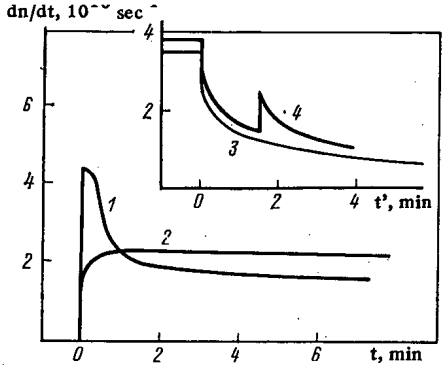

Fig. 4. Rate of desorption of gases from niobium at 78°K vs time after resumption and cessation of ion bombardment; t = 0 at beginning of ion-beam bombardment of target (1, 2); t' = 0 when the beam is removed from the target (3, 4); 1, 3, 4) nitrogen desorption; 2) hydrogen desorption.

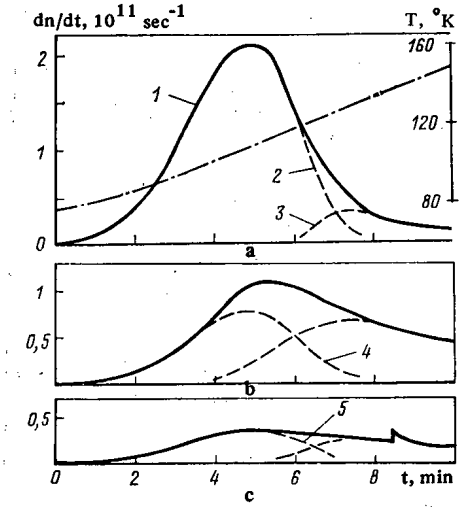

Fig. 5. Rate of desorption of nitrogen from niobium vs time with annealing for irradiation doses of: a) 10^{14}, b) $2 \cdot 10^{14}$, and c) $4 \cdot 10^{14}$ cm^{-2}; ——— · ——— · ———) target temperature T vs time; ———) experiment; - - - -) calculation.

because of diffusion from the bulk, while under such conditions hydrogen does not remain on the target surface. The spike on the hydrogen desorption curves (see Fig. 2, curves 2, 4) can be explained in part by the adsorption, on the target surface, of hydrocarbons which cannot form on the ion-purified target surface in a high vacuum ($1.33 \cdot 10^{-9}$ Pa). With the onset of irradiation, the total pressure of hydrocarbons in the target chamber increases substantially because of desorption from the target surface, which is in accord with the data of [6]. Evidently, the presence of adsorbed gas on the target surface affects the gradient of hydrogen concentration in the surface layer of the target, and in the final account the hydrogen desorption rate dn/dt may depend on this.

Proof of the stability of the radiation defect-impurity complexes can be provided by the curves of spontaneous isothermal gas desorption (after cessation of bombardment of the target with an ion beam). With the cessation of the ion bombardment, the pressure in the target chamber approaches the background pressure (P_0) in only a few minutes, while the characteristic pumpdown time for the given conditions is ~ 0.1 sec. Figure 4 shows the time dependence of the spontaneous desorption of nitrogen (curve 3) from niobium at $T_M = 78°K$. The character of the spontaneous desorption of hydrogen from niobium, as well as from copper, is similar. For roughly 100 sec after the ion beam is switched off, the desorption curves have the shape of a simple exponential.

The curves of thermally activated desorption of gases from a target previously bombarded with molybdenum ions can serve as proof of the stability of various complexes of radiation defects with impurity atoms. Figure 5 shows the desorption of nitrogen from niobium when the target is heated from 78 to 293°K after different doses of irradiation. The bombardment-heating cycles were carried out on one and the same target in succession. In the first cycle the dose was 10^{14} cm^{-2} (Fig. 5a), and in the second and third it was $2 \cdot 10^{14}$ and $4 \cdot 10^{14}$ cm^{-2} (Figs. 5b, c). Up to T $\approx$ 120°K curve 1 (see Fig. 5a) is approximated well by

$$dn/dt = K_0 (N - n) \exp\{-E/kT\}, \tag{3}$$

which is obtained from the kinetic equation, familiar from defect annealing theory, for a first-order reaction [7]; to do this, the number of defects of migration activation energy E which remain in the specimen by the time t is replaced by the difference N − n, where N is the initial number of these defects and n is the number of defects which have already reached the surface. The number of defects already at the surface, equal to $\int_0^t \frac{\partial n}{\partial \vartheta} d\vartheta$, was calculated by graphical integration. By the method of least squares we obtained K_0 = (400 ± 40) sec^{-1}, N = (43.0 ± 0.6)·10^{12}, and E = (0.097 ± 0.001) eV. From the values of dn/dt, found from the formula above by numerical integration, we constructed curve 2, Fig. 5a. It is natural to attribute $\int_0^\infty \frac{\partial n}{\partial \vartheta} d\vartheta - N \approx 8 \cdot 10^{12}$ to sucessive portions of thermally activated liberated gas (see Fig. 5a, curve 3). Curves 4 (Fig. 5b) and 5 (Fig. 5c) were constructed from the data of curve 2 (Fig. 5a), decreased in amplitude by a factor equal to the ratio of the maximum dn/dt values on these curves. It is seen from Fig. 5 that as the irradiation dose increases, the distribution of the intensity of successive portions of gas decreases.

Diffusion of radiation defect-impurity complexes should lead to gas filling the cavities of diverse origin which are present in the specimen. When certain conditions are attained, cavities near the surface can open. This most likely is responsible for single pulses of gas pressure in the target chamber, both during the bombardment (see Fig. 2, curve 1) and for some time after it (see Fig. 4, curve 4), as well as during annealing (see Fig. 5c). It must be pointed out that in the case of niobium such pulses have been observed only for mass 28 and only when the irradiation temperature was 78°K. From the ideas about the formation of mobile complexes incorporating impurity atoms, it follows that any irradiation involving the formation of mobile defects in a solid leads to the redistribution of impurities in the solid and, in particular, to gas filling the cavities which exist in the solid.

LITERATURE CITED

1. N. P. Kartich and N. S. Sidel'nikova, in: Production and Properties of Single Crystals and Scintillators [in Russian], No. 3, VNIImonokristallov (All-Union Scientific-Research Institute of Single Crystals), Kharkov (1979), No. 3, p. 68.
2. N. P. Kartich and V. N. Kanishchev, Prib. Tekh. Eksp., No. 5, 176 (1980).
3. E. S. Borovik, N. P. Kartich, and G. T. Nikoleav, At. Energ., 18, No. 2, 91 (1965).
4. N. P. Kartich and N. M. Lifshitz, in: Single Crystals and Engineering [in Russian], No. 12, Izd. VNIImonokristallov (All-Union Scientific-Research Institute of Single Crystals), Kharkov (1975), p. 32.
5. S. Dushman and J. M. Lafferty, Scientific Foundation of Vacuum Technique, 2nd ed., Wiley New York (1962).
6. N. P. Kartich and G. T. Adonkin, in: Methods of obtaining and Studying Single Crystals and Scintillators [in Russian], No. 5, Izd. VNIImonokristallov, (All-Union Scientific-Research Institute of Single Crystals), Kharkov (1980), p. 49.
7. A. C. Damask and G. J. Dienes, Point Defects in Metals, Gordan and Breach (1964).

SIMULATION OF REACTOR CONDITIONS IN INVESTIGATIONS OF RADIATION DAMAGE OF THE SURFACE OF MATERIALS

B. A. Kalin

UDC 621.039.531

The study of radiation damage of a surface under bombardment with light ions is of interest for estimation of the durability of materials in fusion reactors and, as a rule, is based on models [1-3]. To a certain degree this is justified by the fact that hitherto the exact spectra of plasma radiation, the mechanical loads and stressed state of the structural elements of discharge chambers, and the corrosion reaction with coolants have not been known. Moreover, a large number of reactor projects exist, the most advanced being the INTOR project.

In this situation, it is very important to investigate radiation damage under conditions simulating the conditions under which materials will operate in future fusion reactors. In order to simulate the effect of the expected integrated energy spectrum, e.g., materials have been bombarded successively with monoenergetic helium-ion beams of various energies. In this case it has been shown [4-7] that with the same total dose of implanted helium, blistering and erosion turned out to be less than under bombardment with a helium beam of the same energy.

For an assessment of the influence of synergism on radiation surface damage, experiments on the successive and simultaneous bombardment of materials with helium and hydrogen (deuterium) ions are of certain interest. Successive bombardment of steel at room temperature with 20 keV helium and hydrogen ions to dose of 10^{22} and $5 \cdot 10^{21}$ ions/m^2, respectively, resulted in a lowering of the temperature at which hydrogen liberation begins when the target is heated as compared with the case of bombardment with only hydrogen ions [8]. The blistering parameters in the case of successive bombardment at room temperature practically did not differ from those observed in the case of helium bombardment, but after annealing the blister density was twice as high [9]. It has also been established [10] that implantation of 20-keV deuterium to a dose of $6 \cdot 10^{22}$ ions/m^2 prior to implantation of 40-keV helium ions to a dose of $1 \cdot 10^{22}$ ions/m^2 led to a decrease in the diameter of the blisters and an increase in their density, as well as to a reduction of the rate of radiation damage in comparison with that observed for bombardment with only helium ions. Simultaneous bombardment with helium and hydrogen ions, however, intensifies the erosion, causing flaking of three layers of material with the erosion coefficient reaching 2.2 atoms/ion [10]. These results indicate that in studying the action of plasma on the material of the first wall one must take synergism effects into account.

In investigations of the influence of external stresses on blistering and erosion of materials [11, 12], it has been established that external stresses increase the critical dose or even suppress the formation of blisters, and are conducive to an intensification of erosion through flaking, with the critical dose for exfoliation growing under the influence of both tensile and compressive stresses. Experiments at fixed ion-incidence angles [13-17] revealed that the incidence angle of the ions has a substantial influence on blistering and erosion of a material.

In the light of available information, it seemed appropriate to investigate the radiation damage of a number of promising structural materials under bombardment with monoenergetic beams of 15 and 20 keV helium ions, taking account of the effect of some other factors: the continuous cyclical variation of the incidence angle of the ions, the mechanical load, previous testing for creep in lithium, and prior neutron irradiation. It must be pointed out that the use of monoenergetic one-component ion beams makes it possible to obtain the most exact values of the coefficients of erosion, and leads to more serious surface damage than does bombardment with nonmonoenergetic ion beams [18].

Influence of the Ion-Incidence Angle. In order to study the effect that the incidence angle of ions has on radiation erosion, the target was rotated continuously [19], thus to a

Translated from Atomnaya Energiya, Vol. 53, No. 6, pp. 382-386, December, 1982. Original article submitted June 3, 1981.

0038-531X/82/5306-0837$07.50

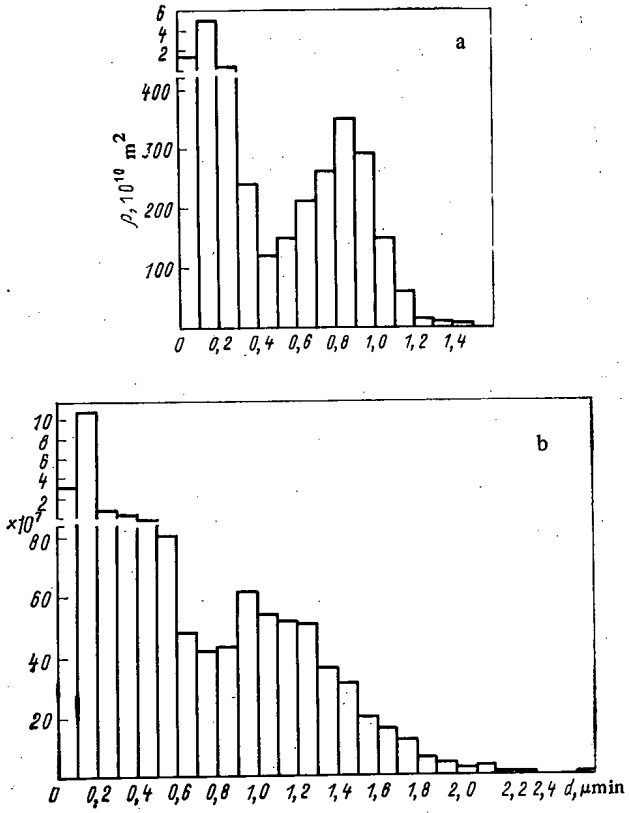

Fig. 1. Histograms of the size distribution of blisters on the surface of molybdenum for rotating (a) and stationary (b) targets.

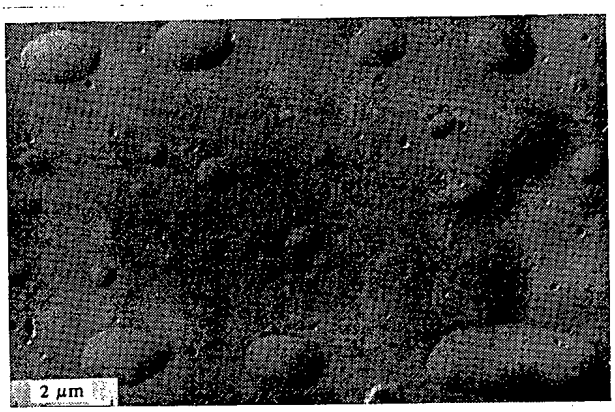

Fig. 2. Electron-microscopic photograph of surface of TsM-6 alloy after bombardment with 20 keV helium ions to a dose of $5 \cdot 10^{21}$ ions/m^2 with a tensile stress of 400 MPa.

certain degree simulating cylindrical bombardment of materials with a nonmonoemergetic ion beam. Electron-microscopic examination of molybdenum and vanadium specimens revealed that the blister parameters and erosion coefficients differ from those obtained for a stationary target bombarded with 20 keV helium ions to a dose of $2 \cdot 10^{22}$ ions/m^2 (Fig. 1). In the case of rotating targets, the size of large blisters decreases, the density of small blisters decreases, and the density of blisters with a size of $(3\text{-}13) \cdot 10^2$ nm grows. As a result, the fraction of the surface occupied by blisters rises from 68 to 95%, while the number of blisters of maximum size drops. Similar changes, observed by other investigators as well [14, 17], are clearly due to the fact that in the rotating target the implanted helium ions are arranged closer to the surface and the distribution becomes more symmetric. This is also confirmed by the data of [19] on the reduction of the thickness of blister lids, which, together with the decrease in the blister size, leads to a lowering of the erosion coefficients of molybdenum and vanadium.

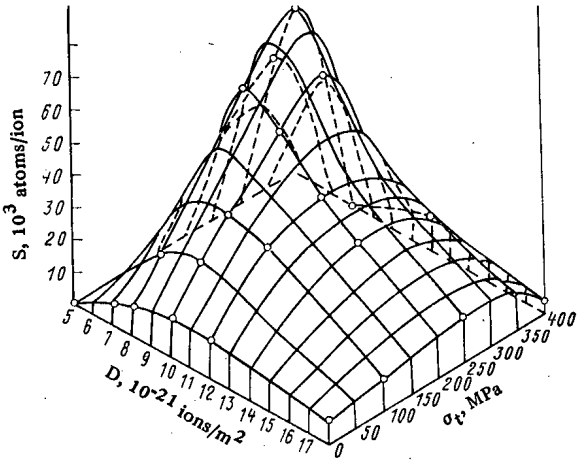

Fig. 3. Diagram of dependence of the radiation erosion S on the dose and the tensile stress.

Since fusion reactors will be characterized by a broad spectrum of angles of ion incidence on the wall and by the cyclical (quasistationary) nature of the bombardment, the results obtained are extremely important for the development of methods to combat radiation erosion.

Influence of Mechanical Stresses. The influence of tensile loads of up to 500 MPa on blistering and radiation erosion of molybdenum alloys has been investigated in the case of bombardment at room temperature with 20 keV helium ions to a dose of $4 \cdot 10^{21}$–$6 \cdot 10^{22}$ ions/m^2. It has been established [20] that processes of blistering and exfoliation of materials depends on the level of stresses and the dose of implanted helium ions. At low doses [$(2\text{-}4) \cdot 10^{21}$ ions/m^2] and external stresses below the yield point ($\sigma_{0.2} \approx 360$ MPa), the blisters decrease somewhat in size, which indicates a delay in the blistering process, as noted earlier [11]. At a dose of about $5 \cdot 10^{21}$ ions/m^2 and a stress of 400 MPa, a stitch-like arrangement of blisters is observed, with an increasing fraction of large ellipsoidal blisters whose major axis coincides with direction of tension (Fig. 2). This occurrence of large blisters creates conditions for an undesirable growth of the erosion coefficient during further bombardment with helium ions. At a dose of $8 \cdot 10^{21}$ ions/m^2, the erosion coefficient increases as the stress grows to 300 MPa and then falls off sharply with the onset of plastic strain (approximately 400 MPa). The general dependence of the radiation erosion on the uniaxial tensile stress and the dose of the implanted helium can be represented in the form of a three-dimensional diagram (Fig. 3). An exact estimate of the stressed state of the material is thus necessary for predicting the durability of the first wall of a fusion reactor and the level of impurities in the plasma.

Influence of Creep Strain. The radiation erosion of the alloy Nb + 1% Zr + 0.1% C in the case of bombardment with 15 keV helium ions at room temperature to a dose of 10^{22} ions/m^2 was measured after prior testing for creep in lithium at 1373-1418°K and a stress of 50-100 MPa [21]. Electron-microscopic examination showed that alloys tested in lithium possess an increased tendency toward radiation erosion. According to estimates, the sputtering coefficient is close to $(2\text{-}4) \cdot 10^{-2}$ atom/ion, i.e., reaches maximum value [22]. Because of sputtering, the relief of grains is revealed and craters of 20-30 nm are formed. The largest number of craters ($5 \cdot 10^{13}$ m^{-2}) was detected in specimens kept in lithium for a long time and coincides with the surface concentration of dislocations in deformed solids. As is known, when niobium alloys are held at a high temperature under stress, a developed network of dislocations surrounded by finely divided (up to 20 nm) precipitates of the carbide phase forms [23], with the sites at which dislocations emerge on the surface being liable to intense sputtering under ion bombardment. Thus, as pertains to fusion reactors, mechanical loads and corrosion activity on the structural materials may lead to an intensification of radiation erosion.

Influence of Neutron Irradiation. As is known, neutron irradiation has a substantial effect on the mechanical properties and durability of fusion-reactor materials; it has also been suggested [14] that it reduces blistering of the first wall. In order to study the effect that prior neutron irradiation has on blistering and exfoliation, specimens of OKh16N15M3B steel were irradiated at 520-570°K in an unsteady neutron flux of $1.5 \cdot 10^{19}$ neutrons/cm^2 • sec. The fluence of thermal neutrons was $2.21 \cdot 10^{22}$ neutrons/m^2 and that of fast neutrons ($E > 0.1$ MeV) was $6 \cdot 10^{20}$ neutrons/m^2. The irradiated specimens were bombarded with 20 keV helium ions

TABLE 1. Erosion Coefficient of Steel, Atoms/Ion

Steel specimens	Dose of implanted helium, 10^{21} ions/m^2									
	1	2	3	4	5	6	7	8	9	10
Initial	0	Blistering	Onset of exfoliation	$(12\pm3)\cdot10^{-2}$	$(24\pm6)\cdot10^{-2}$	$(37\pm9)\cdot10^{-2}$	$(47\pm12)\cdot10^{-2}$	$(54\pm14)\cdot10^{-2}$	$(57\pm14)\cdot10^{-2}$	$(56\pm14)\cdot10^{-2}$
After neutron irradiation	0	0	Blistering	Onset of exfoliation	$(10\pm3)\cdot10^{-3}$	$(15\pm4)\cdot10^{-3}$	$(20\pm5)\cdot10^{-3}$	$(60\pm15)\cdot10^{-3}$	$(19\pm5)\cdot10^{-2}$	$(37\pm9)\cdot10^{-2}$

to a dose of 10^{21}–10^{22} ions/m^2. Electron-microscopic examination of the surface of OKh16N15M-3B steel specimens after bombardment revealed an increase in the critical doses for blistering and exfoliation of the surface; the maximum of the radiation erosion of the steel shifted in similar fashion (see Table 1). In all of the experiments prior neutron irradiation suppressed exfoliation of the steel.

A short anneal (1173°K, 15 min) of the neutron-irradiated specimens before the ion bombardment practically eliminated the restraining effect of the neutron irradiation. Thus, at a dose of $6.5 \cdot 10^{21}$ ions/m^2 the radiation erosion of the initial specimens and specimens annealed after neutron irradiation proved to be the same ($\sim$ 0.45 atoms/ion). This permits the assumption that the suppression of blistering and exfoliation of the steel is due to radiation point defects that are effective traps for helium atoms. Moreover, an excess of point defects in the initial stage of ion bombardment can promote radiation creep and, therefore, relaxation of internal stresses, thus intensifying the blistering process [25]. The suppression of blistering and exfoliation of steel under the influence of neutron irradiation is extremely important for demonstration and experimental fusion reactors of the first generation, in which the neutron load on the first wall be fairly small, while the wall temperature will be high.

The results presented above indicate the need to continue investigations of tensile and compressive loads as well as of prior irradiation of materials with neutrons, to study the effects of synergism in the bombardment of materials with light ions over wide ranges of energy, temperature, and dose, and initials investigations of the influence of other factors, particularly thermocyclical heating with constant and cyclical loads, prior bombardment of materials with charged particles, etc.

LITERATURE CITED

1. M. Das and M. Kaminski, Radiat. Effects on Solid Surfaces, Adv. in Chemistry, No. 158, 112 (1976).
2. B. A. Kalin, D. M. Skorov, and V. L. Yakushin, Problems of Atomic Science and Engineering. Series "Physics of Radiation Damage and Radiation Materials Science" [in Russian], No. 2 (13), 72 (1980).
3. M. I. Guseva and Yu. V. Martynenko, Usp. Fiz. Nauk, 135, No. 4, 671 (1981).
4. M. I. Guseva et al., J. Nucl. Mater., 85-86, part B, 1111 (1979).
5. M. I. Guseva et al., J. Nucl. Mater., 63, No. 1, 245 (1976).
6. S. K. Das et al., in: Proceedings of All-Union Conference on Engineering Problems of Thermonuclear Reactors [in Russian], Vol. 3, NIIEFA, Leningrad (1977), p. 256.
7. S. K. Das et al., Fiz. Khim. Obrab. Mater., No. 4, 94 (1977).
8. D. M. Skorov et al., Problems of Atomic Science and Engineering. Series "Physics of Radiation Damage and Radiation Materials Science" [in Russian], No. 1 (6), 46 (1978).
9. A. D. Gurov et al., At. Energ., 40, No. 3, 254 (1976).
10. B. G. Vladimirov et al., At. Energ., 50, No. 1, 25 (1981).
11. L. I. Ivanov et al., J. Nucl. Mater., 76-77, No. 1-2, 211 (1978).
12. A. P. Komisarov and N. A. Makhlin, Problems of Atomic Science and Engineering. Series "Physics of Radiation Damage and Radiation Materials Science" [in Russian], No. 3(11), 47 (1979).
13. R. Behrisch et al., in: Proc. 9th symp. on Fusion Technology, Garmisch-Partenkirchen, Pergamon Press, Oxford (1976), p. 531.

14. M. Risch, I. Roth, and B. Scherzer, J. Nucl. Mater., 82, No. 2, 220 (1979).
15. Yu. A. Gribanov et al., Problems of Atomic Science and Engineering. Series "Physics of Radiation Damage and Radiation Materials Science" [in Russian], No. 3(11), 64 (1979).
16. V. V. Gann et al., At. Energ., 48, No. 4, 266 (1980).
17. M. I. Guseva. S. M. Ivanov, and Yu. V. Martynenko, J. Nucl. Mater., 96, 208 (1981).
18. I. Roth, R. Behrisch, and B. Scherzer, J. Nucl. Mater., 57, 365 (1975).
19. B. A. Kalin et al., At. Energ., 49, No. 2, 132 (1980).
20. B. A. Kalin et al., in: Proc. Sixth All-Union Conf. "Interaction of Atomic Particles with Solids" [in Russian], Vol. 2, Minsk. Radiotekh., Minsk (1981), p. 146.
21. B. A. Kalin, D. M. Skorov, and G. N. Shishkin, in: Investigation and Development of Fusion Reactor Materials [in Russian], Nauka, Moscow (1981), p. 128.
22. M. I. Guseva and Yu. V. Martynenko, J. Nucl. Mater., 63, 241 (1976).
23. G. G. Maksimovich et al., Probl. Prochn., No. 3, 111 (1978).
24. W. Wolfer and F. Garner, J. Nucl. Mater., 85-86, 583 (1979).
25. M. Risch, I. Roth, and B. Scherzer, in: Proc. Int. Symp. on Plasma Wall Interaction, Pergamon Press, Oxford (1977), p. 391.

ANALYSIS AND ESTIMATE OF NEUTRON CROSS SECTIONS OF CURIUM ISOTOPES

T. S. Belanova

UDC 621.039.556

The presence of curium isotopes in power-reactor fuel creates many problems in reactor operation and design, in repeated fuel reprocessing and actinide waste disposal, and also in the production of transuranium elements. A quantitative estimate of the rate of buildup and decay of Cm nuclei requires data on the neutron capture and fission cross sections in both the resonance and thermal energy regions. The measurement of neutron cross sections presents great difficulties because of the small amount of Cm available, its large number of isotopes, and its high radioactivity (up to 90-96% ^{244}Cm is commonly accumulated in reactors, while the enrichment of the other isotopes varies from 1.5 to 10%). These facts are the main cause of the small amount of information available on neutron differential cross sections and their low accuracy. Thus, there are no data on the fission cross section of ^{242}Cm, and limited information on the total cross sections of $^{242,243,245-247}$Cm and the fission cross sections of ^{243,244,246,247}Cm. Such an important quantity as the neutron capture cross section has not been measured for all the Cm isotopes, and probably will not be measured within the next few years. These cross sections can only be estimated from statistical computational models, and this requires systematizing the information on the basic nuclear parameters (level spacing, average radiation width, force function) which can be obtained from data on the transmission of neutrons in the resonance region.

Information on neutron integral cross sections is in a somewhat better state, but here also there are practically no data for ^{242}Cm, and only isolated measurements have been performed with ^{243}Cm.

In the present article we attempt to systematize the published experimental data on neutron cross sections for Cm isotopes, and to estimate values at thermal and resonance energies.

Summary of Data on Differential and Integral Measurements of Cross Sections. Papers on differential measurements of neutron total cross sections σ_t, fission cross sections σ_f, and capture cross sections σ_c are listed in Table 1. This table includes the characteristics of the spectrometers used and the samples investigated, and indicates the accuracy of the measurements of the cross sections, neutron width Γ_n, radiation width Γ_γ, fission width Γ_f, and total width Γ. Since the accuracy of Γ_n, Γ_γ, and Γ_f varies from resonance to resonance, Table 1 lists the error limits of these values.

The difficulties of measuring σ_f are related mainly to the problem of detection. All Cm isotopes have a high background of alpha radiation. The even isotopes have a high level of radioactivity accompanying spontaneous fission, and this is difficult to separate in recording induced fission of the nuclei. In addition, σ_f for the even Cm isotopes is small (5-10%

Translated from Atomnaya Énergiya Vol. 53, No. 6, pp. 386-391, December, 1982. Original article submitted April 21, 1982.

0038-531X/82/5306-0841$07.50

TABLE 1. Cumulative Information of Differential Cross Sections.

Reaction cross section	Cm isotope	Max. enrichment	Sample thickness, 10^{20} nuclei/cm^2	Neutron source	Resolution of method, nsec/m	Energy range, eV	Accuracy of data, %	Reference
σ_t	244 246	96,5 21,5	22,4 0,74	Chopper ANL	55 55	0,01—275 0,01—20	$\Gamma = 15$, $\Gamma_n = 10$—25 $\Gamma_n = 40$	[1]
σ_t	243 244 245 246	1,51 93,84 4,04 3,94	2,80 177 7,59 7,43	Chopper MTR	147—280	0,01—26 0,01—90 0,01—30 0,01—20	Γ_n, $\Gamma = 15$—30 $\Gamma_n = 10$—20 Γ_n, $\Gamma = 15$—30 $\Gamma_n = 10$	[2]
σ_t	242 243 244 245 246 248 247	8,7 43,77 83,6 9,57 51,85 6,79 1,61	7,52 16,26 110 25,7 20,6 2,7 0,64	Chopper CM-2	70 70 70 70 70 70 120	1—265 0,4—66 0,1—220 0,5—50 0,1—160 0,1—100 0,5—20	Γ_n, $\Gamma_n = 10$—35 $\Gamma \approx 10$—25, $\Gamma_n = 10$—20 $\Gamma \approx 15$, $\Gamma_n = 10$—20 $\Gamma = 10$—25, $\Gamma_n = 10$—20 $\Gamma \approx 10$, $\Gamma_n = 3$—25 $\Gamma \approx 10$, $\Gamma_n = 3$—15 Γ, $\Gamma_n = 10$—40	[3] [4] [5] [6]
σ_t	244 246 248	82,5 3,11 96,82	8,2 0,51 16,0	Accelerator ORELA	40 40 40	10—530 0,5—160 0,5—2400	Γ, $\Gamma_n = 10$—20 $\Gamma_n = 10$—30 $\Gamma \approx 8$, $\Gamma_n = 3$—15	[7] [8]
σ_f	245 245	99,96 99,96	5,75 * 189 *	Accelerator LLL		0,01—36 10^{-3}—10^4	$\Gamma_f = 10$—25, $\Gamma_n = 5$—20	[9] [10]
σ_f	248 246	96,89 96,89	29,9 * 17,0	Spectrometer RINS		1—10^5	$\sigma_f = 14$—60	[11]
σ_f	243 244 245 246 247 248	89 98,5 76,5 94,7 20,9 89,3	210 * 83,5 * 34,1 * 16,3 * 26,9 * 67,6 *	Nuclear explosion Physics-8	20 20 20 20 20 20	15—80 20—980 20—60 20—400 20—60 20—100	Even isotopes of Cm Γ_n, $\Gamma_f = 10$—60	[12] [13]
σ_c	244	79,2	13,3	Physics-8	20	20—10^4	$\sigma_c \approx 20$	[13]

*Mass of sample, μg

of the absorption cross section). As result of all this, the accuracy of σ_f varies from 10 to 60% [2, 11, 13].

The basic data on the fission of Cm nuclei were obtained in an underground nuclear explosion [12, 13] for microgram amounts of the fissionable material and rather high enrichment of the isotopes being studied. The energy range of resolved resonances in these experiments was 20-80 eV.

The difficulties in measuring σ_t and σ_c are the result of a lack of a sufficient amount of monoisotopic chemically pure curium. This prevents the use of conventional methods of measuring capture cross sections (neutron choppers, accelerators), and in the final analysis is the reason for the lack of information. Only one measurement of σ_c is known in an underground nuclear explosion [13] permitting a determination of the resonance parameters of the ^{244}Cm levels. The great importance of data obtained in nuclear explosions should be noted — for many years they have remained the only source of information on σ_f and σ_c.

Total cross sections have been measured mainly with neutron choppers [1-6] for sample of a mixture of Cm isotopes. In spite of the small percentage content of the $^{242,243,245-248}$Cm isotopes in the samples, their absolute "thickness" turned out to be quite adequate for a measurement of transmission. However, the overlapping of levels complicated their identification and decreased the accuracy of the calculation of the parameters. The resolution of the choppers (Table 1) limited the energy range of the investigations of the resonance structure, and caused many levels to be missed. As a result, the errors in the determination of σ_t varied from 5 to 40%. An attempt to measure σ_t, in particular for ^{244}Cm, in a nuclear explosion [13] was unsuccessful.

TABLE 2. Resonance Parameters of ^{244}Cm

E, eV	Γ_n, meV	Γ_γ, meV	E, eV	Γ_n, meV
13,62	1,82	34,2	131,3	3,6
30,33	3,1	54,9	148,7	24,0
37,5	4,4	76,6	154,6	11,5
60,1	23,6	38*	235,2	51
89,3	12,5		245,3	71
103,4	5,4		265,3	68

*For all levels above 60.1 eV, $\langle\Gamma_\gamma\rangle$ = 38 meV.

TABLE 3. Resonance Parameters of ^{243}Cm

E, eV	$2g\Gamma_n$, meV	Γ, meV	E, eV	$2g\Gamma_n$, meV	Γ, meV
—0,14	0,104	343	22,73	0,87	66
0,671	0,044	485	23,60	0,084	200
1,137	0,049	412	24,47	2,48	151
1,466	0,029	200	25,70	2,78	145
2,046	0,019	120	27,41	0,076	200
2,3.9	1,61	563	28,60	1,25	322
2,757	0,016	120	29,83	0,95	203
3,073	0,68	212	30,84	0,17	200
3,734	0,63	150	31,29	1,57	401
5,682	0,58	471	32,71	1,31	108
6,145	1,44	892	33,04	0,083	100
7,211	1,95	342	36,29	2,96	674
8,175	0,46	402	37,27	0,61	343*
9,107	3,12	1247	39,55	0,16	100
10,571	0,73	679	40,70	1,22	343*
11,854	1,93	180	44,11	0,79	250
12,393	0,052	150	45,24	0,69	250
14,728	0,67	202	46,44	1,95	343*
15,902	3,91	615	47,62	1,37	250
17,298	0,54	210	49,50	1,63	343*
17,773	0,94	417	52,2	0,87	100
18,23	0,16	167	55,59	2,79	343*
18,74	0,31	395	57,23	3,68	343*
19,28	1,24	159	59,39	0,74	250
20,31	0,39	276	62,36	1,06	343*
21,05	0,35	400	66,03	31,0	1308
21,58	2,43	682			

*Average value of Γ over first 37 levels.

Improvement of detectors for measuring σ_f (use of chambers with internal discrimination against alpha particles) [9, 11], the availability of practically pure samples of Cm with isotopic enerichment to 97-99% [8-10], and their investigation on spectrometers with a high neutron flux [11] and high energy resolution [7-10] increased the amount of information and raised the accuracy of σ_t and σ_f to 5-20%.

A very small amount of the material under study is required for integral measurements of cross sections. The main mass of data was obtained by the cadmium difference method [14-24], but some measurements were performed by the accumulation method [25-28], which ensures an accuracy of 25-50%. A similar accuracy of cross sections is characteristic of earlier experiments in which the samples used has a very low content of ^{242,243,245}Cm (1.5-2%) and ^{247}Cm (up to 20%) [21, 24]. Bringing the enrichment of the appropriate Cm isotopes up to 80-99% [14, 16, 19] increased the accuracy of the data to 5-10%.

Cross Sections in the Resonance Region. Tables 2-8 list the estimated resonance parameters for seven Cm isotopes, obtained by analyzing the data of [1-13], and taking account of the inadequate accuracy of part of the data. For example, σ_t for ^{246}Cm [1], ^{243,245}Cm [2], and ^{247}Cm [6] was measured with very thin samples, which contributed to the missing of levels. In calculating the cross sections of ^{243}Cm [4], ^{245}Cm [5, 9], and ^{247}Cm [6], the Breit—Wigner one-level formalism was used, not excluding interlevel interference, which may be the cause both of missing levels and of the appearance of spurious levels. In the data for ^{243}Cm [2, 4]

E, eV	Γ_n, meV	Γ_γ, meV	Γ_f, meV	E, eV	Γ_n, meV	Γ_f, meV
—3,5	2,51	36,0	7,50	264,8	11,4	0,90
7,67	10,1	35,1	0,85	274,2	21,5	0,60
16,78	1,85	37,1	1,40	317,4	5,5	0,30
22,85	0,85	35,4	3,70	329,5	42,3	0,30
35,0	3,94	36,4	2,5	343,6	45,0	1,16
52,8	0,56	36,0*	1,7	353,1	117,4	1,28
70,0	0,65		3,0	361,8	23,0	1,03
86,0	24,8		0,65	364,6	8,8	2,10
96,3	6,48		1,50	386,3	26,1	1,10
132,8	14,5		1,20	397,6	18,8	0,66
139,1	2,4		2,80	414,0	20,3	0,27
171,1	3,3		1,3	420,6	118,0	0,89
181,6	9,0		2,1	426,9	18,5	0,35
197,0	32,8		1,00	443,7	67,8	0,82
209,8	42,9		0,52	471,1	44,3	1,84
222,0	41,3		1,25	489,2	18,4	0,50
230,7	15,9		0,40	492,1	54,0	0,45
234,5	3,9		0,85	511,1	123,0	0,20
242,7	1,29		2,20	520,6	36,6	2,50

*For all levels above 52.8 eV, Γ_γ = 35 meV.

TABLE 5. Resonance Parameters of ^{245}Cm

E, eV	$2g\Gamma_n$, meV	Γ_γ, meV	Γ_f, meV	E, eV	$2g\Gamma_n$, meV	Γ_γ, meV	Γ_f, meV
—0,1	0,144	40	300	31,7	0,60	170	690
0,90	0,102	100	800	33,0	0,40	40	4
1,98	0,219	45	175	34,6	0,23	60	60
2,49	0,11	120	300	35,3	6,00	36	4195
4,70	2,06	35	325	36,3	2,58	167	190
5,75	0,14	300	300	39,5	0,65	60*	102
7,53	1,91	40	300	40,7	2,16		582
8,80	0,53	75	500	42,8	4,20		10
9,20	0,30	43	200	43,3	1,73		535
10,15	0,33	350	200	44,8	1,9		690
11,34	0,75	25	140	45,7	0,6		900
13,34	0,06	55	30	47,6	4,9		30
13,84	0,26	20	140	49,2	2,6		1400
16,0	0,57	40	400	50,5	1,8		750
21,4	3,20	27	490	51,6	0,6		210
24,8	3,20	40	225	53,6	12,35		900
25,8	0,04	60	550	54,6	0,3		1060
26,8	0,80	50	130	56,3	1,4		505
27,6	0,70	25	200	58,5	13,8		395
29,5	3,76	25	350	60,0	0,6		520

*For all levels above 39 eV, $\langle\Gamma_\gamma\rangle$ = 60 meV.

and ^{245}Cm [2, 5, 9] there are differences in the positions of levels and the values of the neutron width. In addition, in [2] for ^{243}Cm up to 26 eV, 15 levels were missed, and two extraneous levels (^{243}Am and ^{245}Cm) were observed; in ^{245}Cm nine resonances were missed up to 30 eV. Taking account of the fact that in [2] thinner samples with a lower content of the respective isotopes were investigated on a spectrometer with inferior resolution (Table 1), we have based our estimates of the ^{243,245}Cm parameters on the data of [4] and [5, 9], respectively. The estimated values for each level are the weighted averages (isolated deviations will be discussed).

The values of Γ_n for all isotopes were estimated over a wide energy range. The values of Γ_n for ^{245}Cm in [13] in the range 20-30 eV are systematically from 15 to 25% lower than the values in [2, 5, 9], but agree with the data in those papers within the indicated limits of error. This enabled us to use the data of [13]. The radiation width of each isotope was generally measured for only the first two or three levels, and all the remaining levels were assigned a constant value representing the weighted average of the measured values of Γ_γ.

TABLE 6. Resonance Parameters of [illegible]Cm

E, eV	Γ_n, meV	Γ_γ, meV	Γ_f, meV	E, eV	Γ_n, meV	Γ_f, meV
4,315	0,332	31,9	0,40	250,8	9,34	0,38
15,33	0,538	32,0	0,36	278,7	7,01	1,30
84,62	22,17	32*	0,70	288,7	59,4	0,31
91,91	12,83		0,17	313,6	24,8	0,15
				361,0	55,7	0,31
158,7	28,9		0,73	381,1	117,1	0,18

*For all levels above 84 eV $\langle\Gamma_\gamma\rangle$ = 32 meV.

TABLE 7. Resonance Parameters of ^{247}Cm

E, eV	$2g\Gamma_n$, meV	Γ, meV	Γ_f, meV	E, eV	$2g\Gamma_n$, meV	Γ_f, meV
1,247	0,56	74		40,0	0,01	170
2,919	0,10	70		40,6	0,03	50
3,189	1,0	103		41,3	0,66	20
9,55	0,91	166		41,8	0,05	550
18,1	3,7	210		43,4	0,19	5
21,3	0,12		405	44,9	2,10	30
24,0	0,04		135	45,2	0,58	60
25,3	0,01		25	47,9	1,17	165
26,2	0,02		220	48,9	6,80	80
28,0	0,06		55	50,1	2,36	55
30,2	3,45		4	50,7	3,18	50
30,6	0,19		50	51,8	1,66	15
32,2	0,51		25	52,2	1,26	4
36,4	1,63		60	53,6	0,45	325
37,7	0,03		555	55,1	0,53	40
38,8	1,33		13	56,2	0,66	70
39,5	0,01		705	59,7	15,73	115

TABLE 8. Resonance Parameters of ^{248}Cm

E, eV	Γ_n, meV	Γ_γ, meV	Γ_f, meV	E, eV	Γ_n, meV	E, eV	Γ_n, meV
7,26	1,84	34,1	0,062	647,0	109,4	1389	406,2
26,90	20,12	23,7	0,08	688,6	39,4	1505	682,8
35,01	11,6	29,8	1,70	694,3	202,9	1646	129,8
76,10	97,4	28*	3,3	721,5	91,3	1812	544,9
98,95	151,7		0,47	769,4	61,0	1910	118,0
140,3	1,53		1,12†	865,9	491,6	2040	198,7
186,4	4,25			887,1	98,3	2071	782,7
237,9	16,5			958,4	108,4	2138	471,6
258,7	62,7			994,2	123,0	2156	157,9
321,8	26,4			1042	190,5	2215	654,2
380,6	93,6			1103	219,2	2234	85,1
415,7	50,0			1194	328,2	2291	330,3
457,7	75,5			1210	34,8	2369	496,5
484,9	9,7			1262	270,0	2391	322,7
541,8	384,1			1277	178,6		
605,3	105,8			1288	53,8		

*For all levels above 76 eV, $\langle\Gamma_\gamma\rangle$ = 28 meV
†For all levels above 100 eV, $\langle\Gamma_f\rangle$ = 1.12 meV

The values of Γ_f from [13] were used for ^{244,246,248}Cm above 20 eV. Below 20 eV, Γ_f for ^{244}Cm was obtained by calculating σ_f with an approximation to σ_f^{th} and Γ_f measured at the thermal point, and Γ_f for ^{246,248}Cm was based on the experimental values of σ_f [11] and the corresponding resonance parameters of Tables 6 and 8. The value of $\langle\Gamma_f\rangle$ (1.12 meV) calculated from the values of Γ_f for the first five levels of ^{248}Cm was assigned to all the remaining resonances of this nucleus. Below 35 eV, the values of Γ_f from [9, 10] were used for ^{245}Cm, and above 35 eV the values from [13]. Information on the total widths of ^{245}Cm [5] permitted an estimate of Γ_γ for individual levels below 39 eV and a calculation of $\langle\Gamma_\gamma\rangle$ (Table 9). We

TABLE 9. Average Parameters of Curium Nuclei

Cm isotope	$D_{true}(l=0)$, eV	S_0, 10^4	$\langle 2g\Gamma_n^0\rangle$, meV	$\langle\Gamma_f\rangle$, meV	$\langle\Gamma_\gamma\rangle$, meV	E_{max}, eV
242	12,8±2,7	0,65±0,26	0,83	1,71	38	160
243	0,81±0,10	1,71±0,41	0,28	240	33	66
244	11,8±1,2	1,2±0,2*	1,34	1,35	36	500
245	1,38±0,10	1,1±0,2*	0,30	475	60	60
246	30±4	0,6±0,2	1,81	0,48	32	400
247	1,4±0,2	0,93±0,20	0,26	140	85	60
248	25±5	1,3±0,3*	2,9	1,12	28	1290

*S_0 was found graphically.

TABLE 10. Thermal Cross Sections and Resonance Integrals of Curium Isoptopes b*

Cm isotope	Thermal cross sections (v = 2200 m/sec)		Resonance integrals	
	σ_f^{th}	σ_c^{th}	I_f	I_c
242	⩽5	20±10	—	150±40
243	619,2±16,0	130,7±9,6	1552±64	214,4±20,3
244	1,03±0,07	15,1±0,3	13,6±1,0	643±8
245	2074±34	345±4	794±20	102±3
246	0,15±0,01	1,23±0,10	10,2±0,7	121±3
247	84±3	60±20	774±30	567±134
248	0,36±0,04	2,72±0,20	13,2±0,1	273±15

*1 b = 10^{-28} m^2.

recommend the resonance parameters of strong levels from [6] for ^{247}Cm up to 20 eV, and above 20 eV the values from [13].

On the average, the accuracy of the recommended resonance parameters varies from 10 to 20% for Γ_f, and from 5 to 15% for Γ and Γ_n (deviations of up to 25-50% exist). Our values of the resonance parameters for the even isotopes of Cm agree with the corresponding data of [29-32]. The differences observed for the parameters of the ^{243,245}Cm levels [31, 33] are related mainly to the use of appreciably different experimental data in the estimates. The data in Tables 2-8 were used to obtain the average parameters of the Cm nuclei.

In estimating the s-wave strength function S_0, which is determined essentially by the strong resonances, the question of missed levels (or p-wave levels) is not of practical importance, but becomes of primary importance in determining the average level spacing D. A direct method of correcting for the number of missed levels (or taking account of p levels) involves fitting the integral distribution of reduced neutron widths Γ_n^0 of observed resonance in a given energy range to the Porter–Thomas distribution. When extrapolated to small values of the width, this distribution gives corrected values of $\langle\Gamma_n^0\rangle$ and D_{true}. Table 9 gives the values of D_{true}, $\langle\Gamma_n^0\rangle$ for s-wave neutrons obtained in this way, and the values of the maximum energy E_{max} for which the levels were investigated.

The strength function was found from the relation $S_0 = \langle 2\Gamma_n^0\rangle / D_{true}$. For $^{243-245,248}$Cm nuclei which have a larger number of levels, S_0 was determined from the graph of $\Sigma 2g\Gamma_n^0$ vs E, since this method is insensitive to the omission of levels with small values of Γ_n^0.

When Γ_f or Γ_γ have not been measured, their average values, as a first approximation, were determined from the relation $\langle\Gamma_f\rangle = \langle\Gamma_\gamma\rangle I_f/I_c$. This method gave $\langle\Gamma_f\rangle = 1.71$ meV for ^{242}Cm (the ratio $I_f/I_c = 0.045$ from [34]), $\langle\Gamma_\gamma\rangle = 32.7$ meV for ^{243}Cm ($I_c/I_f = 0.136$ from [9]), and $\langle\Gamma_\gamma\rangle = 85$ meV for ^{247}Cm (from data in Tables 9 and 10).

In the resonance region the neutron cross sections are well described by the one-level Breit–Wigner formula. Curves of σ_c vs neutron energy below 100 eV were calculated for the isotopes ^{242,244,246,248}Cm from the recommended resonance parameters. Since the dimensions

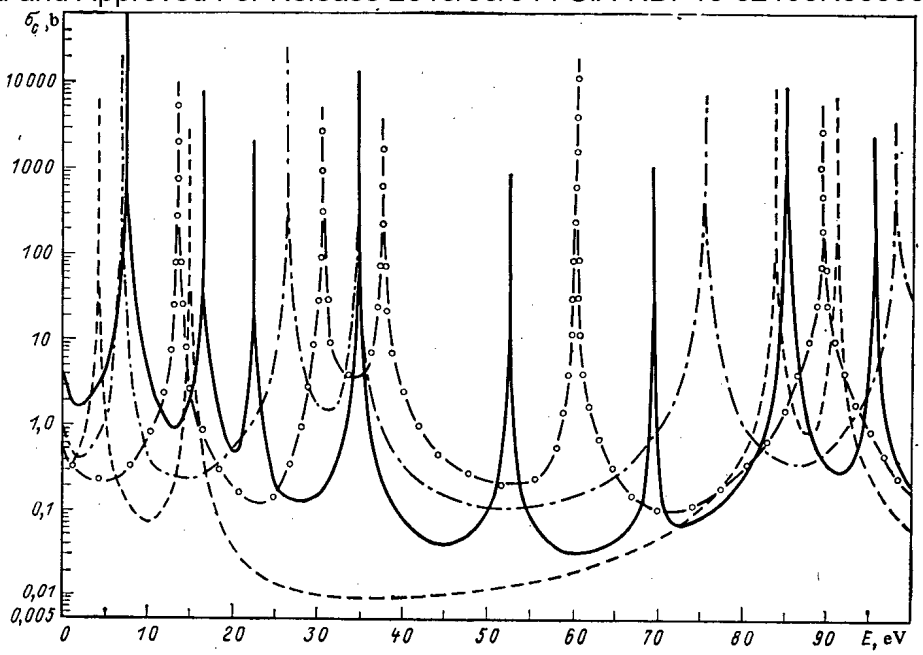

Fig. 1. Calculation of σ_c below 100 eV for ^{242}Cm (○); ^{244}Cm (——); ^{245}Cm [Sic] (---) and ^{248}Cm (-.-).

and locations of resonances were found to be similar for all even Cm isotopes, we can assume that the ^{242}Cm levels below 13 eV and the ^{246}Cm levels between 15 and 85 eV were missed.

Thermal Cross Sections and Resonance Integrals. Integral cross sections are measured in reactor spectra by comparison with known standards. The thermal and epithermal parts of a reactor spectrum are separated by using cadmium filters to cut the part of the spectrum below ∿ 0.5 eV. It is assumed that the neutron flux above the thermal Maxwellian distribution is inversely proportional to the neutron energy, and the cross section for each Cm nucleus in the thermal region is inversely proportional to the neutron velocity.

The recommended values were determined as the weighted mean, agreeing within the indicated limits of error of the corresponding cross sections (deviations will be discussed). The recommended values of the cross sections (Table 10) were obtained from an analysis of the data of [14-28]: the thermal capture σ_c^{th} and fission σ_f^{th} cross sections for neutron velocities of 2200 m/sec, and the resonance capture I_c and fission I_f integrals. The values of σ_f^{th} for ^{243}, ^{245,247}Cm measured for average thermal [21, 24] and reactor [25, 26] spectra, and also I_f for ^{245,247}Cm obtained without taking account of the contribution of the hydrogen contained in the filter material [17], were not taken into account in the calculation.

In a number of papers only the thickness of the cadmium filters was given, and as a result the cutoff of the reactor spectrum can vary from 0.5 to ∿1 eV. However, the first levels of the $^{242,244,246-248}$Cm nuclei lie well above the indicated energy region, and therefore the data of the papers listed were used to estimate the resonance integrals.

The values of σ_c^{th} and σ_f^{th} for ^{242}Cm were obtained by a recalculation using effective reactor cross sections from [26] and I_c from [27]. The results of single measurements of σ_c^{th}, σ_f^{th}, and I_c for ^{242}Cm [26, 27], and σ_c^{th}, I_c for ^{243}Cm [19] were taken as the recommended values.

After the errors in I_f = (18 ± 1)b for ^{244}Cm [15], σ_f^{th} = (1900 ± 100)b for ^{245}Cm [16], σ_f^{th} = (2018 ± 37)b for ^{245}Cm [15], σ_f^{th} = (120 ± 12)b for ^{247}Cm [17], and σ_c^{th} = (10.7 ± 1.5)b for ^{248}Cm [16] were increased, these data were used in the estimates.

On the average, the recommended values of thermal cross sections and resonance integrals were obtained with an accuracy of 5-10%, and for the most part agree with the corresponding values in [29-32, 35] (deviations of up to 25% are observed). The existing differences in σ_c^{th} for ^{244}Cm [35] and ^{248}Cm [30], I_f for ^{244,246}Cm [35], and I_c for ^{247}Cm [35, 36] result from the use of appreciably different experimental data. It should be noted that in all the estimates the most consistent data were obtained for $^{244-246}$Cm and ^{248}Cm [29-32, 35, 37]. Disagreements observed for ^{242,243}Cm and ^{247}Cm [30, 33, 35-37] are difficult to resolve with the existing lack of experimental data: new measurements are needed for these isotopes.

LITERATURE CITED

1. R. Cote, R. Barnes, and H. Diamond, Phys. Rev., 134B, 1281 (1964).
2. J. Berreth, F. Simpson, and B. Rusche, Nucl. Sci. Eng., 49, 145 (1972).
3. V. S. Artamonov et al., in: Neutron Physics, Part 2 [in Russian], TSNIIatominform, Moscow (1977), p. 257.
4. V. A. Anufriev et al., At. Energ. 51, 330 (1981).
5. T. S. Belanova et al., [3], p. 260.
6. T. S. Belanova et al., At. Energ., 47, 206 (1979).
7. O. Simpson et al., Rep. USNDC-3 (1972), p. 4.
8. R. Benjamin et al., Nucl. Sci. Eng., 55, 440 (1974).
9. J. Browne, R. Benjamin, and D. Karakker, Nucl. Sci. Eng., 65, 166 (1978).
10. R. White et al., in: Proc. Int. Conf. on Nuclear Cross Sections for Technology, Knoxville (1979), p. 496.
11. H. Maguire et al., Trans. Am. Nucl. Soc., 38, 648 (1981): R. Block et al., ibid., 39, 876 (1981).
12. M. Silbert, Rep. BNL-NCS-21000 (1976), p. 94.
13. M. Moore and G. Keyworth, Phys. Rev., C3, 1656 (1971).
14. K. D. Zhuravlev, N. I. Kroshkin, and A. P. Chetverikov, At. Energ., 39, 285 (1975); 47, 55 (1979).
15. R. Benjamin, K. MacMurdo, and J. Spencer, Nucl. Sci. Eng., 47, 203 (1972).
16. V. D. Gavrilov and V. A. Goncharov, At. Energ., 44, 246 (1978); 41, 185 (1976).
17. J. Halperin et al., Rep. ORNL-4581 (1970), p. 37.
18. J. Halperin et al., Rep. ORNL-4437 (1969), p. 20.
19. C. Bemis et al., Nucl. Sci. Eng., 63, 413 (1977).
20. R. Druschel et al., Rep. ORNL-4891 (1973), p. 23.
21. H. Diamond et al., J. Inorg. Nucl. Chem., 30, 2553 (1968).
22. R. Schuman, Prog. Rep., WASH-1136 (1969), p. 54.
23. M. Thompson, M. Hyder, and R. Reuland, J. Inorg. Nucl. Chem., 33, 1553 (1971).
24. K. Hulet et al., Phys. Rev. 107, 1294 (1957).
25. J. Smith et al., in: Proc. Conf. on Nuclear Cross Sections and Technology, Vol. 11, Washington (1968), p. 1285.
26. H. Ihle et al., J. Inorg. Nucl. Chem., 34, 2427 (1972).
27. R. Schuman, Prog. Rep. WASH-1136 (1969), p. 53.
28. G. Hanna et al., Phys. Rev., 81, 893 (1951).
29. R. Benjamin et al., Rep. DP-1447 (1977).
30. S. Mughabghab et al., BNL-325, 3rd ed. (1973).
31. T. Martinelli et al., CNEN, Rep. RT/FI (80), 7, 10 (1980).
32. S. Igarasi and T. Nakagawa, Rep. JAERI-M-7733 (1978); Rep. JAERI-M-7733 (1978); Rep. JAERI-M-7175 (1977).
33. T. Nakagawa and S. Igarasi, Rep. JAERI-M-9601 (1981).
34. B. Hinkelman, in: Proc. IAEA Symp. on Nuclear Data for Reactors, Vol. 2, Helsinki (1970), p. 721.
35. Compilation of Actinide Neutron Nuclear Data, KDK-35, Stockholm (1979).
36. T. Martinelli et al., in: Proc. Second Technical Meeting on the Nuclear Transmutation of Actinides, Ispra (1980), p. 171.
37. G. Maino et al., CNEN Rep. RIT/FIS(81), 1-2 (1981).

NEUTRON-TRANSMISSION FUNCTION FOR THE REGION OF UNRESOLVED RESONANCES

A. V. Komarov and A. A. Luk'yanov

UDC 539.170.013

An important part in the urgent problem of increasing the accuracy of reactor-physics calculations is played by investigations of the resonant self-screening in the retardation, absorption, and diffusion of decelerating neutrons in reactor media. The most complete information on the peculiarities of this structure and its importance for the estimation of self-screening effects is given by experimental data on neutron transmission as a function of the sample thickness. In the general case the transmission function measured experimentally is determined by the integral

$$T(n, E) = \langle \exp(-n\sigma) \rangle = \int \exp[-n\sigma(E')] F(E, E')\, dE', \quad (1)$$

where n is the sample thickness; F(E, E') is the normalized function of the experimental resolution, characterizing the energy scatter of the neutrons in the incident beam with respect to the mean energy E. If the cross section varies weakly with energy in the limits of integration in Eq. (1), or the neutrons in the beam are monochromatic, then the transmission is directly determined by the cross section: $T = \exp(-n\sigma)$; $\sigma = (1/n)(-\ln T)$. However, in the region of neutron resonances, as a rule, the influence of the finite resolution must be taken into account: in various methods of determining the cross section from the transmission in Eq. (1), the characteristic parameter is found to be the ratio between the width of the individual resonances Γ to the width of the resolution function Δ. The case when $\Gamma \gg \Delta$ corresponds to a resolved resonance. In this case, methods of determining the cross section from data on the neutron transmission through thin and thick targets are known [1, 2]. In the region of unresolved resonances, where $\Gamma < \Delta$, it is usually only possible to determine the mean cross section over the energy, on the basis of data on neutron transmission through relatively thin targets.

In investigating the energy structure of the neutron cross sections, the main interest centers on improvements in the experiment, with a view to improving the resolution and increasing the accuracy of the measurements. Data of experiments on the transmission of energetically broad neutron beams as a function of the sample thickness, including fairly thick beams (beam attenuation by 2-3 orders of magnitude) are also of some significance. The accumulation of very broad experimental material has proven to be possible, mainly by Soviet researchers [3-6]. As a rule, the measured values of the mean transmission over the energy interval (energy group) in the region of resonances $\langle \exp(-n\sigma) \rangle$ for thickness with $n\langle\sigma\rangle \geqslant 0.5$ are markedly different from $[-n\langle\sigma\rangle]$ (Fig. 1) [6]. It is interesting that even in those intervals where there are data on the detailed structure of the cross section obtained with the best resolution, the values calculated from them, of the transmission at large thickness may diverge significantly from the results of measurements in broad beams [7, 8]. This is usually associated with inadequate accuracy of the cross-section measurements in experiments with thin targets close to the interference minima, often determining the transmission at large thickness. In the region of resolved resonances, the cross sections at the minima must be more carefully determined, using measurements for relatively thick targets [8].

The problem of determining the transmission function over a broad range of variation in the thickness for the region of unresolved resonances proves to be more complex in its general formulation. Direct experimental information on the energy structure of the cross section is lacking; only the means of the cross section over the energy $\langle\sigma\rangle$ are known. However, this structure evidently appears indirectly in the deviation of the observed transmissions from exponential. The theoretical interpretation of data on transmission as a function of the sample thickness requires corresponding theoretical models of the energy structure of the cross section in the region of unresolved resonances, reflecting the features which are char-

Translated from Atomnaya Énergiya, Vol. 53, No. 6, pp. 392-395, December, 1982. Original article submitted December 25, 1981.

0038-531X/82/5306-0849$07.50

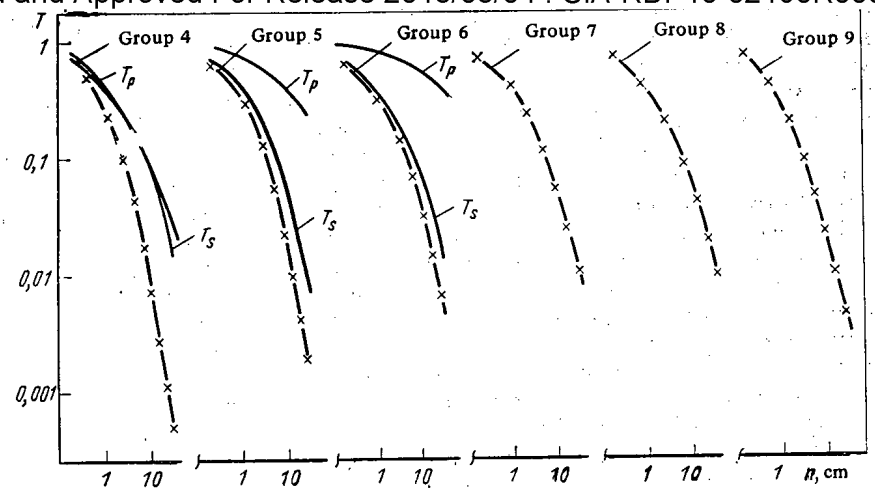

Fig. 1. Transmission function T in the groups; the curves correspond to calculation and the crosses correspond to experiment (in groups 4-6, the partial transmissions for s and p neutrons are shown).

acteristic for transmission. This problem was considered in [9] for the calculation of the mean cross section over the momentary resonances $\langle\sigma^k\rangle$. In practice, however, the method of representing the transmission as a sum of a small number of exponentials is well known and widely used; it is very expedient for reactor-physics applications using experimental data on the transmission in energy groups [10].

In the present work, the transmission function in the region of unresolved resonances is determined using a model cross section corresponding to the case of identical equidistant resonances with mean resonant parameters. For nonfissile nuclei, in which the radiational capture is sufficiently small, an approximate multilevel expression for the cross section may be written in terms of the periodic function

$$\sigma = \sigma_{min} + \sigma_0 \frac{(\cos\varphi - s^{-1}\operatorname{tg} z \sin\varphi)^2}{1 + s^{-2}\operatorname{tg}^2 z}, \tag{2}$$

where σ_{min} is the minimum cross section; σ_0, cross section at resonance; $s = \pi\Gamma/2D$, force function and φ, potential-scattering phase, which are assumed to be energy-independent parameters in the individual energy groups; and $z = \pi E/D$ (D is the mean distance between resonances) [2]. Averaging over the energy in the present model is equivalent to averaging over the period $-\pi/2 \leqslant z \leqslant \pi/2$. Thus, the mean cross section is

$$\langle\sigma\rangle = \frac{1}{\pi}\int_{-\pi/2}^{+\pi/2} \sigma(z)\, dz = \sigma_{min} + \sigma_0 \frac{\sin^2\varphi + s\cos^2\varphi}{1+s}, \tag{3}$$

and the mean square (second moment) is

$$\langle\sigma^2\rangle = \langle\sigma\rangle^2 + s\sigma_0^2/2(1+s)^2. \tag{4}$$

The transmission function in the present model is determined by the integral

$$T = \exp(-n\sigma_{min})\frac{1}{\pi}\int_0^{\pi} \exp\left\{-n\sigma_0 \frac{(s\cos\varphi - \operatorname{tg} z \sin\varphi)^2}{s^2 + \operatorname{tg}^2 z}\right\} dz, \tag{5}$$

the mathematical properties of which were described in detail in [11, 12]. Only the asymptotic expression at large $n\sigma_0$ will be given here

$$T \approx \exp(-n\sigma_{min})\frac{1}{\sqrt{\pi n\sigma_0}}\frac{s}{\sin^2\varphi + s^2\cos^2\varphi} \tag{6}$$

TABLE 1. Parameters of the Transmission Function for Iron in Individual Groups for a Single System of Levels

Group no.	Energy range, MeV	σ_{min}, b *	φ	s	σ_0, b
4	1,4—2,5	1,04	0,567	0,069	6,61
5	0,8—1,4	0,847	0,643	0,146	4,77
6	0,4—0,8	0,671	0,609	0,226	6,23
7	0,2—0,4	0,426	0,524	0,163	7,99
8	0,1—0,2	0,445	0,424	0,113	15,9
9	0,0465—0,1	0,49	0,323	0,052	32,7

* $1\text{b} = 10^{-28}$ m^2.

as well as the expression for the area under the transmission curve

$$\int_0^\infty \langle \exp(-n\sigma)\rangle\, dn = \left\langle \frac{1}{\sigma} \right\rangle = \frac{(\sqrt{\sigma_{min}} + s\sqrt{\sigma_{max}})(\sqrt{\sigma_{max}} + s\sqrt{\sigma_{min}})}{\sqrt{\sigma_{min}\sigma_{max}}\,(\sqrt{\sigma_{min}} + s\sqrt{\sigma_{max}})^2 + \sigma_0(1-s^2)\sin^2\varphi}, \quad (7)$$

where $\sigma_{max} = \sigma_0 + \sigma_{min}$ is the maximum cross section.

Analysis of the transmission function measured experimentally reduces, in the given approach, to determining the consistent set of parameters (σ_{min}, σ_0, s, and φ) that best describe the given integral Eq. (5). To calculate how well these model parameters coincide with the analogous parameters of the theory of mean cross sections, the experimental data on neutron transmission through iron samples obtained in [6] for a broad range of variation in sample thickness, in various energy groups, are objected to detailed analysis. The group intervals correspond to those adopted in the well-known BNAB system of group constants [10]. Consideration is limited to the range from 46.5 keV to 2.5 MeV (groups 4-9), where resonant-structure effects evidently appear in the transmission.

In the groups of lower energy (9, 8, and 7), the parameters of the transmission function in Eq. (5) are determined directly by comparison with the experimental data. This is accomplished by the least-squares method, realized on a BÉSM-6 computer by the FUMILI library program. In this case, as well as the experimental data on the transmission described by the integral in Eq. (5), values of the mean cross sections in the group [12] analyzed using Eq. (3) are also used. It is also assumed that the s wave predominates in these groups, and $\sigma_0 = 4\pi K^{-2}$. The results obtained are shown in Table 1 and Fig. 1.

The parameters $s = \pi/2\, s_0\sqrt{E}$ and $\varphi = KR$ of the present model are found, within the limits of the error obtained, to be close to the corresponding theoretical estimate of the reduced force function $s_0 = 1.6 \cdot 10^{-4}$ and the optical radius of the nucleus $R = 5 \cdot 10^{-13}$ cm (see, e.g., [13], [12]. The minimum cross section σ_{min} obtained in the present analysis is new in comparison with the usual parameters of the theory of a mean cross section (see Table 1); the errors in its determination are large (5-10%) [12]. The values of σ_{min} obtained are in qualitative agreement with the expected cross sections at the interference minima for s-wave resonances.

In the higher groups (4-6), the parameters of the present fitting in the given approximation — Eq. (5) — are found to be formal (model) parameters to a considerable extent, and diverge from the theoretical estimates. The reason for this is the pronounced contribution to the corresponding energy from p- and d-wave resonances, and also, in groups 4 and 5, from inelastic scattering of the neutrons. To take these effects into account, it is assumed that the position of the resonances of various systems of levels in the group interval is uncorrelated. Then the transmission may be approximately represented as the product of the partial transmissions $T = T_S T_p \ldots$, where $T_p = T_{p_1} T_{p_2}$, which corresponds to two possible systems of resonances for p neutrons with a total moment equal to 1/2 and 3/2.

In analyzing the ratio T/T_S (Fig. 1), where T_S is calculated for the given groups with parameters s_0 and R, as for the lower groups, it is assumed that $T/T_S = T_{p_1} T_{p_2}$, where T_{p_1} and T_{p_2} are described by the functions in Eq. (5) with the parameters $s_{p_1} = s_{p_2} = s_p$, $\varphi_{p_1} = \varphi_{p_2} = \varphi_p$, $\varphi_p = KR - \text{arctg}(KR)$, $\sigma_{0p_1} = 0.5\, \sigma_{0p_2}$ [2]; in groups 5 and 6, $\sigma_{0p_1} = \sigma_0$. As a result of fitting to the experimental data in groups 5 and 6, the values of the parameters σ_{min} and s_p

TABLE 2. Parameters of the Transmission Function for Iron in High-Energy Groups, Taking Account of s and p Resonances

Group no.	σ_{min}, b	$4\pi K^{-2}$, b	KR	$\frac{\pi}{2} s_0 \sqrt{E}$	φ_p	s_p	σ_{0p}, b
4	0,523	1,22	1,57	0,54	0,56	0,157	1,76
5	0,507	2,17	1,1	0,26	0,225	0,0677	2,17
6	0,317	3,88	0,83	0,21	0,137	0,0288	3,88

are determined (Table 2). The values of σ_{min} significantly differ from the results of analysis under the assumption of a single system of resonances, i.e., taking the influence of p-wave resonances into account allows σ_{min} to be refined. The values s_p agree with the available data on the reduced force functions for the p wave, within the limits of the error in the determination; it is assumed here that by redefinition of the force function $s_p^* = s_p(E) + s_p(E-0.85)$ in groups 4 and 5, the inelastic scattering of neutrons by the first excited level of ^{56}Fe at $E_{in} = 0.85$ MeV [14] may be effectively taken into account.

In group 4, in addition to inelastic scattering, a significant contribution to the transmission comes from d-wave resonances and, with the limitations of the experimental information, detailed analysis is very difficult here. In this group the parameters obtained by fitting are formal in character, and the set of parameters best describing the experimental data is shown in Table 2.

The present analysis illustrates the possibility of theoretical description of the transmission averaged over the resonances in the whole range of thickness using mean resonant parameters. The only new parameter in the groups is σ_{min}, the variations in which mainly influence the behavior of the transmission at large thicknesses. At present, sufficiently accurate theoretical estimates of this parameter are impossible. The values of σ_{min} in a scheme with a single system of resonances differ from the values in a more detailed scheme where the p wave is separated out. This indicates that the determination of σ_{min} and also other resonant parameters in the upper groups is of model character, to a considerable extent, if no detailed analysis of the partial contributions to the transmission from the various interaction processes between the neutron and nucleus is performed.

Data on neutron transmission in groups are used in reactor-physics calculations to determine the group characteristics [2, 10]. In the present approach, both an approximate scheme of parameterization of the transmission function by the single integral in Eq. (5) and a scheme with the separation of resonances of different systems may be used. The first variant is more expedient from the viewpoint of practical use, since it contains fewer parameters and the expressions for the mean inverse moments and the self-screening coefficients obtained in this approach have a simple analytical form [11, 12]. However, the parameters obtained in this approach are of model character in the case of several systems of resonances, and the values of these parameters cannot be estimated with good accuracy without directly using data on the transmission. The second variant, with the isolation of p waves in the transmission, allows approximate mean resonant parameters to be used in the present case in constructing the function T(n), supplementing them only by the one new parameter σ_{min} determining the behavior of the transmission function at the asymptote ($n\sigma_0 \gg 1$). In this variant, all that is necessary to reproduce the transmission at an arbitrary thickness in the region of unresolved resonances (or in averaging over many resolved resonances) is to supplement the approximate mean resonant parameters in the groups (in the case where good estimates of these parameters exist) with the corresponding group value of σ_{min}, which, from a physical viewpoint, is more systematic than to approximate the transmission by a sum of exponentials [10].

The method proposed in the present work for the analysis of the energetically mean transmission has certain advantages with regard to the production of experimental data in comparison with the subgroup method [10], especially at a large thickness [11], but, at the same time the subgroup method is simpler from the point of view of practical realization.

LITERATURE CITED

1. Yuz Dzh, Neutron Research in Nuclear Reactors [Russian translation], IL, Moscow (1954).
2. A. A. Luk'yanov, Moderation and Absorption of Resonant Neutrons [in Russian], Atomizdat, Moscow (1974).

3. M. N. Nikoleav, V. V. Filippov, and I. I. Bondarenko, At. Energ., 11, No. 5, 445 (1961).
4. A. A. Van'kov, Yu. V. Grigor'ev, and V. F. Ukraintsev, in: Neutron Physics. Materials of Fourth All-Union Conference [in Russian], Vol. 2, TsNIIatominform, Moscow (1977), p. 243.
5. F. Boreli and S. Darden, Phys. Rev., 109, 2079 (1958); G. B. Yan'kov, Dissertation, Institute of Atomic Energy, Moscow (1964).
6. V. V. Filippov, Vopr. At. Nauk, Tekh., Ser, Yad. Konst., No. 8, Part 1, 39 (1972).
7. V. V. Vozyakov and V. V. Filippov, Vopr. At. Nauk. Tekh., Ser, Yad. Konst., No. 20, Part 1, 41 (1975).
8. A. A. Luk'yanov, in: Neutron Physics. Materials of Third All-Union Conference [in Russian] Vol. 2, TsNIIatominform, Moscow (1976), p. 48.
9. D. F. Zaretskii and V. K. Sirotkin, in: Neutron Physics. Materials of Third All-Union Conference [in Russian], Vol. 3, Izd. TsNIIatominform, Moscow (1976), p. 175.
10. M. N. Nikolaev, A. A. Ignatov, and V. F. Khokhlov, At. Energ., 29, No. 1, 11 (1970).
11. A. V. Komarov and A. A. Luk'yanov, Vopr. At. Nauk. Tekh., Ser. Yad. Konst., No. 38, 10 (1980).
12. A. V. Komarov and A. A. Luk'yanov, Vopr, At. Nauk. Tekh., Ser. Yad. Konst., No. 42, 3 (1981).
13. V. M. Byhkov, V. V. Vozyakov, and V. N. Manokhin, in: Neutron Physics. Materials of Third All-Union Conference [in Russian], Vol. Izd. TsNIIatominform, Moscow (1976), p. 176.
14. A. V. Komarov and A. A. Luk'yanov, Vopr. At. Nauk. Tekh., Ser. Yad. Konst., 45, 23 (1982).

ANALYSIS OF THE SURFACE AND EROSION OF THE GRAPHITE DIAPHRAGM OF THE T-3M TOKAMAK IN THE TEARING MODE

D. G. Baratov, G. V. Gordeeva, M. I. Guseva,
V. N. Dem'yanenko, A. N. Mansurova, S. V. Mirnov,
V. A. Stepanchikov, and V. P. Fokin

UDC 539.175.3;621.039.6

A major difficulty in constructing large tokamaks and tokamak-reactors will be posed by the tearing-mode instability which manifests itself in fast expansions of the current channel (tears) right up to the diaphragms and walls of the discharge chamber.

The tearing time in present-day tokamaks is 10^{-5}–10^{-3} sec, and with the growth of the size of tokamaks it may well increase to $(20\text{-}30) \cdot 10^{-3}$ sec. Tearing is characterized by the break-up of the magnetic configuration of the tokamak into magnetic islands constituting packets of current. They, in the first place, come into contact with the diaphragm and the wall. The rapid disruption of the magnetic configuration is accompanied by a regime in which the heat fluxes on the wall and diaphragm increase. In this case the heat loads (albeit brief) can run to tens of kW/cm^2. The pulsed temperature of the diaphragm surface reaches 1000°C or more during tearing [1]. Thus, it is a practical interest to study the processes of erosion of diaphragms during tearing.

At least five different possible mechanisms of erosion during tearing are known: melting under the action of the heat flux of electrons and ions of the basic plasma; melting under the action of accelerated ("escaping") electrons; sputtering under the action of ions accelerated by the potential difference of the Langmuir layer arising at the diaphragm-plasma interface; erosion under the action of unipolar arcs initiated between the diaphragm and the plasma by that potential; and an electrodynamic mechanism of erosion under the action of arcs arising when the diaphragm cuts off packets of current [2]. The last mechanism seems to be one of the most timely for present-day tokamaks and was the object of investigation in experiments carried out earlier on the T-3M materials-testing tokamaks stand [3].

A diaphragm (4 × 8 cm) of two parallel graphite (USB-15) plates (Fig. 1), separated by an insulator, was introduced into the T-3M tokamak in a discharge regime with I_d = 20–30 mA, magnetic field B_z = 1 T, major radius R = 95 cm, and minor radius of the plasma filament r = 16 cm across the magnetic field B_z. The diaphragm could be moved into the plasma filament to a depth l = 3 cm. Upon connecting the plates by an electrical shunt, it is possible to measure the current I_d flowing in the "shadow" of the diaphragm and, have measured the voltage drop V_d between the insulated plates, to estimate the scale of the high voltage between the plasma and the diaphragm. It turned out that during tearing the currents I_d flowing "through" the diaphragm immersed in the plasma can reach 1 kA while $V_d \approx 500$ V. This voltage would be sufficient to ignite an arc.

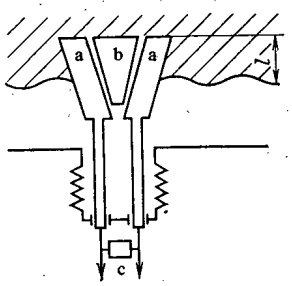

Fig. 1. Diagram of movable diaphragm (view from top): a) graphite plates; b) insulator; c) shunt; l is depth of immersion in the plasma.

Translated from Atomnaya Énergiya, Vol. 53, No. 6, pp. 396-398, December, 1982. Original article submitted April 6, 1982.

 0038-531X/82/5306-0854$07.50

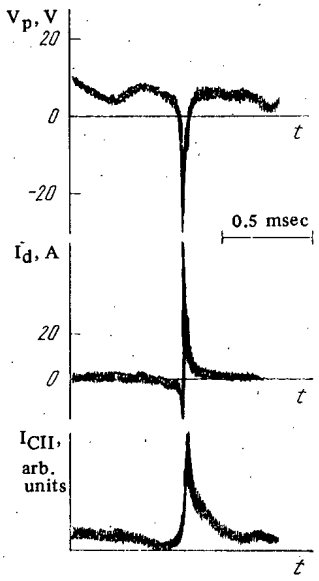

Fig. 2. Oscillograms of the voltage $V_p(t)$ on the periphery, the current I_d, and the intensity of the CII line during tearing.

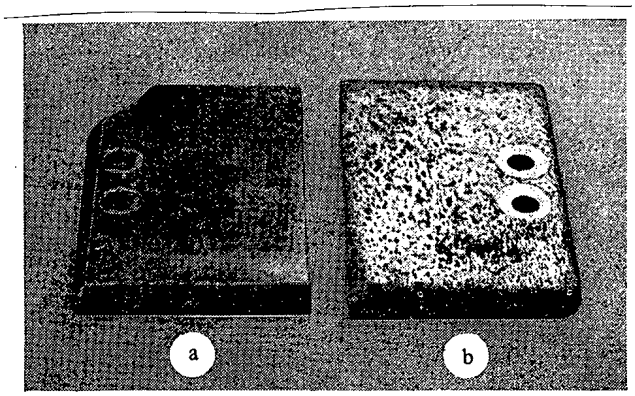

Fig. 3. Electron (a) and ion (b) plates of movable diaphragm after 100 discharge pulses with tearing.

Figure 2 shows time oscillograms of the voltage $V_p(t)$ on the periphery of the torus, the current $I_d(t)$, and the intensity of the CII spectral line, illustrating the course of erosion. The current $I_d(t)$ is bipolar. The small negative precursor (opposite to the direction of the main current) probably corresponds to the region of absolute negative current having been cut off by the diaphragm, while the large positive peak corresponds to the destruction of an island on reaching the diaphragm and to the expansion of the entire current channel [4]. The erosion correlates with the onset of I_d.

The maximum value reached by I_d is 1 kA. This value has a tendency to decrease with the purification of the chamber and the aging of the diaphragm. In order to maintain a current of 1 kA, the ion side of the diaphragm, which acts as a cathode with respect to I_d, would have had to emit electron currents with an average density of ~ 40 A/cm^2. This permitted the assumption that on the ion side, emission during the tearing is ensured by arcs [5].

No deep traces of erosion are visible on the electron side of the diaphragm (Fig. 3), while the ion side is filled with traces of cathode spots — arc craters. The space between the craters on the ion side is covered with films with characteristic iridescent tarnishes. It is these films that gave the ion plate of the diaphragm the highlight in Fig. 3b.

Figures 4a, b show scanning electron miroscope photographs of eroded parts of the ion plate. Traces of two kinds of arc are easily distinguished. A large part of them are in the form of elongated spots (arcs of the first kind [5]) with a width of ~ 500 μm and a length of ~ 1500 μm, mainly oriented across the total magnetic field (see Fig. 4a). Each spot is a set of overlapping craters with a characteristic diameter of 3-5 μm and a density of 10^6 cm^{-2}

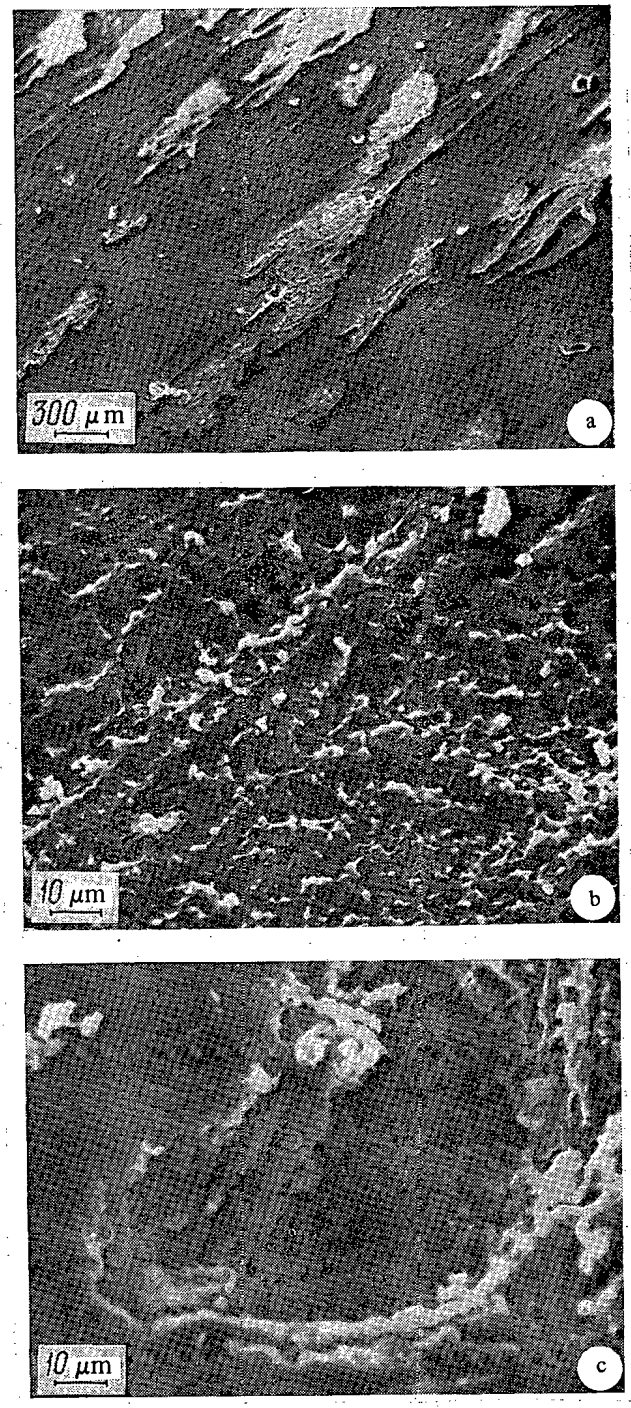

Fig. 4. Magnified images of arc craters of the ion plate of the diaphragm shown in Fig. 3: a) region of eroded surface; b, c) regions of craters formed by arcs of the first and second kinds, respectively.

(see Fig. 4b). In addition to these, we can distinguish individual deep craters, resembling the traces of microexplosions (see Figs. 4a, c), with a diameter of up to 100 μm (arcs of the second kind [5]), distributed comparatively sparsely over the surface of the plate, with an average density of 300 cm^{-2}.

The amount of carbon carried off from the ion surface (electron transfer coefficient) was $\sim 0.7 \cdot 10^{-4}$ g/C, or 0.6 atom/electron, with respect to the current flowing "through" the diagram during tearing. Such coefficients are typical of destruction of the surface in quasi stationary cathode spots [5]. This can be used, e.g., to estimate the scale of the electrodynamic erosion in INTOR-type tokamaks during tearing. At a current of $5 \cdot 10^{-2}$ I_d in the packets and a tearing duration of $4 \cdot 10^{-2}$ sec, the scale of electrodynamic erosion in the INTOR

is $\sim$ 1 g of material of the diaphragm (wall) in a tearing. This value seems to be quite modest. The surface of the withdrawn diaphragm was analyzed with an Auger spectrometer and by the backscattering method. The phase composition of the surface and bulk of the diaphragm was analyzed by the x-ray diffraction method. On the basis of this analysis we can conclude that the phase composition of the surface did not change and the deposited films are apparently amorphous.

The Auger analysis and backscattering showed that the films on the ion side of the diaphragm were formed mainly by metals present in the wall of the discharge chamber (Fe, Ni). The thickness of the films is $\sim 15 \cdot 10^{-6}$ cm. On the electron side the metal content is lower than on the ion side by a factor of at least five. The metal content in the arc craters was also low.

In order to explain this pronounced difference, it is usually assumed [6] that the plasma column rotates as a whole along the torus in the direction of the main current I_d (i.e., in the ion direction) at the speed V_0. If it is assumed that along the magnetic field the metal ions have a Maxwellian distribution, shifted by V_0, then this explanation becomes valid when V_0 exceeds 0.4 of the mean thermal velocity of the ions. Assuming the temperature of ions near the boundary to be 5-20 eV, we get $V_0 = (2\text{-}4) \cdot 10^5$ cm/sec (a comparatively high value).

Another explanation of the asymmetric arrival of ions at the diaphragm is that they are extracted from the plasma and accelerated by an electrical potential V_d, which arises between the plasma and the ion side of the diaphragm during a tearing, in the stage preceding the development of arcs. This explanation requires further investigation.

Thus, we can make the following conclusion: Investigations of the surface of the T-3M diaphragm have estiblished that in tearing experiments the electrodynamic mechanism, causing arcs to form on the ion side of the diaphragm, was the dominant mechanism of diaphragm erosion. The formation of metal films on the ion side of the diaphragm indicates, first, that in tearing modes the plasma column comes into contact with the walls, despite the presence of the diaphragm. Second, metal ions either participate in directed motion along the torus with a velocity of $(2\text{-}4) \cdot 10^5$ cm/sec or are extracted from the plasma and accelerated by the electric potential in the raw material itself. The asymmetry of the electron and ion sides of the diaphragm during tearing must be taken into account when designing tokamak diaphragms.

LITERATURE CITED

1. Thermal Load on the TFR Tokamak Limiter During Additional Heating Pulses and Major Plasma Disruptions, TFR Group EUR-CEA-FC-1114, Fontenay-aux-Roses (1981).
2. S. V. Mirnov, Fiz. Plazmy, 7, No. 3, 687 (1971).
3. D. Baratov et al., in: Proc. X European Conf. on Controlled Fusion and Plasma Physics, Moscow (1981), Vol. 1, Paper J11.
4. S. Mirnov and I. Semenov, in: Proc. Conf. on Plasma Physics and Controlled Nuclear Fusion IAEA, Vienna (1977), Vol. 1, p. 291.
5. G. A. Lyubimov and V. I. Rakhovskii, Usp. Fiz. Nauk, 125, No. 4, 665 (1978).
6. V. Chicherov et al., J. Nucl. Mater., PA 93-94, 133 (1980).

PHOTONEUTRONS FROM THICK D_2O, Be and Pb CONVERTERS AT E_{max} = 15 MeV

A. V. Drobinin, M. Leonard,
and Yu. M. Tsipenyuk

UDC 539.164:539.172.3

Neutron escape is one of the basic channels of an excited nucleus. Neutrons may be emitted at various stages in a nuclear reaction. The energy spectrum of the decay products from an intermediate or heavy nuclide is due, in the main, to the decay of the compound nucleus, but it also contains a high-energy component corresponding to the decay of the ingoing state into the continuum; part of the spectrum is due to the preequilibrium decay from more complicated configurations. A recent survey [1] deals with the energy spectra of nuclides with A > 40.

In the case of light nuclide, we encounter a completely different situation: The nuclear levels are widely spaced and each of them has individual features. For example, photofission of the deuteron is in fact an extreme case of dividion of a nucleus into two fragments, namely a neutron and proton, while for beryllium we find 3-particle decomposition:

$$^9\mathrm{Be}+\gamma\rightarrow n+{}^8\mathrm{Be}\rightarrow n+{}^4\mathrm{He}+{}^4\mathrm{He}. \quad (1)$$

Fairly detailed experimental studies have been made of neutron emission from intermediate and heavy nuclides, but there are only a few papers on deuterium and beryllium. A study has been made [2] of the photoneutron spectrum at E_n > 2 MeV in terms of the recoil protons in stilbene for an electron energy of 17 MeV, while in [3] the process was examined at 85 MeV. A fairly surprising result was that the fine structure in the neutron spectrum is retained with this very large difference in the maximum spectrum energies. Also, in [3] there were two strong neutron groups with $E_n \approx 1$ MeV and $E_n \approx 3$ MeV.

The neutron carries off a definite energy in the breakup of the deuteron:

$$E_n=(E_\gamma-B_n)/2. \quad (2)$$

Here B_n = 2.23 MeV is the neutron binding energy and E_γ is the γ-ray energy. Therefore, the photoneutron spectrum should virtually reproduce the photon spectrum if a continuum is used. However, if heavy water is used as the converter, the spectrum is greatly altered by the neutron moderation. Calculations have been made [4] on the neutron spectra when D_2O is exposed to continuous spectra of various energies; however, we know of no experimental study on D_2O.

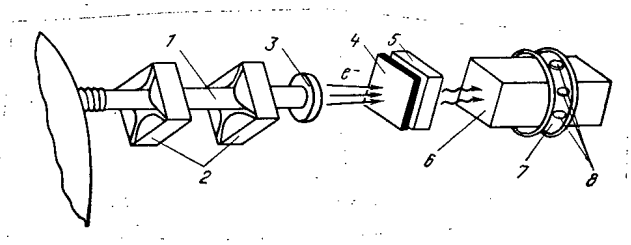

Fig. 1. Experiment scheme: 1) electron guide; 2) quadropole lenses; 3) exit window; 4) W target; 5) Al absorber; 6) neutron converter; 7) cadmium screen; 8) specimens.

Translated from Atomnaya Énergiya, Vol. 53, No. 6, pp. 398-399, December, 1982. Original article submitted April 16, 1982.

 0038-531X/82/5306-0858$07.50

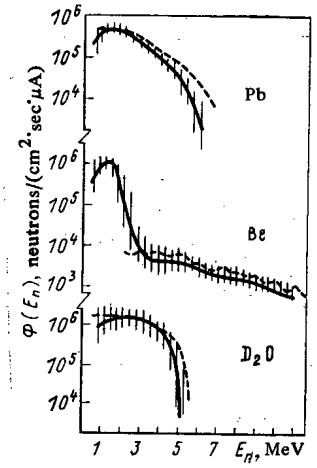

Fig. 2. Energy spectra of photoneutrons from Pb, Be, and D_2O for E_{max} = 15 MeV; the broken lines show the results of [8], [2], and [4].

As we lack information on photoneutrons from D_2O and Be, and as the substances are very important as neutron sources at low electron energies, we have measured the photoneutron spectra from these substances and Pb at an electron energy of 15 MeV and have also examined the scope for performing activation analysis using such photoneutrons. The choice of electron energy was not accidental. The yield of neutrons falls at lower energies, while at higher energies the major rock-forming elements begin to be activated by the γ rays.

The experiments were performed with a microtron with 17 orbits at the Institute of Physical Problems, Academy of Sciences of the USSR [5]. Figure 1 shows the system. The electron beam was extracted from the accelerator chamber through a thin aluminum window (thickness 0.15 mm) and was focused by a pair of quadrupole lenses into a spot of diameter 5 mm on the target, which consisted of 1 mm of tungsten and 10 mm of aluminum. Directly behind this target was the neutron converter made of one of these materials, dimensions 5 × 5 × 10 cm. The heavy water was contained in a thin tinplate box of the same dimensions.

The neutron spectra were recorded by means of threshold detectors [6], which were either pure substances (In, Al, Ni, Mg, Fe, Pb) or certain compounds [HgO, $(NH_4)_2HPO_4$, SiO_2] of mass 0.5-1 g. The detectors were set up in a circle around the converter in a cadmium screen. The gamma activity was determined by means of a Ge (Li) detector of volume 15 cm^3 and efficiency 1.5% for the ^{137}Cs line. The irradiation time was 15 min with an average beam current of 10 μA. The activation integrals were calculated from γ-activity measurements:

$$q = \frac{\lambda s \mu}{\eta_g \eta_\gamma x M N_A} \frac{1}{(1-e^{-\lambda t_1})(e^{-\lambda t_2}-e^{-\lambda t_3})}, \qquad (3)$$

where $\lambda = 0.693\ T_{1/2}$ is the decay constant; s, number of γ rays recorded; η_g, recording efficiency of the detector; η_γ, yield of quanta of a given energy per decay; x, abundance of the isotope used; μ, molecular mass of the compound; M, mass of the detector; N_A, Avogadro's number; and T_1, T_2, T_3, times for the end of the irradiation, the cooling period, and the measurement, respectively.

The values of the activation integrals constitute initial data for the calculation of the neutron spectrum from a system of integral equations

$$q_i = \int_0^\infty \varphi(E)\,\sigma_i(E)\,dE, \qquad (4)$$

where φ(E) is the unknown spectrum and σ(E) is the reaction cross section. System (4) was solved numerically by computer using maximum likelihood, which was first employed in such cases by Tarasko [7]. In some cases there were difficulties in correcting for the contributions of the photonuclear reactions to the γ activities of the detectors (Mg and Pb), so we performed a series of calculations on the spectra, with various numbers of activation integrals. Figure 2 shows the average results for the neutron spectra and the error range characterizing the spread in various forms of processing. Our results agree well with detailed

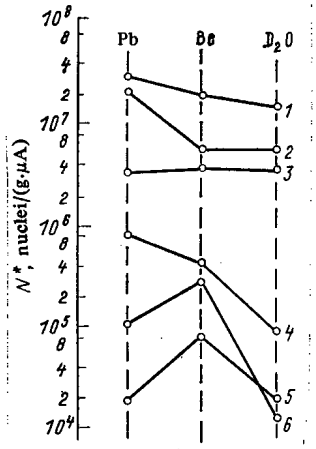

Fig. 3. Absolute yields of γ-active isotopes in natural mixtures of the elements In, Ni, Hg, Al, Fe, Si, formed by irradiation with photoneutrons from Pb, Be, and D_2O for 15 min at a distance of 3.5 cm from the axis of a converter of dimensions 5 × 5 × 10 cm: 1) In (n, n'); 2) Ni (n, p); 3) Hg (n, n'); 4) Al (n, p); 5) Fe (n, p); 6) Si (n, p).

measurements performed by neutron time-of-flight in lead [8], which indicates that the results with D_2O and Be are reliable.

The energy spectra have the following features: Most of the neutron spectrum from Pb at 15 MeV is [8] closely described by the evaporation model; at lower electron energies, the structure of the nuclear levels begins to make itself felt even for lead [9]; and the upper limit to the spectrum is naturally determined by the neutron binding energy.

In the case of the beryllium converter, there was a very gently sloping high-energy part of the spectra for E_n from 3-12 MeV, but the main contribution to the total neutron yield came from the low-energy part where $E_n \approx 1.5$ MeV. The latter is due not to the Maxwellian character of the spectrum but to cascade neutrons: Because the spectrum is widely spaced in ^{9}Be, the irradiation width Γ_γ and the neutron width Γ_n may be of the same order even at a high excitation energy, and therefore a process of (n, γn') type is possible, so the spectrum is enriched at low neutron energies. Also, the cross section for (γ, n) on ^{9}Be has peaks at quantum energies of 1.7 and 3 MeV, which correspond to the first levels of ^{9}Be; therefore, if we make allowance for the shape of the γ-ray spectrum, the contribution from the low-energy neutrons should be predominant. The spectrum is also softened by the partial moderation of the fast neutrons in the converter.

The neutron spectrum from D_2O differs from the spectra from Pb and Be in having a plateau at 1-4 MeV and then falling sharply in accordance with kinematic condition (2).

These features of the spectra make themselves felt in the yields of radioactive nuclides as shown in Fig. 3. For elements with low reaction thresholds [In (n, n'), Hg (n, n')] the yields of radioactive species are practically the same for all the neutron converters, whereas the yield is highest for the D_2O converter if the nuclide has a threshold in the range 3-5 MeV (Si, P), and reactions with high thresholds occur only with the photoneutrons from Be. This feature of photoneutron activation can be used in activation analysis with electron accelerators. According to (2), the upper boundary to the spectrum with the D_2O converter is a linear function of the electron energy.

The ratios between the fast-neutron fluxes from these converters and the absolute values are in good agreement with the results of [10, 11].

We are indebted to P. L. Kapitsa for interest, S. P. Kapitsa for useful discussions, and A. A. Kolosov and B. G. Korol'kov for technical assistance.

LITERATURE CITED

1. B. S. Ratner, Elem. Chast. At. Yad., 12, 1492 (1981).
2. M. Thompson and J. Taylor, Nucl. Phys., 76, 377 (1966).

3. R. Garfagnini, G. Pragino, and A. Zanini, Nuovo Cimento, 63B, 670 (1969).
4. T. Gozani, Radiation Engineering in the Academic Curriculm, IAEA, Vienna, 25 (1975).
5. S. P. Kapitsa et al., Prib. Tekh. Eksp., No. 1, 13 (1969).
6. E. A. Kramer-Ageev, V. S. Troshin, and E. G. Tikhonov, Activation Methods of Neutron Spectrometry [in Russian], Atomizdat, Moscow (1976).
7. M. Z. Tarasko, FÉI-156 Preprint, (1969).
8. I. Kimura et al., Ann. Rep. Res. Reactor Inst. Kyoto Univ., 3, 75 (1970).
9. N. Sherman et al., Phys. Rev. Lett., 35, 1215 (1975).
10. V. K. Brovtsyn, V. N. Samosyuk, and Yu. M. Tsipenyuk, At. Energ., 32, No. 5, 383 (1972).
11. Yu. N. Burmistenko, O. A. Val'dner, and A. V. Shal'nov, in: Accelerators [in Russian], Issue 10, Atomizdat, Moscow, (1968), p. 238.

DIRECT CHARGED-PARTICLE ENERGY CONVERSION IN A SYSTEM COMPOSED OF A MAGNETIC EXPANDER AND PLANAR COLLECTOR

S. K. Dimitrov and A. V. Makhin

UDC 621.039.637

Direct energy conversion should be used with charged particles emerging from plugs, in order to improve the efficiency of a fusion reactor based on an open trap and to solve the problem of cooling constructional components.

Several forms of converter have been described. Post's expander [1] has a periodic electrostatic retardation system and gives an efficiency of 0.8. A magnetic expander is required to transform the energy of rotation of the particles around the magnetic field $W_\perp$ into energy of motion along it $W_\parallel$. Model experiments in a system with oblique diaphragms [9] have given an efficiency of about 0.9. However, the dimensions of a real converter are always extremely large (about 100 m for one plug). One can reduce the dimensions substantially if magnetic expansion in one plane is replaced by a expander [3], whose dimensions along with the retardation system may be ~ 30 m.

We have examined the electron retardation in a conical magnetic expander with a planar collector. The electron beam (Fig. 1) lay at the top of a conical vacuum chamber with a semivertex angle of 30° in the region of maximum magnetic field. Beam parameters: diameter 3 cm, energy 500 eV, perveance 0.25, and divergence angle 45-60°. The magnetic field followed the law

$$B(z)=\frac{B_{\max}}{(Az+1)^2},$$

where $A = 0.29 \cdot 10^{-7}\frac{B_{\max}}{\sqrt{W_{\perp\,\mathrm{init}}}}$ in the inertial system and W_{init} is the initial energy of rotation of an electron around the magnetic field.

The retardation system consisted of grids C_1 and C_2, together with the collector K, and was placed at 30 cm from the gun. Grid C_1 was at ground potential to prevent the electric field from penetrating into the expander. Grid C_2 was the antidynatron one. Figure 2 shows the potential distribution on the electrodes. Figure 3 shows the retardation characteristics.

The recuperation performance η is given by

$$\eta=(I_c/I_0)(u_c/u_0),$$

where I_C is the current in the collector circuit; I_0, current entering the recuperator; and u_C, u_0, potentials of the collector and the gun cathode. The maximum efficiency of 0.7 was obtained with a degree of retardation $u_C/u_0 = 0.74$. The particles are retarded between C_1 and C_2, while C_2 is at a potential with respect to ground close to the cathode potential, so it is obvious that the degree of retardation in the region of this grid is considerably more than 0.74.

Translated from Atomnaya Énergiya, Vol. 53, No. 6, pp. 400-401, December, 1982. Original article submitted May 14, 1982.

0038-531X/82/5306-0861$07.50

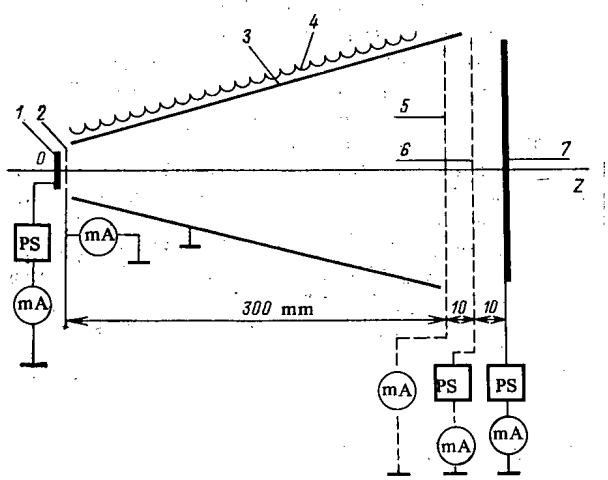

Fig. 1. The apparatus (PS power supply): 1) cathode; 2) anode; 3, 4) expander and winding; 5, 6) grids C_1 and C_2; 7) collector.

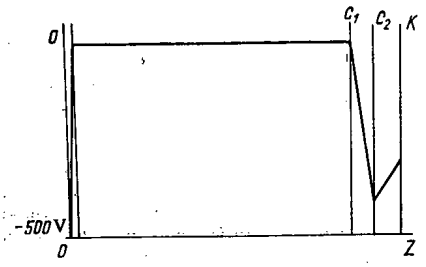

Fig. 2. Distribution of the potential φ along the system axis.

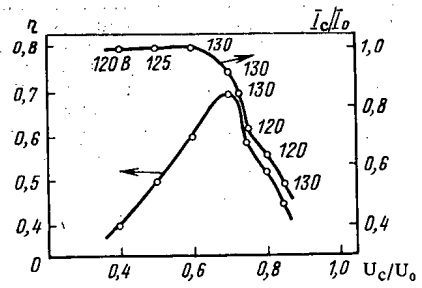

Fig. 3. Dependence of the efficiency η of the recuperator and the current collection factor I_c/I_0 on the degree of retardation u_c/u_0 (the numbers by the points are the optimum negative potentials on the grids C_2 relative to the collector).

The electric field was simulated with an electrolytic tank, which showed that the degree of retardation was 0.94 for the optimum potential distribution. In that case, about 90% of the particles passed through C_2 and fell on the collector (Fig. 3), which means that the angular spread in the beam at the entrance to the retardation system was reduced to 14° by conversion of $W_\perp$ to $W_\parallel$.

In the case of an ion beam in this system, where there is no need for an antidynatron grid, the latter was replaced by the collector, which would collect 90% of the particles with a degree of retardation of 0.94, i.e., $\eta \approx 0.85$.

Reactors currently being developed on the basis of ambipolar adiabatic traps can be used with such a converter even in the one-collector form to ease the conditions for heat removal and also to provide a plasma in the plug at zero potential, and the over all efficiency of the reactor is improved by about 1-3%. Here the ion collector is also at ground potential

and does not require an additional power supply. The real converter for the reactor was a cone with a semivertex angle of 30° and an overall length of ∿30 m.

LITERATURE CITED

1. R. Post, in: Proc. Conf. BNES on Nuclear Fusion Reactors, Paper 2.1, 88 (1969).
2. S. K. Dimitrov and V. V. Morozov, Nuclear Science and Engineering: Thermonuclear Synthesis Series [in Russian], Issue 2(8), 70 (1981).
3. R. Smith, UCRL-51373 (1973).

CURRENTS GENERATED IN PYROELECTRICS BY γ IRRADIATION

B. A. Levin

UDC 539.227

Since the first publications [1-3] which reported that pyroelectric detectors show promise as dosimeters, particularly for pulsed γ radiation, very few papers [4-6] have appeared on the use of pyroelectrics for the dosimetry of ionizing radiations.

We have investigated the individual components of the short-circuit current $I_{s.c.}$ or the charge generated in ferroelectric ceramics ZTP-19 (Zr–Ti–Pb), $BaTiO_3$, and a single crystal of $LiNbO_3$ under continuous and pulsed gamma irradiation at dose rates $W_\gamma = 16\text{-}3 \times 10^8$ R/sec (1 R = 2.58×10^{-4} C/kg). We have studied the effect of the input parameters of the pyroelectrics and of the irradiation conditions on the photovoltaic current and other components of the short-circuit current. For W_γ = 16-600 R/sec we used an arrangement with ^{60}Co, and for $W_\gamma = 10^3\text{-}4 \times 10^8$ R/sec we studied the effect of a single pulse of γ radiation of 2-3 msec duration at the IIN [7] and "Hydra" reactors.

We measured the photovoltaic emf (P_{ph}) for W_γ = 440-470 R/sec. Doses were measured with SGD-8 and IKS-A glass dosimeters. The irradiated samples were drenched with ceresin and placed in thin-walled metal capsules. Measurements were performed on ceramic samples 20 mm in diameter and 2 and 0.5 mm thick (unpolarized samples of ZTP-19) with Ag electrodes. The 10 × 10 × 2 mm $LiNbO_3$ crystal had an iron content < 10^{-4}–10^{-5}%. The large faces of the crystal were coated with a layer of Aquadag. The pyroelectric coefficients γ_o for ZTP-19 and $LiNbO_3$ were measured by a steady-state method using the charge of a large capacitor. The value of E_{ph} was found from the experimentally determined dependence of the steady component of $I_{s.c.}$ on the external load resistance (0-10^{11} Ω), and also by measuring the potential drop across the electrodes of the pyroelectric with an electrostatic voltmeter. The values of E_{ph} at room temperature were 500-680 V/cm for ZTP-19 ($\gamma_o \approx 38.7$ nC/cm² • K). For an unpolarized sample E_{ph} = 0; for $LiNbO_3$, 50 V/cm ($\gamma_o \approx 5.3$ nC/cm² • K); for $BaTiO_3$, 95 V/cm (γ_o = 19-40 nC/cm² • K). At 60-70°C, E_{ph} = 25 V/cm for $BaTiO_3$.

Under steady irradiation $I_{s.c.}$ was measured with a low input impedance electrometric amplifier. Under pulsed irradiation the charge on the electrodes of the pyroelectric was measured and "stored" in an RC circuit with a time constant of 1.5 sec. The charge–discharge signal from the RC circuit was amplified by an electrometric amplifier with an input impedance of more than 10^8 Ω, and recorded on the screen of an S-1-29 storage oscillograph. Under steady irradiation conditions the curves for the time dependence of $I_{s.c.}$ generally have the shape shown in Fig. 1. At the instant certain samples of ZTP-19 are introduced into the irradiation zone, a current appears in the opposite direction; this disappears with repeated introduction of the sample into the irradiation chamber. Evidently the observed effects are due to screening currents of spontaneous polarization by excess carriers, or the effect of the latter on possible electret states. The peaks on the $I_{s.c.}$ curve observed as the sample is introduced into and withdrawn from the irradiation zone are due to the pyroelectric current I_{py}. The steady component I_s of the short-circuit current is related to the photovoltaic I_{ph} and Compton I_c components. The latter is approximately proportional to W_γ, does not depend on the magnitude or direction of polarization, and results from ionization currents produced in the pyroelectric and cable by Compton electrons. The value and sign of I_c for a steady W_γ depends on the orientation of the sample in the irradiation chamber. Measurements showed that I_{ph} varies by a factor of 1.5-2 in samples of the same size with the same values of γ_o.

Translated from Atomnaya Énergiya, Vol. 53, No. 6, pp. 401-402, December, 1982. Original article submitted January 25, 1982.

0038-531X/82/5306-0863$07.50

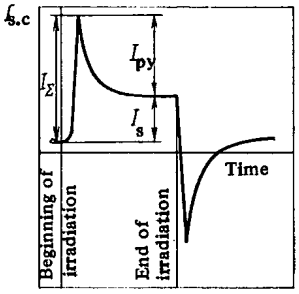

Fig. 1. Time dependence of $I_{s.c.}$ in pyroelectrics under steady gamma irradiation.

There is a tendency for I_{ph} to increase with increasing γ_o. The value of I_{ph} in ZTP-19 samples with $\gamma_o \leqslant 10$ nC/cm² • K is comparable with I_c. The values of $I_{s.c.}$ and its components were measured for dose rates W_γ = 16-600 R/sec for a sample of ZTP-19 with $\gamma_o \approx 38.7$ nC/cm² • K. The measurements showed that I_{ph} and I_c vary linearly with W_γ. The current densities j_{ph} and j_c corresponding to these components are 1.2 and 0.13 (pA/cm²)/(R/sec), respectively. The current density j_{py} corresponding to I_{py} is $\sim$ 0.8 (pA/cm²)/(R/sec). The dependence of I_{ph} on the radiation dose was studied for one ZTP-19 sample with $\gamma_o \approx 25$ nC/cm² • K. The sample was irradiated for 690 h at 60-70°C. The radiation dose was 1565 MR. Within the limits of error of the measurements (±5%), I_s remained constant. Within these same limits, a change in temperature of the sample did not affect this part of $I_{s.c.}$. The observed increase in I_{py} can be completely attributed to the increase of γ_o with temperature [3, 8]. Experiments of the temperature dependence of γ_o show that in the range 20-70°C the relative change in γ_o per degree in various samples of ZTP-19 is 1-2%. When the temperature of a $BaTiO_3$, sample was increased to 60-70°C, I_s was halved. In measuring the charge generated in a ZTP-19 sample ($\gamma_o \approx 38.7$ nC/cm² • K) when irradiated by a 2 msec pulse of gamma radiation, it was established that for $W_\gamma \approx 2 \times 10^4$-$2.9 \times 10^8$ R/sec the total surface charge density j_Σ was 1.05 (pC/cm²)/R (mean square error ±0.08).

The contribution to the total charge from I_c was $\sim$ 20% in measurements made near the reactor core, and $\sim$ 6% at distances > 2-3 m from the core. Taking account of the contribution from I_c decreases j_Σ to 0.9 (pC/cm²)/R. For $W_\gamma < 2 \times 10^4$ R/sec, fluctuations are observed in j_Σ and in the leading edge of the charge-discharge pulse. For $W_\gamma = 1.5 \times 10^3$-$2 \times 10^4$ R/sec, j_Σ varies from 1 to 1.9 (pC/cm²)/R, and the leading edge varies from a few milliseconds to 400-500 msec. The maximum value of j_Σ = 1.9 (pC/cm²)/R for $W_\gamma = 1.5 \times 10^3$ R/sec. To determine the contribution of the pyroelectric charge to j_Σ under adiabatic conditions, we measured the temperature increase of a ZTP-19 calorimeter as a result of irradiating it with a pulse of reactor radiation with $W_\gamma = 3.6 \times 10^7$ R/sec. The value of the pyroelectric charge density γ_d, found from the temperature increase of the calorimeter per Roentgen (3×10^{-5} °C/R) and the value of γ_o, was 1.16 (pC/cm²)/R. The mean square error of the determination of the pyroelectric charge density was $\sim$ ±15%. From measurements of the temperature increase of the calorimeter and the specific heat of ZTP-19 (440 J/kg • °C) [9], the total absorbed energy was found to be 1.3 rd (ZTP-19)/R. The corresponding pyroelectric charge density was γ_d = 0.88 (mean square error ±0.15). The conversion factor ($\sim$ 1) from R to rd (ZTP-19) for ^{60}Co gamma radiation was found by calculating the ratio (1.08) of the energy absorption in ZTP-19 and water. The energy absorption coefficients of the elements constituting these compounds [10] were used in the calculations. The conversion factors obtained were used to determine the pyroelectric charge density γ_d from the values of j_Σ and j_{py}, measured for pulsed and continuous irradiation, respectively. The values found in this way, $\gamma_d = (7 \pm 1.1) \times 10^{-1}$ (pC/cm²) rd (ZTP-19) and $(7.7 \pm 1.1) \times 10^{-1}$ (pC/cm²)/rd (ZTP-191 are in good agreement with one another and, within the limits of error of the measurements, with the value $(8.8 \pm 1.5) \times 10^{-1}$ (pC/cm²) rd (ZTP-19) calculated for this sample from γ_o and the specific heat. A comparison of j_Σ 0.9 (pC/cm²)/R and γ_d = 1.16 (pC/cm²)/R shows that they agree within the limits of error of the measurements, and that there is no contribution to j_Σ from j_{ph}. The increase in j_Σ (to values measured under steady irradiation) with a decrease in W_γ of pulsed irradiation and the appearance of a slow component in the charge-discharge capacitance pulse can be explained by the relative increase in the contribution of I_{ph} to I_Σ. For $W_\gamma > 2 \times 10^4$ R/sec, I_{ph} reaches saturation and doses not depend on $W\gamma$. The agreement between j_Σ and γ_d obtained in [1, 3] for a ZTP sample $Pb(Zr_{0,65}\ Ti_{0,35})O_3$ + 1 wt. % Nb_2O_5 (γ_o = 30 nC/cm² • K) is related to this same effect of I_{ph} saturation for $W_\gamma > 10^6$ rd (H_2O)/sec. The agreement obtained by these same authors [2, 3] between $j_\Sigma \approx 1$ (pA/cm²)/(rd (H_2O)/sec) and the pyroelectric current

density 0.6 (pA/cm^2)/(rd (ZTP)/sec) for W_γ = 245 rd (H_2O)/sec is clearly incorrect for the following reasons: 1) Their use of an incorrect value (1.65) of the conversion factor from rd (H_2O) to rd (ZTP) (it is appreciably different from the calculated value 1.08); 2) the identification of $j_\Sigma = j_{py} + j_s$ [j_{py} = 0.7 (pA/cm^2)/(rd (H_2O)/sec); $j_s \approx 0.3$ (pA/cm^2)/(rd (H_2O)/sec)] with j_{py}. (It is possible that in this case the pyroelectric current I_{py} is superimposed on I_s). In $BaTiO_3$ the current densities j_s, j_{py}, and j_Σ vary by factors of 2-3 from irradiation to irradiation. Probably this can be explained by the fact that the temperature of the sample (15-25 °C) was close to the phase transition temperature (13 °C) [18]. This transition probably affects the decrease of E_{ph} (by approximately a factor of 4) and I_s (by a factor of 2) measured at 60-70°C. For both steady and pulsed irradiation $W_\gamma = 7 \times 10^4$ - 3.6×10^7 R/sec), j_{py} and j_Σ are changed within these same limits. Evidently this is related to the manifestation of the saturation effect of I_{ph} in $BaTiO_3$ for large values of W_γ. Measurements of I_{ph} and I_c in $LiNbO_3$ for W_γ = 16 and 600 R/sec show that $j_{ph} = (3\text{-}4) \times 10^{-1}$ (pA/cm^2)/(R/sec), and j_c is within the same limits as in ZTP-19; I_{py} is observed separately in $LiNbO_3$ only when I_{ph} and I_c have opposite signs. The values of γ_0 found from I_{py} and the specific heat [11] exceed the directly measured value of γ_0 (5.3 nC/cm^2 • K) by more than a factor of 1.5. Repeated introduction of the sample into the irradiation zone causes a decrease in I_{py}. Measurement of j_Σ for $LiNbO_3$ for $W_\gamma = 16\text{-}4 \times 10^8$ R/sec shows that in the range 10^3-10^5 R/sec there is a quite pronounced anomaly, manifesting itself in a change of sign and in a sixfold increase in j_Σ. When W_γ is increased, the sign of j_Σ is restored, and its value approaches (5-6) $\times 10^{-1}$ (pC/cm^2)/R measured for steady γ irradiation. This anomaly may be caused by screening currents with a different polarity which "saturate" with increasing W_γ. The relatively large j_{ph} and small E_{ph} in $LiNbO_3$ (as for x rays [12]) is due to the conductivity produced by carriers which do not take part in the generation of E_{ph}.

LITERATURE CITED

1. D. Hester, D. Glower, and L. Overton, IEEE Trans. Nucl. Sci., NS-11, No. 5, 145 (1964).
2. D. Glower and D. Hester, Trans. Am. Nucl. Soc. Ann. Meeting 8, No. 1, 66 (1965).
3. D. Hester and D. Glower, Nucl. Appl., 2, 41 (1966).
4. D. A. Kaushanskii, V. M. Pluzhnikov, and B. P. Glazunov, in: Effect of High-Energy Radiation on Catalysts and Polypropylene [in Russian], Naukova Dumka, Kiev (1974), p. 83.
5. L. S. Kremenchugskii and R. Ya. Strakovskaya, At. Energ., 41, No. 3, 190 (1976),
6. R. Ya. Strakovskaya, L. S. Kremenchugskii, and G. A. Dimoglo, Prib. Tekh. Eksp., No. 5, 61 (1976).
7. A. I. Smirnov, V. M. Talyzin, and V. E. Khvostionov, Preprint IAE-1962, Moscow (1968).
8. W. Cook, D. Berlincourt, and F. Scholz, J. Appl. Phys., 34, No. 5, 1392 (1963).
9. L. S. Kremenchugskii and O. V. Roitsina, Prib, Tekh. Eksp., No. 3, 7 (1976).
10. E. Storm and H. Israel, Nucl. Data Tables, Sec. A, 7, No. 6 (1970).
11. V. K. Novik, N. D. Gavrilova, and N. B. Fel'dman. Pyroelectric Transducers [in Russian], Sov. Radio (1979).
12. O. Schirmer, J. Appl. Phys., 50, No. 5, 3404 (1978).

REACTOR TESTS OF TWO THERMOEMISSION ELECTRIC POWER GENERATING ELEMENTS IN A SINGLE LOOP CHANNEL

V. P. Baril'chenko, V. P. Berzhatyi, A. S. Karnaukhov,
V. P. Kirienko, V. A. Maevskii, V. K. Morozov,
A. V. Nikonov, N. N. Parkhomenko, V. S. Pastukhov,
V. V. Sinyavskii, and Yu. A. Sobolev

UDC 621.039.572

An important stage for the technical achievement of thermoemissive energy conversion is the complex reactor investigations of the thermoemission electric power generating elements (EPGE) and multielement assemblies [1-3]. One of the problems of these tests is the verification of the reproducibility and stability of the power generating characteristics of EPGE of the same kind. Comparison of the results of EPGE tests or tests of EPGE assemblies, conducted nonsimultaneously, is not always correct, in view of the different test conditions. It is difficult to ensure identical working parameters in different tests, e.g., heat release, temperature of individual components of the channel, pressure of the working substance, etc. Therefore, in order to eliminate this indeterminacy it is desirable to test the individual EPGE or their assemblies simultaneously and in one loop channel. For this purpose, a loop channel was developed and tested, with two independent identical EPGE.

Construction of Experimental Assembly. The general form of the experimental assembly with individual EPGE is shown in Fig. 1. The cylindrical emitter with a diameter of 0.01 m and a length of 0.022 m is made of tungsten–rhenium alloy (27% Re), and, by means of a metal crosspiece of niobium foil, was braced to the current lead. The emitter contains pellets of UO_2. The current lead was joined with a leak-tight inlet fitting by a flexible link of an assembly of foils. In the lower cover of the emitter, there is a channel with a diameter of $5 \cdot 10^{-4}$ m and a length of $9 \cdot 10^{-3}$ m for the extraction of gaseous fission products. The emitter was aligned along the axis with a rod and rigid metal arresting devices for the inter electrode jumpers. In the spacing system there are also two continuous bands of beryllium-oxide spacers, installed in the cylindrical grooves of the collector. The niobium collector was at the same time hermetically sealed to the casing of the EPGE. In the upper part it was joined by a vacuum seal to the leak-tight assembly and the current busbar, and the lower part was joined to the nozzle leading to the vacuum–cesium system.

It was proposed to test the elements over a wide range of electric power density. Therefore, the conditions of optimum dimensions of the coaxial EPGE, considered in [4], specified the choice of a smaller length than for the tests, e.g., of the ES-1-1 element [2]. By comparison with [2], the initial interelectrode gap also was reduced to $(1.4\text{-}1.6) \cdot 10^{-4}$ m.

Two experimental assemblies with identical EPGES were installed in graphite sleeves of the heat removal system of the loop channel. The cesium thermostat, located in the lower part of the loop channel, was common for these assemblies. The vacuumization system of the loop channel also was common, and consisted of an external pumping-out system and an ion-getter pump built into the channel [1]. The loop channel with the electric power generating elements was installed in a cell of a VVR beryllium reflector.

Comparison of the Characteristics of the Two Elements. The main problem of the investigations was the comparison of the characteristics of two similar EPGE in reactor conditions over a wide range of electric power density. Because, in the first and last stages of the lifetime tests, one of the elements functioned unstably, an accurate comparison of the results of the investigations can be conducted only for the second stage of the tests (from 180 to 270 h of the lifetime), when a normal stable operation of both elements was observed. In this period, almost total coincidence of all the power generating characteristics was observed. For example, the static volt–ampere characteristics coincide in both the slope and the absolute value. The characteristics were determined for a volume heat release density in the core of the emitter of $5.2 \cdot 10^8$ W/m^3, a temperature of the cesium thermostat of 380°C, and a temperature of the collector of 800-850°C.

Translated from Atomnaya Énergiya, Vol. 53, No. 6, pp. 402-404, December, 1982. Original article submitted January 18, 1982.

 0038-531X/82/5306-0866$07.50

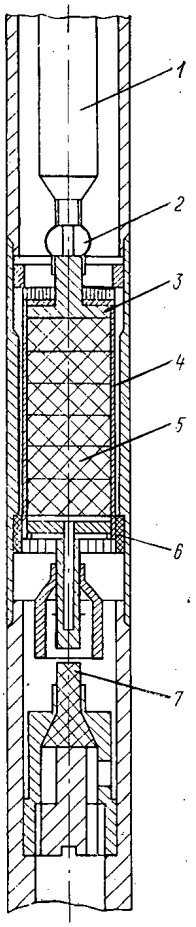

Fig. 1. General view of the experimental assembly: 1) current lead; 2) crosspiece; 3) spacers; 4) EPGE emitter; 5) uranium-dioxide pellets; 6) cover; 7) ceramic rod.

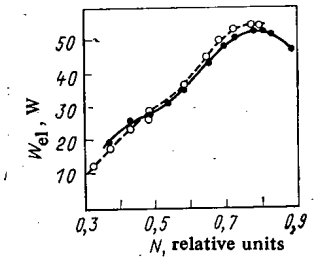

Fig. 2. Dependence of the electric power of the elements EPGE-1 (o) and EPGE-2 (●) on the thermal power of the reactor.

An identical change of other characteristics was also observed, in particular the dependence of the electric power W_{el} of the EPGE on the thermal power of the reactor N, the cesium vapor pressure P_{Cs}, and the temperature of the collector T_c. The optimum values of the temperature of the collector and the cesium vapor pressure almost coincided, For example, for an average electric power density $W = (1.2\text{-}1.4) \cdot 10^5$ W/m^2, the optimum temperature of the collector T_c^{opt} for both elements amounted to 740-760°C. The optimum cesium vapor pressure for these same values of the electric power corresponded to a temperature of the cesium thermostat of T_{Cs} = 380-390°C, i.e., it was higher than the value of T_c^{opt} obtained in similar conditions when testing multielement assemblies with an interelectrode gap of $3 \cdot 10^{-4}$ m [3]. With T_{Cs} = 350-400°C, the characteristics of both elements were almost independent of T_{Cs}, and were almost linear, with an identical slope.

In individual cases, a small difference of the characteristics was observed, which can be

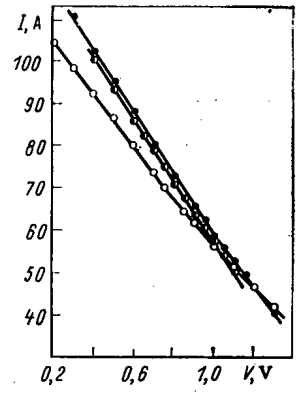

Fig. 3. Dependence of the change of static volt–ampere characteristics of the EPGE-2 on the lifetime tests: ●, ◐, and o) 61, 118, and 169 h, respectively.

explained, nevertheless, by slight differences of the test conditions of the two EPGEs (Fig. 2). Because the characteristics of the heat removal system of the two EPGEs were slightly different, the temperature of the EPGE-1 collector was always 20-40°C higher than for the EPGE-2. The temperature of the collectors of both EPGEs, determined as $T_{C_{1,2}} = T_W + T_{1,2}(q)$ (T_W is the temperature of the cooling water, and $T_{1,2}(q)$ is the temperature drop in the heat removal system, depending on the thermal flux), increased with increase of the thermal power of the reactor. The temperature of the EPGE-2 collector was close to the optimum for a low thermal power of the reactor, and for EPGE-1 it was close to the optimum for a high reactor power. As a result, the electric power of EPGE-1 was slightly lower than the electric power of EPGE-2 for a low thermal power, and slightly higher for a high thermal power (see Fig. 2).

The approximately identical initial change of the characteristics, similar to those observed in the course of the reactor tests of the ES-6-3 assembly [4], should also be noted; they are expressed in an increase of the volt–ampere characteristics (increase of current for a short circuit, and a reduction of the effective value of the no-load voltage), which obviously is due to internal surface phenomena in the thermoemission converter, which lead to an increase of the effective vacuum performance of the emitter (Fig. 3). A change of slope of the characteristic curve occurred most intensively at the start of the tests and continued during 250-300 h; it then gradually slowed down and ceased.

Thus, during tests of two identical thermoemission EPGEs over a quite wide range of electric power, it was established that for their normal operation almost complete coincidence of the characteristics was observed. Deviations of the characteristics, due to possible random variations in the manufacturing technology or to other uncontrollable conditions, were not detected.

LITERATURE CITED

1. V. I. Berzhatyi et al., At. Energ., 31, No. 6, 585 (1971).
2. V. I. Berzhatyi et al., Zh. Tekh. Fiz., 42, No. 11, 2439 (1972).
3. E. S. Bekmukhambetov et al., At. Energ., 35, No. 6, 387 (1973).
4. V. V. Sinyavskii, Zh. Tekh. Fiz., 44, No. 3, 599 (1974).

INDEX

SOVIET ATOMIC ENERGY

Volumes 52-53, 1982

SOVIET ATOMIC ENERGY

Volumes 52-53, 1982

(A translation of Atomnaya Énergiya)

A

Abdukadyrova, I. Kh. - 183, 498
Abramov, B. D. - 783
Adadurov, A. F. - 205
Adamovskii, L. A. - 164
Afrikanov, I. N. - 421
Akap'ev, G. N. - 652
Akrachkova, L. L. - 768
Alekhin, I. A. - 546
Aleksakov, A. N. - 285, 747
Aleksakov, G. N. - 724
Aleksandrov, V. D. - 422
Alekseenko, N. N. - 491, 734
Alekseev, É. F. - 690
Alekseev, P. N. - 67
Alekseev, Yu. A. - 112
Alekseeva, I. S. - 272
Aleshin, A. A. - 356
Alimov, V. Kh. - 443
Al'tovskii, I. V. - 443
Anan'ev, E. P. - 10
Andreeva, A. B. - 10
Andronov, V. A. - 797
Androsenko, A. A. - 123
Androsenko, P. A. - 123
Antonov, V. A. - 778
Antonov, V. L. - 587
Anufriev, V. A. - 478
Apel', P. Yu. - 652
Arinkin, F. M. - 438, 778
Arkhipkin, V. M. - 673
Arm, E. M. - 794
Avramov, A. M. - 95
Azizov, É. A. - 112

B

Babad-Zakhryapin, A. A. - 254, 272
Babadzhanyants, N. V. - 559
Babenko, A. G. - 673
Babenko, S. P. - 546
Babich, S. I. - 478
Bagdasarov, Yu. E. - 1
Balaev, V. I. - 797
Barabanova, A. V. - 546
Baranov, I. A. - 331, 559
Baranov, V. N. - 803
Baratov, D. G. - 854
Barenbaum, A. A. - 410
Baril'chenko, V. P. - 866
Barit, I. Ya. - 424
Barkovskii, A. N. - 150
Baronov, V. A. - 528
Barsov, P. A. - 209
Bashilov, S. M. - 638
Batyrbekov, G. A. - 438, 778
Bazhin, V. G. - 24
Bekmukhambetov, E. S. - 727
Bekmurzaeva, Z. B. - 438
Belanova, T. S. - 841
Belokopytov, V. S. - 753
Belovodskii, L. F. - 251
Belyakov, V. P. - 103
Bergman, A. A. - 403
Berzhatyi, V. P. - 866
Berzina, I. G. - 648
Bespalov, D. F. - 283
Bibichev, B. A. - 596, 669
Bilenko, V. I. - 800
Blinkin, V. A. - 720
Blyskavka, A. A. - 778
Bobkov, A. F. - 254
Bobkov, Yu. V. - 690
Bobrov, Yu. G. - 128, 638
Bochvar, I. A. - 149
Boldyrev, V. M. - 664
Bol'shakov, E. P. - 458
Bondarenko, A. V. - 270
Bondarenko, Yu. I. - 193
Bondars, Kh. Ya. - 436
Borisovskii, A. F. - 135
Brevnov, N. N. - 112
Budnikov, A. T. - 758
Bulanenko, V. I. - 622
Bulgakov, Yu. V. - 512
Bulovich, V. - 296
Burmistenko, Yu. N. - 714
Bushkovskii, V. S. - 753
Bushuev, A. V. - 776
Butra, F. P. - 690
Bychkov, A. S. - 187
Bykhovskaya, T. A. - 319

C

Chachin, V. V. - 776
Chebyshev, V. M. - 707
Chechetkin, Yu. V. - 10, 738
Chelnokov, O. I. - 202
Cherdantsev, Yu. P. - 202
Cherednichenko-Alchevskii, M. V. - 393, 417, 419, 421
Cherednichenko-Alchevskii, V. M. - 443
Cherepkov, V. G. - 74
Chernikov, V. N. - 396
Chernobrovin, V. I. - 458
Chernobrovkin, Yu. V. - 374
Chernov, I. I. - 396, 533, 697
Chernov, I. P. - 202
Chernova, A. A. - 351
Chernyi, S. S. - 805
Chervinskii, Yu. F. - 565
Chetverikov, V. V. - 551
Chetvertkov, V. I. - 458
Chirkst, D. É. - 327
Chuev, V. I. - 443, 690
Chuvilin, D. Yu. - 422
Chuyanov, V. A. - 112

D

Daukeev, D. K. - 727
Davies, J. A. - 324
Demenyuk, V. N. - 251
Demichev, V. F. - 112
Demin, N. A. - 785
Dem'yanenko, V. N. - 854
Denisov, A. A. - 577
Desyatnik, V. N. - 427, 565
Devdariani, O. A. - 642
Devochkin, A. V. - 141
Dianov, E. M. - 797
Dimitrov, S. K. - 861
Dmitriev, P. P. - 99
Dmitriev, S. A. - 707
Dmitriev, V. S. - 19
Dmitrieva, Z. P. - 99
Dolgov, V. M. - 43
Doroshenko, G. G. - 432
Drobinin, A. V. - 858
Drozdova, L. P. - 587
Drushchits, A. V. - 648

Drutman, K. D. - 340
Duba, V. V. - 195
Dubinin, A. A. - 572
Dubrovskii, I. S. - 10
Dulin, V. A. - 213
Dushin, P. G. - 270
Dyadin, Yu. V. - 714
Dymkov, Yu. M. - 45
Dynin, E. A. - 381
Dzantiev, B. G. - 87, 764

E

Efimov, V. N. - 164
Eliseenkova, S. A. - 319
Elokhin, A. P. - 440
Emel'yanov, E. I. - 270
Emel'yanov, I. Ya. - 157, 285, 515, 747
Emel'yanov, V. S. - 157, 515
Eperin, A. P. - 141, 828
Ermakov, A. N. - 87, 764
Erokhin, K. M. - 736
Eshcherkin, V. M. - 10

F

Fabritsiev, S. A. - 494
Fedik, I. I. - 504, 506
Fedorov, S. A. - 482
Fedoseev, V. E. - 738
Fedotov, P. I. - 596, 669
Fedotova, L. P. - 351
Fefelov, P. A. - 145
Filatov, V. M. - 19
Finkel', É. É. - 768
Flerov, G. N. - 652, 714
Fokin, V. P. - 854
Fomin, V. I. - 199
Fotchenkov, A. A. - 183
Frolov, V. V. - 622

G

Gaevoi, V. K. - 251
Galiev, N. B. - 147
Galkin, N. P. - 45
Galkov, V. I. - 334, 776
Gataullin, N. G. - 738
Gavrilin, A. I. - 29, 738
Gavrilyuk, S. A. - 724
Gazizov, R. K. - 753
Gel'perin, I. I. - 773
Gese, A. - 241
Gimadova, T. I. - 149
Ginzburg, S. R. - 546
Gizatulin, Sh. Kh. - 438
Glazunov, M. P. - 272
Glazyrin, A. M. - 690
Glebov, I. A. - 112
Glukhikh, V. A. - 103, 112, 458
Glushkov, E. S. - 743
Gol'din, M. L. - 144
Golikov, I. V. - 690
Golovanov, A. G. - 576
Golovanov, V. N. - 753
Golovchenko, Yu. M. - 791
Golovin, I. N. - 117, 655
Gol'tsov, V. A. - 145, 482
Golubchikova, I. G. - 673
Golubnichii, P. I. - 331
Goncharov, E. E. - 697
Gordeeva, G. V. - 854
Gorodetskii, A. E. - 443
Grabovskii, E. V. - 458
Grachev, N. S. - 24
Grebennik, V. S. - 365
Grigorov, V. P. - 805
Grigorovich, B. V. - 690
Grushkova, É. D. - 496
Gruzdeva, A. A. - 587
Gudkov, A. N. - 576
Gul'ko, V. M. - 280
Gurevich, N. Yu. - 277
Gur'yanov, G. M. - 128, 638
Guseinov, A. G. - 123
Gusev, É. B. - 648
Gusev, O. A. - 458
Guseva, M. I. - 202, 303, 341, 396, 697, 854
Gverdtsiteli, I. G. - 487, 489

H

Howe, L. M. - 324

I

Ibragimov, Sh. Sh. - 781
Ignatenko, E. I. - 436
Il'inskii, A. A. - 794, 797
Ilyasov, V. M. - 673
Ilyushkin, A. I. - 572
Ioltukhovskii, A. G. - 633
Isaenkova, M. G. - 299
Isakova, L. Ya. - 306
Iskhakov, K. A. - 123
Istomin, Yu. A. - 458
Ivanov, M. V. - 533
Ivanov, S. M. - 303, 341
Ivanov, V. P. - 91
Ivannikov, V. P. - 825

K

Kadomtsev, B. B. - 103, 112
Kagan, A. M. - 773
Kalandarishvili, A. G. - 487, 489
Kalashnikov, M. V. - 331
Kalin, B. A. - 396, 533, 697, 837
Kalinin, V. P. - 365
Kalinkin, Yu. A. - 732
Kaminskii, V. A. - 642
Kanishchev, V. N. - 832
Kantor, M. M. - 633
Kantsedalov, V. G. - 465
Kaptel'tsev, A. M. - 690
Kapyshev, V. K. - 145
Karasev, B. G. - 112
Karasev, V. B. - 519
Karnaukhov, A. S. - 866
Karus, E. V. - 797
Katanaev, A. O. - 43
Katrich, N. P. - 758, 832
Katyshev, S. F. - 427, 565
Kavun, A. M. - 103
Kazakov, V. V. - 356
Kazanskii, Yu. A. - 213, 229
Kazantsev, V. V. - 576
Kebadze, B. V. - 164, 374
Kenzhebaev, Sh. - 317
Kham'yanov, L. P. - 825
Kharlamov, Yu. M. - 187
Khenven, A. R. - 732
Kholev, S. R. - 266
Khomchik, L. M. - 707
Khudasko, V. V. - 24
Khudyakov, A. V. - 173
Kirienko, V. P. - 866
Kirillov, P. L. - 24
Kirillovich, A. P. - 469, 753
Klemin, A. I. - 157, 515
Klimentov, V. B. - 487
Klykov, L. M. - 417, 419
Koba, Yu. V. - 458
Kobozev, M. G. - 123
Kobylyanskii, V. V. - 187
Kochevanov, V. A. - 199
Kolchin, V. A. - 386
Koldobskii, A. B. - 576
Kolobashkin, V. M. - 576
Kolomenskii, A. V. - 209
Kolomiets, N. F. - 280
Kolesov, V. E. - 572
Kolosovskii, A. G. - 403
Kolotinskii, V. N. - 633
Komarov, A. V. - 849
Komin, S. F. - 561
Kondrat'ko, M. Ya. - 629
Konev, V. N. - 473
Konobeev, Yu. V. - 563, 785
Konoplenko, V. P. - 299
Kornilov, V. A. - 525
Korotenko, M. N. - 487
Korotkov, V. P. - 334
Koryakin, Yu. I. - 515
Kosheleva, T. A. - 251

Koskinen, Eeva - 49
Kostenko, A. I. - 103
Kostromin, A. G. - 555, 270
Koltunova, E. S. - 235
Kovalenko, V. D. - 103
Kovalenko, V. V. - 576
Kovarskii, A. P. - 128, 638
Kovyrshin, V. G. - 570
Kozachok, I. A. - 787
Kozhevnikov, O. A. - 697
Kozlov, F. A. - 682
Kozlov, S. K. - 587
Kozlov, V. F. - 825
Kozlov, Yu. D. - 496
Kozlovskii, K. I. - 280
Kraiko, A. V. - 292
Kraitor, S. N. - 432, 546
Krasheninnikov, I. S. - 577
Kravchuk, S. P. - 177
Krayushkin, A. V. - 816
Krayushkin, V. V. - 496
Krivonosov, S. D. - 487
Krivtsov, A. S. - 572
Krsheminskii, V. S. - 74
Krtil, I. - 296
Kruglov, A. K. - 79
Kruglov, V. P. - 699, 673, 825
Krutikov, P. G. - 83, 141
Kruzhilin, G. N. - 10
Krylov, V. A. - 112
Kuchikhidze, V. A. - 489
Kudlenko, V. G. - 331
Kudryavtsev, A. V. - 724
Kudryavtsev, V. A. - 91
Kukavadze, G. M. - 254
Kuksanov, N. K. - 768
Kulichenko, V. V. - 707
Kulik, V. V. - 787
Kulikauskas, V. S. - 648
Kulikov, E. V. - 10
Kulikov, V. I. - 150, 729
Kulikov, V. I. - 553
Kurbatov, D. K. - 361
Kurbatov, I. M. - 348
Kurbatov, N. N. - 427
Kushnereva, K. K. - 432, 546
Kushnikov, V. V. - 528
Kut'in, L. N. - 217
Kutuzov, A. A. - 776
Kuzin, A. P. - 145
Kuzin, E. N. - 229
Kuz'min, L. E. - 424
Kuz'mina, I. A. - 169
Kuz'minov, B. D. - 536
Kuznetsov, I. A. - 1, 274
Kuznetsov, M. G. - 655
Kuznetsov, O. L. - 797
Kuznetsov, V. I. - 652
Kuznetsova, G. A. - 149
Kuznetsova, T. V. - 432

L

Lapenas, A. A. - 436
Lapin, A. N. - 697
Lapshev, O. B. - 587
Larionov, B. A. - 112
Latmanizova, G. M. - 458
Latyshev, V. V. - 145, 482
Lavrinovich, Yu. G. - 469, 753
Lazurik, V. T. - 205
Leonard, M. - 858
Leonchuk, M. P. - 190
Leonov, E. S. - 432
Leont'ev, G. G. - 14, 828
Lepikhov, A. N. - 173
Leppik, P. A. - 370
Levin, B. A. - 863
Lifanov, S. I. - 576
Lifant'ev, A. N. - 19
Lifits, A. L. - 277
Linev, A. F. - 280
Lityaev, V. M. - 229
Lobov, V. I. - 436
Lomakin, S. S. - 436
Lomidze, V. L. - 312
Longe, I. I. - 572
Lozhkin, V. V. - 687
Lugonov, A. F. - 45
Luk'yanov, A. A. - 849
Luzanova, L. M. - 825
Luzhnov, A. M. - 677

M

Madoyan, A. A. - 465
Maevskii, V. A. - 866
Maiorov, V. P. - 596, 669
Makarov, O. I. - 95
Makarov, S. A. - 424
Makarov, S. P. - 509
Makarov, V. M. - 682
Makhin, A. V. - 861
Makhin, V. M. - 791
Makhonko, K. P. - 354
Maksimovich, Z. - 296
Malikzhonov, A. - 403
Malinovskii, V. V. - 536
Malyshev, I. F. - 103, 112
Mamonova, T. I. - 652
Mamontov, V. F. - 213
Mansurova, A. N. - 697, 854
Marin, S. V. - 288
Markin, S. A. - 164
Markovskii, D. V. - 422
Martynenko, S. P. - 803
Martynenko, Yu. V. - 202, 341
Mashinin, V. A. - 736
Mashkovich, V. P. - 572
Matveenko, I. P. - 95
Matveev, L. V. - 358
Matveev, V. V. - 577, 587
Medvedev, A. A. - 714
Medvedev, A. N. - 403
Mekhedov, B. N. - 673
Mel'nichenko, N. A. - 334, 776
Mel'nikov, V. A. - 551
Memelova, L. Ya. - 254
Men'shenin, A. I. - 74
Metzger, B. É. - 794
Mikerin, E. I. - 544
Mikhailov, B. A. - 738
Minashin, M. E. - 270
Mints, A. Z. - 280, 283
Mirnov, S. V. - 854
Mironov, Yu. V. - 567
Miroshnikov, V. S. - 14, 551
Mishin, E. V. - 797
Mitenkov, F. M. - 217
Mityaev, Yu. I. - 223
Mogil'nitskii, G. M. - 319
Mokhnachev, A. G. - 828
Monoszon, N. A. - 103, 112
Mordovskii, M. V. - 403
Morozov, A. G. - 436
Morozov, V. B. - 157
Morozov, V. K. - 866
Mosesov, A. V. - 629
Moskalev, Yu. I. - 153
Moskvin, L. N. - 14, 551, 828
Motorov, B. I. - 217
Mozhaev, V. K. - 213
Mozin, I. V. - 112
Mskhalaya, B. A. - 487
Mukhin, I. P. - 89
Musurmankulov, R. T. - 727
Myaé, É. A. - 258
Myagkikh, A. I. - 187

N

Nalivaev, V. I. - 504, 506
Nazarov, V. K. - 555
Nedospasov, A. V. - 117
Nefedov, V. N. - 478
Nekrest'yanov, S. N. - 14, 828
Nemirov, N. V. - 141
Nesterenko, V. B. - 34
Neverov, V. A. - 791
Ngo Kwang Zui - 312
Nikiforov, A. S. - 443
Nikitin, Yu. M. - 519
Nikolaev, E. V. - 747
Nikol'skii, Yu. V. - 303
Nikonov, A. V. - 487, 866
Novikov, I. I. - 633
Novikov, V. M. - 177, 422
Novikov, V. V. - 299

Novoselov, G. P. - 528
Novosel'skii, O. Yu. - 519
Nozhkina, I. N. - 199

O

Obnorskii, V. V. - 331, 559
Ochkin, D. V. - 356
Odintsov, V. I. - 112
Ogorodnik, S. S. - 438
Oleinik, G. M. - 458
Onufriev, V. D. - 421, 443
Opanasenko, A. N. - 377
Orlenkov, I. S. - 551
Orlov, V. V. - 288, 361
Ozerkov, V. N. - 776

P

Panarin, M. V. - 99
Panin, V. M. - 285, 747
Paraev, B. V. - 285
Parkhomenko, N. N. - 866
Parshin, A. M. - 494, 697
Pasechnikov, A. M. - 458
Pashkov, P. T. - 258
Pastukhov, V. S. - 866
Pavlov, S. P. - 370
Pavlov, V. I. - 659
Pavlova, G. Yu. - 187
Pelshakova, R. P. - 280
Percherskii, O. P. - 458
Perlin, A. S. - 458
Perlovich, Yu. A. - 299
Pershin, A. V. - 619
Pertsovskii, E. S. - 74
Peshkov, V. P. - 334
Petrosyan, L. G. - 797
Petrzhak, K. A. - 629
Petukhov, V. P. - 512
Petushkov, V. N. - 546
Pevchev, V. P. - 458
Piksaikin, V. M. - 536
Pimonov, Yu. I. - 469
Pis'mennyi, V. D. - 112
Pitkevich, V. A. - 195
Pivovarov, V. A. - 229
Pleshakov, L. D. - 406
Pleshakova, R. P. - 283
Plyutinskii, V. I. - 370
Pocevin, A. T. - 825
Podladchikov, Yu. N. - 732
Podlazov, L. N. - 285, 747
Podosenov, S. A. - 60, 429
Polyachenko, A. L. - 410
Polyakov, A. A. - 561
Ponomarev-Stepnoi, N. N. - 743
Popilyuk, S. F. - 659
Popkov, G. N. - 103
Popkov, K. K. - 150, 553, 729
Popov, O. P. - 732
Popov, S. V. - 673
Popov, V. D. - 438, 487
Popov, V. N. - 87, 764
Posobilo, T. S. - 135
Potapenko, P. T. - 601, 608
Potetyunko, G. N. - 98, 137
Prasolov, P. F. - 299
Priimak, S. V. - 504, 506
Proimin, G. S. - 334
Prokhorov, A. M. - 797
Prokhorov, A. V. - 95
Pronina, V. N. - 19
Pronman, I. M. - 424
Protasenko, Yu. M. - 669
Protasov, V. I. - 336
Pushkin, V. V. - 587
Pushnov, A. S. - 773
Pustynskii, L. N. - 266
Putvinskii, S. V. - 112
Pyatakhin, V. I. - 794, 797

R

Rabotnova, F. A. - 354
Rabukhin, V. B. - 140
Radzievskii, G. B. - 329
Rainer, Kh. - 303
Rakhov, N. A. - 707
Rakov, I. V. - 123
Reutov, V. F. - 781
Rineiskii, A. A. - 807
Rogov, K. D. - 141
Rogova, V. D. - 747
Romanenko, V. S. - 816
Romanichev, M. K. - 587
Romanov, V. P. - 677
Rubisov, V. N. - 400
Rudakov, L. I. - 458
Rudenko, V. S. - 193
Rudik, A. P. - 79, 352
Rudnev, S. I. - 563
Rudovskii, B. P. - 365
Rukhlo, V. P. - 561
Rumyantsev, G. Ya. - 339
Rutberg, F. G. - 112
Ryzhov, N. V. - 577

S

Sakharov, V. K. - 572
Sakovich, E. V. - 519
Sakovich, V. A. - 209
Salimov, R. A. - 74, 768
Sal'nikov, A. A. - 714
Samoilenko, P. B. - 465
Samoilenko, V. P. - 465
Samoilov, O. B. - 217
Samoilova, L. I. - 652
Samsonov, A. E. - 403
Samsonov, B. V. - 791
Sapozhnikova, G. A. - 319
Savel'eva, L. M. - 512
Savinskii, A. K. - 329
Savitskii, V. I. - 346
Savvatimova, I. B. - 254
Sednev, A. R. - 682
Sedov, V. M. - 83, 141
Semenova, N. N. - 536
Serebryakov, V. P. - 528
Sergeev, G. P. - 682
Shabalin, E. P. - 312
Shadrin, V. N. - 202
Shamardin, V. K. - 753
Shan'gin, N. N. - 377
Shapar', A. V. - 229
Sharapa, A. I. - 803
Sharapov, V. M. - 270
Shatalov, G. E. - 117, 288, 422
Shchegolev, V. A. - 652
Shchekina, G. B. - 173
Shcherbina, V. G. - 828
Shepeleva, E. R. - 329
Shermakov, A. E. - 587
Sheshunov, V. P. - 791
Shestopalov, E. V. - 264
Shikanov, A. E. - 280, 283
Shishin, B. P. - 57
Shishkin, G. N. - 396, 533, 697
Shishkov, L. K. - 67
Shkuratova, I. G. - 247
Shkurpelov, A. A. - 440
Shmelev, V. E. - 10
Shokod'ko, A. G. - 501
Shpanskii, S. V. - 567
Shtein, Yu. Yu. - 687
Shulepin, V. S. - 339
Shumskii, R. V. - 687
Shvetsov, Yu. E. - 190
Shvoev, A. F. - 669
Sidorenko, V. D. - 596
Sidorkin, N. A. - 91
Sidorov, G. I. - 213
Sigal, M. V. - 664
Silant'ev, A. N. - 247
Simonov, V. D. - 659
Sinyavskii, V. V. - 438, 778, 866
Skachkov, E. V. - 736
Skatkin, V. M. - 577
Skorov, D. M. - 396, 417, 419, 421, 533, 697
Skvortsov, S. A. - 664
Slavyagin, P. D. - 825
Sluchevskaya, V. M. - 501
Slyusarenko, A. O. - 576
Smirnov, A. V. - 258
Smirnov, M. V. - 24
Smirnov, V. P. - 458

Smirnov, Yu. A. - 687
Smirnova, N. S. - 190
Sobolev, I. A. - 707
Sobolev, Yu. A. - 438, 778, 866
Soifer, V. N. - 187
Sokolov, I. N. - 10
Sokurskii, Yu. N. - 443, 690
Solovkin, A. S. - 400
Spirchenko, Yu. V. - 112
Stanc, S. - 241
Starkov, O. V. - 89, 264
Starostin, Yu. M. - 91
Stavisski, B. A. - 103
Stepakov, L. V. - 336
Stepanchikov, V. A. - 303, 854
Stepennova, N. M. - 528
Stetsyuk, V. N. - 732
Stolov, A. M. - 112
Storozhuk, O. M. - 393, 417, 419, 421
Strelkov, V. S. - 103
Suglobova, I. G. - 327
Sukhotin, L. N. - 673
Sulaberidze, G. A. - 642
Sulaberidze, V. Sh. - 619
Sulema, V. N. - 202
Sultanov, N. V. - 614
Sunchugashev, M. A. - 669
Sus, F. - 296
Suvorov, A. L. - 254
Sych, A. P. - 791

T

Tagi-Zade, R. F. - 677
Talalaev, V. A. - 123
Tanskaya, N. A. - 199
Tarasov, V. M. - 334
Taratunin, V. V. - 157
Tashlykov, I. S. - 324
Tebus, V. N. - 443, 690
Teodorovich, O. A. - 629
Terekhov, G. P. - 724
Teterev, Yu. G. - 714
Tevzadze, G. A. - 642
Timko, Yu. N. - 768
Timofeev, I. G. - 743
Titarenko, Yu. E. - 561
Titov, V. F. - 24
Titov, V. I. - 729
Tkachenko, V. D. - 144
Toistikov, V. A. - 403
Tolmachev, Yu. N. - 272
Tombak, M. I. - 149
Tomik, J. - 241
Tonov, B. I. - 682
Torlin, B. Z. - 473
Totskii, Yu. I. - 280
Trekhova, N. A. - 515
Trofimov, B. A. - 436
Trubin, S. B. - 491, 734
Trukhanov, G. Ya. - 60, 429
Tselykovskii, O. P. - 504, 506
Tsenter, É. M. - 358, 622
Tsimbalov, S. A. - 292
Tsipenyuk, Yu. M. - 858
Tsirlin, Ya. A. - 277
Tsitovich, T. B. - 319
Tsitsin, A. G. - 741
Tsoglin, Yu. L. - 438
Tsykanov, V. A. - 10, 791
Tsypin, S. G. - 677
Tulinov, A. F. - 648

U

Ulanov, V. E. - 128
Usanov, V. I. - 346
Utkelbaev, B. D. - 781
Utkin, Yu. A. - 169

V

Vagin, S. P. - 781
Vaimugin, A. A. - 270
Van'kov, A. A. - 229
Vargin, E. P. - 587
Vashilov, S. M. - 128
Vasilenko, I. Ya. - 153
Vasil'ev, N. N. - 117, 655
Vasil'ev, V. K. - 633
Vasil'eva, K. I. - 274
Velikhov, E. P. - 112, 458
Vergun, I. I. - 283
Verkhovetskii, N. A. - 825
Vertman, E. G. - 574
Veryatin, U. D. - 45
Veselov, V. P. - 440
Vetsko, V. M. - 642
Videskii, V. G. - 195
Vikulov, V. K. - 223
Vinogradov, V. I. - 336
Viograd, É. L. - 277
Vladimirov, B. G. - 341
Volchkov, L. G. - 682
Volkov, A. F. - 145
Volkov, E. P. - 504, 506
Volkov, V. A. - 327
Volkov, Yu. V. - 555
Volkova, O. I. - 319
Volobuev, P. V. - 491, 734
Vorobei, M. P. - 469
Vorob'eva, V. G. - 536
Voropaev, A. I. - 229
Vorotyntsev, M. F. - 229
Vorov'ev, E. D. - 652
Vozyakov, V. V. - 229
Vyrskii, M. Yu. - 572

W

Wasatjerna, Frej - 49

Y

Yakhonin, I. F. - 45
Yakubov, V. Ya. - 504, 506
Yakubson, K. I. - 410
Yakushin, G. V. - 266
Yampol'skii, I. R. - 458
Yaroshevich, V. D. - 494, 697
Yarullov, B. G. - 559
Yaryna, V. P. - 147
Yuditskii, V. D. - 525

Z

Zabelin, A. I. - 10
Zagryadskii, V. A. - 422
Zaitsev, S. V. - 254
Zaitsev, V. I. - 458
Zakharov, A. P. - 396, 443
Zakharova, K. P. - 319
Zakladnoi, G. A. - 74
Zaletin, V. M. - 199
Zaluzhnyi, A. G. - 393, 417, 419, 421, 443
Zamyatnin, Yu. S. - 714
Zaritskaya, T. S. - 79, 352
Zaritskii, S. M. - 67
Zav'yalova, N. Yu. - 633
Zbonarev, A. V. - 776
Zemskov, E. A. - 306
Zhelnin, V. D. - 89
Zhemerev, A. V. - 207
Zhernov, V. S. - 577, 587
Zhilkin, A. S. - 264, 274
Zhitomirskii, V. M. - 87, 764
Zhokina, I. A. - 614
Zhotabaev, Zh. R. - 727
Zhukova, S. V. - 319
Zhuravlev, V. I. - 95
Zlepko, V. F. - 365
Zolotov, A. F. - 776
Zolotukhin, S. T. - 83, 141
Zoltowski, T. - 540
Zvyagintsev, A. L. - 145

SOVIET ATOMIC ENERGY

Volumes 52-53, 1982

(A translation of Atomnaya Énergiya)

Volume 52, Number 1 January, 1982

	Engl.	Russ.
Nonsteady and Emergency Conditions of Fast-Reactor Operation and Their Role in Safety Systems — Yu. E. Bagdasarov and I. A. Kuznetsov	1	3
Efficiency of the Use of a Neutral-Oxygen Water-Chemical Regime in the Operation of a Nuclear Power Station with a Pressurized Boiling Reactor — E. P. Anan'ev, A. B. Andreeva, I. S. Dubrovskii, V. M. Eshcherkin, A. I. Zabelin, G. N. Kruzhilin, E. V. Kulikov, I. N. Sokolov, V. A. Tsykanov, Yu. V. Chechetkin, and V. E. Shmelev	10	10
Operative Automated Monitoring of the Fission Product Radioactivity in the Water Coolant of a Nuclear Reactor — L. N. Moskvin, G. G. Leont'ev, V. S. Miroshnikov, and S. N. Nekrest'yanov	14	14
An Investigation of the Stress State of Large-Diameter Tubes for High-Powered Channel Reactors — V. S. Dmitriev, A. N. Lifant'ev, V. N. Pronina, and V. M. Filatov	19	17
Calculation of a Heat-Exchange Crisis in Steam Generators Heated by Sodium — P. L. Kirillov, V. F. Titov, N. S. Grachev, M. V. Smirnov, V. V. Khudasko, and V. G. Bazhin	24	21
Mass- and Heat-Exchange Processes in Fuel-Element Assembly Models — A. I. Gavrilin	29	24
Influence of the Thermal Effects of Chemical Reactions in a Dissociating Coolant on the Thermodynamic Efficiency of an Atomic Power Station — V. B. Nesterenko	34	28
Radioactive Corrosion Products in the Loop of a Fast Reactor with a Dissociating Coolant — V. M. Dolgov and A. O. Katanaev	43	34
The Conversion of Uranium Hexafluoride to Dioxide — N. P. Galkin, U. D. Veryatin, I. F. Yakhonin, A. F. Lugonov, and Yu. M. Dymkov	45	36
Methods of Calculating Radial Boundary-Conditions for Flux Trap Control Assemblies — Frej Wasastjerna and Eeva Koskinen	49	39
Determination of the Reciprocal Period of a Highly Supercritical Reactor — B. P. Shishin	57	44
Propagation of Retarded-Neutron Pulse in a Heavy Medium with Arbitrary Scattering and Capture Cross Sections — S. A. Podosenov and G. Ya. Trukhanov	60	47
Methods of Solving Inhomogeneous Equations of Generalized Perturbation Theory — P. N. Alekseev, S. M. Zaritskii, and L. K. Shishkov	67	52
Industrial Application of Radiation Deinsectification of Grain — G. A. Zakladnoi, A. I. Men'shenin E. S. Pertsovskii, R. A. Salimov, V. G. Cherepkov, and V. S. Krsheminskii	74	57
LETTERS TO THE EDITOR		
A Computational-Experimental Method for the Determination of ^{237}Np in Spent Nuclear Fuel — T. S. Zaritskaya, A. K. Kruglov, and A. P. Rudik	79	60

Chemical Treatment of the Internal Surfaces of Nuclear Power Stations before Startup — V. M. Sedov, P. G. Krutikov, and S. T. Zolotukhin..... 83 62
An Apparatus for Examining the Radiolysis of Steam under Flow Conditions — V. N. Popov, A.N. Ermakov, V. M. Zhitomirskii, and B. G. Dzantiev..... 87 64
Heat Resistance of 10Kh18N9 Stainless Steel in Sodium Containing Hydroxide at 500°C — O. V. Starkov, I. P. Mukhin, and V. D. Zhelnin..... 89 65
Television Monitoring and Observation Systems in Nuclear Engineering — V. P. Ivanov, N. A. Sidorkin, Yu. M. Starostin, and V. A. Kudryavtsev..... 91 67
Effect of a Reflector Made Out of UO_2 on the Kinetics of Prompt Neutrons in a Fast Reactor — A. M. Avramov, V. I. Zhuravlev, O. I. Makarov, I. P. Matveenko, and A. V. Prokhorov..... 95 69
Problem of Empirical Formulas for the Stopping Power of a Material — G. N. Potetyunko..... 98 71
^{76}Br, ^{77}Br, and ^{82}Br Yield in Nuclear Reactions with Protons, Deuterons, and Alpha Particles — P. P. Dmitriev, M. V. Panarin, and Z. P. Dmitrieva..... 99 72

Volume 52, Number 2 February, 1982

ARTICLES

The T-15 Tokamak. Basic Characteristics and Research Program — V. P. Belyakov, V. A. Glukhikh, A. M. Kavun, B. B. Kadomtsev, V. D. Kovalenko, A. I. Kostenko, I. F. Malyshev, N. A. Monoszon, G. N. Popkov, B. A. Stavisskii, and V. S. Strelkov..... 103 101
The Main Physical and Engineering Problems in Creating a Tokamak with a Strong Magnetic Field and Adiabatic Compression of the Plasma — É. A. Azizov, Yu. A. Alekseev, N. N. Brevnov, E. P. Velikhov, I. A. Glebov, V. A. Glukhikh, V. F. Demichev, B. B. Kadomtsev, B. G. Karasev, V. A. Krylov, B. A. Larionov, I. F. Malyshev, I. V. Mozin, N. A. Monoszon, V. I. Odintsov, V. D. Pis'mennyi, S. V. Putvinskii, F. G. Rutberg, Yu. V. Spirchenko, A. M. Stolov, and V. A. Chuyanov..... 112 108
Hybrid Reactor with Ambipolar Plasma Containment (Project Trol) — N. N. Vasil'ev, I. N. Golovin, A. V. Nedospasov, and G. E. Shatalov..... 117 113
Resonance Effects in the Interaction of Fast Neutrons with Fe and ^{209}Bi Nuclei — A. G. Guseinov, M. G. Kobozev, K. A. Iskhakov, I. V. Rakov, V. A. Talalaev, P. A. Androsenko, and A. A. Androsenko..... 123 118
Structural Alloy Surfaces with Chemical Processing Using the Method of Secondary Ion Mass Spectrometry — S. M. Vashilov, Yu. G. Bobrov, G. M. Gur'yanov, A. P. Kovarskii, and V. E. Ulanov..... 128 122

LETTERS TO THE EDITOR

Influence of Pressure on the Penetration of Hydrogen Through Oxidized Steel and Alloys at 685°C — A. F. Borisovskii and T. S. Posobilo..... 135 128
Verifying the Addition Rule for the Proton-Retarding Power of Multicomponent Materials — G. N. Potetyunko..... 137 129
String Method of Measuring the Density of Irradiated Metallic Crystals — V. B. Rabukhin..... 140 131
Chemicotechnological Regime during Preparation of the Third Block of the Leningrad Nuclear Power Plant for Physical Start-Up — V. M. Sedov, P. G. Krutikov, N. V. Nemirov, S. T. Zolotukhin, A. V. Devochkin, A. P. Eperin, and K. D. Rogov..... 141 132
Approximation of the Range of Electrons as a Function of Their Energy and Atomic Number — M. L. Gol'din and V. D. Tkachenko..... 144 134
Diffusion Filter for Hydrogen Isotopes — V. A. Gol'tsov, V. V. Latyshev, A. F. Volkov, A. L. Zvyagintsev, A. P. Kuzin, V. K. Kapyshev, and P. A. Fefelov..... 145 135

Nuclear-Physical Characteristics of the AKN-T Set of Neutron Dosimeters — V. P. Yaryna and N. B. Galiev 147 136
Use of $BaSO_4(Eu)$ Thermoluminophore for Dose Measurement in Prolonged Exposure — I. A. Bochvar, T. I. Gimadova, G. A. Kuznetsova, and M. I. Tombak 149 137
Combined Use of S_n and Integral-Equations Methods to Calculate Angular Characteristics of a Radiation Field — A. N. Barkovskii, V. I. Kulikov, and K. K. Popkov 150 138

Volume 52, Number 3 March, 1982

Problem of ^{129}I Contamination of the Biosphere — I. Ya. Vasilenko and Yu. I. Moskalev.... 153 155
Estimation of the Residual Operational Lifetime of Uranium—Graphite Channel Reactors — I. Ya. Emel'yanov, A. I. Klemin, V. V. Taratunin, V. S. Emel'yanov, and V. B. Morozov 157 158
Improved Sensitivity in Cassette Temperature Monitoring in a Sodium-Cooled Fast Reactor — L. A. Adamovskii, V. N. Efimov, B. V. Kebadze, and S. A. Markin 164 164
Effects of Carbon on the Physicomechanical Properties of Kh18N9 Steel Irradiated in a Fast Reactor — Yu. A. Utkin and I. A. Kuz'mina..... 169 168
Helium Liberation from Irradiated Ceramic Materials — A. V. Khudyakov, G. B. Shchekina, and A. N. Lepikhov..... 173 173
Dynamical Stability of the Liquid First Wall of Pulsed Thermonuclear Reactors — S. P. Kravchuk and V. M. Novikov 177 176
Study of the Phase Transition of α-Quartz as a Result of Irradiation with a Large Dose of Fast Neutrons — I. Kh. Abdukadyrova and A. A. Fotchenkov 183 180

LETTERS TO THE EDITOR

Radioactive Background of Potassium in Seawater in the Western Part of the Pacific Ocean — V. N. Soifer, A. S. Bychkov, V. V. Kobylyanskii, A. I. Myagkikh, G. Yu. Pavlova, and Yu. M. Kharlamov 187 185
Simulation of Heat and Mass Exchange with Natural Convection — M. P. Leonchuk, N. S. Smirnova, and Yu. E. Shvetsov 190 187
Use of Deutrons with 3-MeV Energy in Activation Analysis — Yu. I. Bondarenko and V. S. Rudenko..... 193 189
Statistical Modeling of the Slowing Down of Electrons with Energies Below 39 keV in a Tissue-Equivalent Material — V. A. Pitkevich, V. G. Videnskii, and V. V. Duba 195 190
X-Ray and γ-Ray Detectors based on Mercury Diiodide Crystals — V. M. Zaletin, V. A. Kochevanov, I. N. Nozhkina, N. A. Tanskaya, and V. I. Fomin..... 199 193
Effect of Temperature on the Behavior of Implanted Helium in a Ti—V—Al Alloy — M. I. Guseva, Yu. V. Martynenko, O. I. Chelnokov, I. P. Chernov, V. N. Shadrin, Yu. P. Cherdantsev, and V. N. Sulema 202 195
Calculation of Nonequilibrium Distributions of Absorbed Dose and Space Charge during γ Irradiation — A. F. Adadurov and V. T. Lazurik..... 205 197
Neutron-Burst-Induced Light Flash — A. V. Zhemerev..... 207 199
Procedure for Determining the Optimal Dose Ratio of a Deterministic and a Probabilistic Source — P. A. Barsov, A. V. Kolomenskii, and V. A. Sakovich 209 200
Conversion Parameters for Fast Critical BFS Assemblies — Yu. A. Kazanskii, V. A. Dulin, G. I. Sidorov, V. F. Mamontov, and V. K. Mozhaev 213 203

Volume 52, Number 4 April, 1982

ARTICLES

Hydrodynamic Stability of Natural Circulation in a Nuclear Power Plant with Underboiling Coolant — F. M. Mitenkov, L. N. Kut'in, B. I. Motorov, and O. B. Samoilov 217 227
Cassette Permutation to Equalize the Energy Distribution and Improve the Fuel Cycle of the RBMK Reactor — Yu. I. Mityaev and V. K. Vikulov 223 231

Study of Neutron Energy Spectra on BFS Fast Critical Assemblies — Yu. A. Kazanskii, A. A. Van'kov, V. V. Vozyakov, A. I. Voropaev, M. F. Vorotyntsev, E. N. Kuzin, V. M. Lityaev, V. A. Pivovarov and A. V. Shapar' 229 235
Application of Bifurcation Theory to the Investigation of the Dynamics of a Nuclear Reactor — E. S. Koltunova 235 240
Performance Diagnostics of the Thermoelectric Circuits of a System of In-Reactor Monitoring — S. Stanc, A. Gese, and J. Tomik 241 244
Determining the Commercial Contamination of Soil by ^{137}Cs Against a Background of Global Contamination — A. N. Silant'ev, and I. G. Shkuratova 247 248
Exchange between Tritium Oxide Vapor and the Surface of Water — L. F. Belovodskii, V. K. Gaevoi, T. A. Kosheleva, and V. N. Demenyuk 251 252
Extent of Damage of Tungsten in the Helium Plasma of a Glow Discharge — A. L. Suvorov, L. Ya. Memelova, I. B. Savvatimova, A. A. Babad-Zakhryapin, G. M. Kukavadze, A. F. Bobkov, and S. V. Zaitsev 254 253
Efficiency of Suppression of Longitudinal Instabilities of Proton Clusters with the Help of a Landau Resonator — É. A. Myaé, P. T. Pashkov, and A. V. Smirnov 258 256

LETTERS TO THE EDITOR
Cobalt and Other Impurities in Reactor Steels — A. S. Zhilkin, O. V. Starkov, and E. V. Shestopalov 264 261
Possibilities of Neutron Generation with the Help of a High-Voltage Glow Discharge — L. N. Pustynskii, S. R. Kholev, and G. V. Yakushin 266 262
Measurement of Reactivity Coefficients for the Reactor at Bilibinsk Nuclear Power Station — A. V. Bondarenko, A. A. Vaimugin, P. G. Dushin, A. G. Kostromin, M. E. Minashin, and V. M. Sharapov . 270 265
Microstructures of Pyrocarbon Sheaths on Fuel Micropins — I. S. Alekseeva, A. A. Babad-Zakhryapin, M. P. Glazunov, and Yu. N. Tolmachev 272 266
Transport of Radioactive Particles in the Primary Loop of a Reactor — K. I. Vasil'eva, A. S. Zhilkin, and I. A. Kuznetsov 274 267
Activator Concentration and the Stability of the Intrinsic Resolution of NaI(Tl) Crystals — É. L. Vinograd, N. Yu. Gurevich, Ya. A. Tsirlin, and A. L. Lifits 277 269
Construction of a Neutron Tube with a Laser Ion Source — V. M. Gul'ko, K. I. Kozlovskii, N. F. Kolomiets, A. F. Linev, A. Z. Mints, R. P. Pelshakova, Yu. I. Totskii, and A. E. Shikanov . 280 271
Obtaining (d,t) Neutrons in an Accelerator Tube with a Laser Source of Deuterons — D. F. Bespalov, I. I. Vergun, A. Z. Mints, R. P. Pleshakova, and A. E. Shikanov 283 272

Volume 52, Number 5 May, 1982

ARTICLES
Influence of the Steam Reactivity Effect on the Height Stability of the Power Distribution in a Pressurized Water Reactor — I. Ya. Emel'yanov, L. N. Podlazov, A. N. Aleksakov, V. M. Panin, and B. V. Paraev 285 299
Formation of Plutonium Isotopes in the Uranium Fuel of a Hybrid Thermonuclear Reactor — S. V. Marin, V. V. Orlov, and G. K. Shatalov 288 301
Coolant Temperature Distribution at VVÉR-440 Core Inlet — S. A. Tsimbalov and A. V. Kraiko 292 304
Feasibility of Determining Plutonium by the γ-Spectrometric Determination of the Nuclear Fuel Burnup — V. Bulovich, I. Krgil, F. Sus, and Z. Maksimovich 296 308

Influence of Texture on Plastic Tensile Strain of Rolled Zr—1% Nb Alloy — M. G. Isaenkova, V. P. Konoplenko, V. V. Novikov, Yu. A. Perlovich, and P. F. Prasolov 299 310
Temperature Dependence of Radiation Blistering of Aluminum Alloys in Irradiation by Helium Ions — M. I. Guseva, S. M. Ivanov, Yu. V. Nikol'skii, Kh. Rainer, and V. A. Stepanchikov 303 314
Direct Methods in Neutron-Physics Reactor Calculations — E. A. Zemskov and L. Ya. Isakova 306 316
Possibility of Obtaining the Effect of Self-Quenching of Power Pulses from a Pulsed Fast Reactor — V. L. Lomidze, Ngo Kwang Zui, and E. P. Shabalin 312 320
Variational Method in Transport Theory for Neutrons from a Pulsed Source — Sh. Kenzhebaev 317 323
Biostability of Compounds Based on Organic Binders Formed during Solidification of Liquid Medium-Activity Wastes — S. V. Zhukova, G. M. Mogil'nitskii, G. A. Sapozhnikova, S. A. Eliseenkova, T. B. Tsitovich, T. A. Bykhovskaya, O. I. Volkova, and K. P. Zakharova 319 326

LETTERS

Application of the Method of Resonance Nuclear Reactions to Ascertain the Spatial Distribution of Implanted Aluminum in Gallium Arsenide — J. A. Davies, I. S. Tashlykov, and L. M. Howe 324 330
Energy Characteristics of Fluouranates(IV) of Alkali Metals — V. A. Volkov, I. G. Suglobova, and D. É. Chirkst 327 331
Ionization Straggling and the Area of Applicability of the Continuous Electron Retardation Approximation — A. K. Savinskii, E. R. Shepeleva, and G. B. Radzievskii 329 333
Sound Emission from a Liquid Caused by Fission Fragments — I. A. Baranov, P. I. Golubnichii, V. G. Kudlenko, and V. V. Obnorskii 331 335
Automated Facility for Investigating Irradiated Fuel Elements by γ Scanning — V. I. Galkov, V. P. Korotkov, N. A. Mel'nichenko, V. P. Peshkov, G. S. Proimin, and V. M. Tarasov 334 336
High-Speed Program for the Analysis of Complex γ Spectra — V. I. Vinogradov, L. V. Stepakov, and V. I. Protasov 336 338
Albedo—Diffusion Approximation for Reflector Calculations — G. Ya. Rumyantsev and V. S. Shulepin 339 339
Investigation of the Radiation Blistering of Aluminum Alloys during Simultaneous Irradiation with He^+ and D^+ Ions — B. G. Vladimirov, M. I. Guseva, S. M. Ivanov, and Yu. V. Martynenko 341 341
Calculating the Functionals of Radiation Fields over Inhomogeneous Protection Regions — V. I. Usanov and V. I. Savitskii 346 344
Influence of the Relation between the Active-Region Parameters on the Fuel-Element Reliability Index — I. M. Kurbatov 348 346
Possibility of Attaining Criticality in Media Containing ^{234}U — M. V. Kalashnikov, L. P. Fedotova, and A. A. Chernova 351 347
Correlations for the Formation of Actinides in Nuclear Reactors — T. S. Zaritskaya and A. P. Rudik. 352 348
Radiation Monitoring Experience in the Vicinity of Nuclear Power Stations — K. P. Makhonko and F. A. Rabotnova 354 349
Improvement of the Radiochromatographic Gas-Purification System of a Nuclear Power Station — D. V. Ochkin, A. A. Aleshin, and V. V. Kazakov 356 350
Radiation Safety in Working with Natural Thorium — L. V. Matveev and É. M. Tsenter 358 351

Volume 52, Number 6 June, 1982

ARTICLES

Mathematical Model of a Thermonuclear Power Station with a Hybrid Reactor — D. K. Kurbatov and V. V. Orlov. 361 371

Equipment Metal Monitoring at Nuclear Power Stations – V. S. Grebennik, V. F. Zlepko, V. P. Kalinin, and B. P. Rudovskii. 365 374
Mechanism of HF-Resonance Instability of the VK-50 Reactor – P. A. Leppik, S. P. Pavlov, and V. I. Plyutinskii. 370 379
Analysis of Sodium–Water Steam Generator Protection from Magnetic-Flowmeter Signals – B. V. Kebadze and Yu. V. Chernobrovkin 374 382
Hydrodynamics of Mixer Chambers in Nuclear-Power Systems – A. N. Opanasenko and N. N. Shan'gin 377 385
Padé-Approximation Method in Problems of Neutron Moderation – E. A. Dynin. 381 389
Bifurcations and Self-Oscillations in Nuclear Reactors with Linear Feedback – V. A. Kolchin. . 386 393
Buildup of Helium in Structural Materials during Reactor Irradiation – A. G. Zaluzhnyi, O. M. Storozhuk, and M. V. Cherednichenko-Alchevskii. 393 398
Electron-Microscopic Examination of Helium Distribution in a High-Nickel Alloy – M. I. Guseva, A. P. Zakharov, B. A. Kalin, D. M. Skorov, V. N. Chernikov, I. I. Chernov, and G. N. Shishkin 396 401
Calculation of Steady-State Regimes of Technological Extraction Processes from Data on the Thermodynamics of Pu(IV) Extraction with Tri-n-Butyl Phosphate (TBP) from Nitrate Solutions – V. N. Rubisov and A. S. Solovkin. 400 404
Measurement of the Neutron Radiative Capture Cross Section for ^{236}U in the Range of Neutron Energies 0.1-50 keV – A. A. Bergman, A. N. Medvedev, A. E. Samsonov, V. A. Tolstikov, A. G. Kolosovskii, M. V. Mordovskii, and A. Malikzhonov. 403 406
Determination of Characteristics of Radiation Incident on a Detector – L. D. Pleshakov. 406 409
Solving Inverse Problems of Nuclear Geophysics (Method of Equivalent Fields) – A. A. Barenbaum, A. L. Polyachenko, and K. I. Yakubson 410 412

LETTERS TO THE EDITOR

Multipurpose Mass-Spectrometric Facility for Investigating the Buildup and Release of Inert Gases from Reactor Materials – A. G. Zaluzhnyi, D. M. Skorov, O. M. Storozhuk, M. V. Cherednichenko-Alchevskii, and L. M. Klykov. 417 418
Buildup and Behavior of Helium in Iron, Irradiated in the IRT-2000 – A. G. Zaluzhnyi, D. M. Skorov, O. M. Storozhuk, M. V. Cherednichenko-Alchevskii, and L. M. Klykov . 419 419
Buildup of Helium in Structural Materials Containing Nickel, during Irradiation in the BOR-60 Reactor – A. G. Zaluzhnyi, D. M. Skorov, O. M. Storozhuk, M. V. Cherednichenko-Alchevskii, V. D. Onufriev, and I. N. Afrikanov. 421 421
Experimental Investigation of Neutron Spectrum in Lead with a 14-MeV Source – V. D. Aleksandrov, V. A. Zagryadskii, D. V. Markovskii, V. M. Novikov, D. Yu. Chuvilin, and G. E. Shatalov 422 422
Mechanism of the Reduction of the Neutron Yield from Metallotritiated Targets of Type NG-150 Neutron Generators – I. Ya. Barit, L. E. Kuz'min, S. A. Makarov, and I. M. Pronman. 424 423
Density of Melts of Thorium Fluoride with Sodium and Uranium Chlorides – S. F. Katyshev, N. N. Kurbatov, and V. N. Desyatnik 427 425
Distribution Function of Intermediate Neutrons in Heavy Homogeneous Media – S. A. Podosenov and G. Ya. Trukhanov. 429 427
DISNEI-2 Neutron Spectrometer – G. G. Doroshenko, S. N. Kraitor, T. V. Kuznetsova, K. K. Kushnereva, and E. S. Leonov 432 429
Determination of the Fast-Neutron Flux Density in a Reactor of the Kola Atomic Power Plant – Kh. Ya. Bondars, E. I. Ignatenko, A. A. Lapenas, V. I. Lobov, S. S. Lomakin, A. G. Morozov, and B. A. Trofimov. 436 431
Monitoring of Neutron-Physical Parameters during Loop Testing – F. M. Arinkin, G. A. Batyrbekov, Z. B. Bekmurzaeva, Sh. Kh. Gizatulin, S. S. Ogorodnik, V. D. Popov, V. V. Sinyavskii, Yu. A. Sobolev, and Yu. L. Tsoglin. 438 432
Approximate Numerical Method of Solving the Transport Equation for Fast Electrons in Heterogeneous Slab Shields – A. A. Shkurpelov, A. P. Elokhin, and V. P. Veselov. . 440 433

Engl./Russ.

Volume 53, Number 1 July, 1982

ARTICLES

Problem of Helium in the Structural Materials of a Thermonuclear Reactor — A. S. Nikiforov, A. P. Zakharov, V. I. Chuev, A. G. Zaluzhnyi, Yu. N. Sokurskii, V. D. Onufriev, V. N. Tebus, A. E. Gorodetskii, V. Kh. Alimov, I. V. Al'tovskii, and V. M. Cherednichenko-Alchevskii..... 443 3

Module of Angara-5 Facility — E. P. Bol'shakov, E. P. Velikhov, V. A. Glukhikh, O. A. Gusev, E. V. Grabovskii, V. I. Zaitsev, Yu. A. Istomin, Yu. V. Koba, G. M. Latmanizova, G. M. Oleinik, A. M. Pasechnikov, V. P. Pevchev, A. S. Perlin, O. P. Percherskii, L. I. Rudakov, V. P. Smirnov, V. I. Chernobrovin, V. I. Chetvertkov, and I. R. Yampol'skii..... 458 14

Flaw Detector for the Inside Surfaces of Pipes in a Nuclear Power Station — A. A. Madoyan, V. G. Kantsedalov, V. P. Samoilenko, and P. B. Samoilenko..... 465 18

Properties and Behavior of the High-Activity Wastes from the Experimental Gas-Fluoride Reprocessing of Spent Uranium—Plutonium and Uranium Fuel of the BOR-60 — A. P. Kirillovich, Yu. G. Lavrinovich, M. P. Vorobei, and Yu. I. Pimonov..... 469 22

Two-Dimensional Analysis of the Stability of the Neutron Distribution in a Reactor — V. N. Konev and B. Z. Torlin..... 473 25

Measurement of the Neutron Total Cross Sections of ^{109}Ag and ^{110m}Ag — V. A. Anufriev, S. I. Babich, and V. N. Nefedov..... 478 29

Separation of Hydrogen Isotopes by Metal Membranes — V. V. Latyshev, V. A. Gol'tsov, and S. A. Fedorov..... 482 32

LETTERS TO THE EDITOR

Experimental Investigation of the Neutron Flux Regulation by Means of a Two-Phase Equilibrium Reaction — I. G. Gverdtsiteli, A. G. Kalandarishvili, V. B. Klimentov, M. N. Korotenko, S. D. Krivonosov, B. A. Mskhalaya, A. V. Nikonov, and V. D. Popov..... 487 36

Device for Continuous Monitoring of Burning of Nuclear Fuel — I. G. Gverdtsiteli, A. G. Kalandarishvili, and V. A. Kuchikhidze..... 489 37

Kinetic Constants of Radiation Gas Formation in Polyethylene — N. N. Alekseenko, P. V. Volobuev, and S. B. Trubin..... 491 38

Characteristics of the Distribution of Helium Bubbles in a Dislocation Network — A. M. Parshin, S. A. Fabritsiev, and V. D. Yaroshevich..... 494 40

Absorbed Electron Doses in Mixed Liquid-Phase Systems — É. D. Grushkova, V. V. Krayushkin, and Yu. D. Kozlov..... 496 41

Influence of Reactor Radiation and γ Radiation upon the Optical Properties of Quartz Glass — I. Kh. Abdukadyrova..... 498 42

Taking into Account the Variable Background of Delayed Neutrons in Reactivity Measurements with the Aid of Pulsed Neutron Techniques — A. G. Shokod'ko and V. M. Sluchevskaya..... 501 44

Measurement of Transient Variations of Thermoelectromotive Force — E. P. Volkov, V. I. Nalivaev, S. V. Priimak, I. I. Fedik, O. P. Tselykovskii, and V. Ya. Yakubov..... 504 45

Thermoelectromotive Force of VR 5/20 Thermocouples of Various Constructions — E. P. Volkov, V. I. Nalivaev, S. V. Priimak, I. I. Fedik, O. P. Tselykovskii, and V. Ya. Yakubov..... 506 47

Dependence of Spatial Distribution of Neutrons Under Moderation in Polyethylene of Thickness up to 5 cm on Their Initial Energy — S. P. Makarov..... 509 48

Implantation of Radioactive Cesium Ions in Solid Materials — Yu. V. Bulgakov, V. P. Petukhov, and L. M. Savel'eva..... 512 50

Engl./Russ.

Volume 53, Number 2 August, 1982

ARTICLES

Comparison Analysis of the Reliability and Efficiency of Nuclear Power Station Units with One and Two Turbogenerator Sets – I. Ya. Emel'yanov, A. I. Klemin, Yu. I. Koryakin, V. S. Emel'yanov, and N. A. Trekhova 515 67

Operating Efficiency of Steam Separators in Power Plants with RBMK Reactors – V. B. Karasev, Yu. M. Nikitin, O. Yu. Novosel'skii, and E. V. Sakovich 519 70

Modeling Heat and Mass Transfer in the Core of a Heat-Emitting Fuel Element – V. A. Kornilov and V. D. Yuditskii 525 74

Oxidation of Uranium and Plutonium Mononitride and Monocarbide Briquettes – G. P. Novoselov, V. V. Kushnikov, V. A. Baronov, V. P. Serebryakov, and N. M. Stepennova 528 77

Influence of Preliminary Neutron Irradiation upon Helium Blistering in OKh16N15M3B Steel – I. I. Chernov, B. A. Kalin, D. M. Skorov, G. N. Shishkin, and M. V. Ivanov 533 80

Average Number $\bar{\nu}_p$ of Prompt Neutrons in the Fission of ^{236}U Nuclei by Neutrons in the Energy Range 0.8–6 MeV – V. V. Malinovskii, V. G. Vorob'eva, B. D. Kuz'minov, V. M. Piksaikin, and N. N. Semenova 536 83

Nuclear Reactivity of Extractors with a Variation in the Concentration of Fissionable Materials in a Nonsteady Regime – T. Żółtowski 540 86

Status and Prospects of the Production of Radioisotope-Tagged Compounds in the USSR – E. I. Mikerin 544 89

Experience from Application of Radiolyoluminescence and Electron Paramagnetic Resonance to Dosimetry of Accidental Irradiation – I. A. Alekhin, S. P. Babenko, S. N. Kraitor, K. K. Kushnereva, A. V. Barabanova, S. R. Ginzburg, R. D. Drutman, and V. N. Petushkov 546 91

LETTERS TO THE EDITOR

Method for Automatic Monitoring of Iodine Radioactivity in the Water Coolant of an Atomic Power Plant – L. N. Moskvin, V. W. Miroshnikov, V. A. Mel'nikov, I. S. Orlenkov, and V. V. Chetverikov 551 101

γ-Radiation Albedo of Hydrogen-Containing Plane Layers – V. I. Kulikov, and K. K. Popkov 553 102

Quasilinear Approximation in the Statistical Analysis of the Simplest Nonlinear Dynamic Model of a Power Reactor – Yu. V. Volkov, A. G. Kostromin, and V. K. Nazarov 555 103

Sputtering of the Surface of Gold by Fission Fragments – V. V. Obnorskii, I. A. Baranov, N. V. Babadzhanyants, and B. G. Yarullov 559 105

Buildup of ^{233}U with a Specified Content of ^{232}U by the Irradiation of Thorium in a Water-Cooled/Water-Moderated Reactor (VVÉR) – A. A. Polyakov, V. P. Rukhlo, Yu. E. Titarenko, and S. F. Komin 561 106

Estimation of Stacking-Fault Energy of Frank Loops in OKh16N15M3B Austenitic Stainless Steel – Yu. V. Konobeev and S. I. Rudnev 563 107

Density and Viscosity of Fused Mixtures of Uranium Chlorides and Potassium Chloride – S. F. Katyshev, Yu. F. Chervinskii, and V. N. Desyatnik 565 108

Problems in Summarizing Experimental Data on the Heat-Transfer Crisis in Boiling – Yu. V. Mironov and S. V. Shpanskii 567 110

Liberation of Helium in the Heating of Irradiated Boron Carbide – V. G. Kovyrshin 570 112

Multigroup System of Constants for Calculating High-Energy Neutron Transport – M. Yu. Vyrskii, A. A. Dubinin, A. I. Ilyushkin, V. E. Kolesov, A. S. Krivtsov, I. I. Longe, V. P. Mashkovich, and V. K. Sakharov 572 113

Density Distribution of the Flux of Delayed Fission Neutrons in Water – E. G. Vertman . . . 574 116

Determination of the Cumulative Yields of Short-Lived Products of Thermal-Neutron ^{239}Pu Fission by Means of the γ-Spectrometric Method under Cyclic Conditions – A. G. Golovanov, A. N. Gudkov, V. V. Kazantsev, V. V. Kovalenko, A. B. Koldobskii, V. M. Kolobashkin, S. I. Lifanov, and A. I. Slyusarenko 576 117

Volume 53, Number 3 September, 1982

ARTICLES

Distributed Microprocessor-Based System for Monitoring Radiation of Nuclear Power Plants — A. A. Denisov, V. S. Zhernov, I. S. Krasheninnikov, V. V. Matveev, N. V. Ryzhov, and V. M. Skatkin 577 131
Monitoring the Distribution of Radionuclides Throughout the Technological Circuits of a Nuclear Power Station — V. L. Antonov, A. A. Gruzdeva, V. S. Zhernov, S. K. Kozlov, O. B. Lapshev, V. V. Matveev, V. V. Pushkin, M. K. Romanichev, A. E. Shermakov, E. P. Vargin, and L. P. Drozdova 587 138
Distribution of the Flux Density and Hardness of the Neutron Spectrum with Height and Over the Cross Section of the Heat-Generating Assemblies of VVÉR-365 and VVÉR-440 Reactors — B. A. Bibichev, V. P. Maiorov, V. D. Sidorenko, and P. I. Fedotov 596 143
Control of the Neutron Distribution in a Reactor by a Liquid Absorber — P. T. Potapenko 601 147
Harmonic Simulation of a Power Reactor — P. T. Potapenko 608 151
Refinement of Boundary Conditions in the Calculation of Close-Packed Lattices by the Surface Pseudosources Method — N. V. Sultanov and I. A. Zhokina 614 155
Gas Release from Uranium Dioxide — V. Sh. Sulaberidze and A. V. Pershin 619 158
Neutron Yield of the (α, n) Reaction for Multicomponent Media — V. I. Bulanenko, V. V. Frolov, and É. M. Tsenter 622 160
Yields of the Photofission Products of ^{237}Np — M. Ya. Kondrat'ko, A. V. Mosesov, K. A. Petrzhak, and O. A. Teodorovich 629 164
Swelling in Cold-Deformed OKh16N15M3B Steel on Irradiation in a High-Voltage Electron Microscope — M. M. Kantor, V. N. Kolotinskii, I. I. Novikov, A. G. Ioltukhovskii, V. K. Vasil'ev, and N. Yu. Zav'yalova 633 167
Study of the Deactivation Mechanisms for Some Constructional Steels by Secondary-Ion Mass Spectrometry — Yu. G. Bobrov, S. M. Bashilov, G. M. Gur'yanov, and A. P. Kovarskii 638 171
Optimization of Isotope-Separation Processes in Columns — V. A. Kaminskii, V. M. Vetsko, G. A. Tevzadze, O. A. Devdariani, and G. A. Sulaberidze 642 174
Determining Distribution and Concentration of Certain Elements with the Aid of a Charged-Particle Beam — I. G. Berzina, É. B. Gusev, A. V. Drushchits, V. S. Kulikauskas, and A. F. Tulinov. 648 178
Technique for Preparing Microfilters with High Specific Capacity — G. N. Flerov, E. D. Vorob'ev, V. I. Kuznetsov, V. A. Shchegolev, G. N. Akap'ev, P. Yu. Apel', T. I. Mamonova, and L. I. Samoilova . . . 652 181

Volume 53, Number 4 October, 1982

ARTICLES

Some Results of the Parametric Analysis of the Technicoeconomic Indices of a Power Plant with the Trol Hybrid Ambipolar Reactor — N. N. Vasil'ev, I. N. Golovin, and M. G. Kuznetsov. 655 211
Analysis of the Routes to an Economically Advantageous Reorganization of the VVÉR-440 Fuel Cycle — V. D. Simonov, V. I. Pavlov, and S. F. Popilyuk. 659 213
Use of Nuclear Fuel to Cover the Seasonal Maximum Electric Load — V. M. Boldyrev, M. V. Sigal, and S. A. Skvortsov. 664 218
Measurement of Fuel Burnup in VVÉR-365 and VVÉR-440 Fuel-Element Assemblies by Gamma Spectroscopy — B. A. Bibichev, V. P. Kruglov, V. P. Maiorov, Yu. M. Protasenko, M. A. Sunchugashev, P. I. Fedotov, and A. F. Shvoev. 669 222

Tritium Content in Water Systems of a Reactor of the Fifth Unit of the Novovoronezh Nuclear Power Plant — V. P. Kruglov, V. M. Ilyasov, I. G. Golubchikova, B. N. Mekhedov, L. N. Sukhotin, S. V. Popov, V. M. Arkhipkin, and A. G. Babenko . . . 673 225
Problem of Predicting the Radiation Conditions in an Atomic Power Station A. M. Luzhnov, V. P. Romanov, R. F. Tagi-Zade, and S. G. Tsypin . . . 677 227
Small Steam Leaks into Sodium in a Reverse Steam Generator—F. A. Kozlov, G. P. Sergeev, L. G. Volchkov, A. R. Sednev, V. M. Makarov, and B. I. Tonov 682 231
Effect of Gas Dissolved in Water on the Heat-Exchange Crisis — V. V. Lozhkin, Yu. A. Smirnov, Yu. Yu. Shtein, and R. V. Shumskii. 687 234
Influence of Both Reactor Irradiation and Helium Isotopes upon the Mechanical Properties of Titanium and α-Titanium Alloys — V. N. Tebus, É. F. Alekseev, Yu. V. Bobkov, F. P. Butra, A. M. Glazyrin, I. V. Golikov, B. V. Grigorovich, A. M. Kaptel'tsev, Yu. N. Sokurskii, and V. I. Chuev 690 237
Effects of Heat Treatment and Alloying on the Radiation Erosion of Austenitic Stainless Steels and Alloys — E. E. Goncharov, M. I. Guseva, B. A. Kalin, O. A. Kozhevnikov, A. N. Lapin, A. N. Mansurova, A. M. Parshin, D. M. Skorov, I. N. Chernov, G. N. Shishkin, and V. D. Yaroshevich 697 243
Results with Pilot Bitumening Plants — I. A. Sobolev, L. M. Khomchik, V. V. Kulichenko, N. A. Rakhov, S. A. Dmitriev, and V. M. Chebyshev . 707 250
Prospects for the Development of Neutron-Activation Analytical Facilities Based on Powerful Antimony—Beryllium Sources — G. N. Flerov, Yu. N. Burmistenko, Yu. V. Dyadin, Yu. S. Zamyatnin, A. A. Medvedev, A. A. Sal'nikov, and Yu. G. Teterev. 714 255
LETTERS TO THE EDITOR
Stability of a Nuclear Reactor with Natural Circulation of a Liquid Fuel — V. A. Blinkin and E. I. Emel'yanov 720 261
Indicator of the Energy Distribution in the RBMK-1000 Field — G. N. Aleksakov, S. A. Gavrilyuk, A. V. Kudryavtsev, and G. P. Terekhov 724 263
Diffusion of ^{131}I and ^{103}Ru in Single-Crystal Tungsten — E. S. Bekmukhambetov, D. K. Daukeev, Zh. R. Zhotabaev, and R. T. Musurmankulov. 727 265
Characteristics of Reflected γ Rays with a Short Distance between the Detector and the Scattering Surface — V. I. Kulikov, K. K. Popkov, and V. I. Titov. 729 266
Creep in a Carbon—Carbon Material — Yu. A. Kalinkin, Yu. N. Podladchikov, O. P. Popov, V. N. Stetsyuk, and A. R. Khenven 732 268
Formation of Bubbles of Radiolytic Gas in Polyethylene — N. N. Alekseenko, P. V. Volobuev, and S. B. Trubin 734 269
Effect of the Geometry of Measurement on the Attenuation of β Particles — K. M. Erokhin, V. A. Mashinin, and E. V. Skachkov. 736 270
Mechanism of Formation of Deposits on Heating Surfaces Cooled by Organic Coolants — A. I. Gavrilin, N. G. Gataullin, B. A. Mikhailov, V. E. Fedoseev, and Yu. V. Chechetkin. 738 271
Temperature Fields of Electricity Generating Thermal Emission Elements in Changes of the Width of the Gap between the Electrodes — A. G. Tsitsin. 741 273
Calculations of the Irradiation Characteristics in Reactor Tests — E. S. Glushkov, N. N. Ponomarev-Stepnoi, and I. G. Timofeev. 743 274

Volume 53, Number 5 November, 1982

ARTICLES
Synthesis of a System of Local Automatic Regulators for Power Reactors — I. Ya. Emel'yanov, L. N. Podlazov, A. N. Aleksakov, E. V. Nikolaev, V. M. Panin, and V. D. Rogova. 747 301

Corrosion of St.3 and 12Kh18N10T Steels and NP-1 Nickel in High-Level Wastes from Gas-Fluoride Reprocessing of Fast-Reactor Rods — A. P. Kirillovich, R. K. Gazizov, V. S. Bushkovskii, V. N. Golovanov, Yu. G. Lavrinovich, V. S. Belokopytov, and V. K. Shamardin 753 305
Interaction of $^{4}He^{+}$ Ions with Polycrystalline and Single-Crystal Metals — N. P. Katrich and A. T. Budnikov 758 309
Thermoradiation Decomposition of Carbon Dioxide — B. G. Dzantiev, A. N. Ermakov, V. M. Zhitomirskii, and V. N. Popov 764 314
Increase of the Electron-Beam Irradiation Efficiency of Cylindrical Objects by Means of Magnetic Systems — L. L. Akrachkova, N. K. Kuksanov, R. A. Salimov, Yu. N. Timko, and É. É. Finkel' . . 768 317

LETTERS TO THE EDITOR
Distribution of Gas in a Reactor with Spherical Fuel Elements — A. S. Pushnov, I. I. Gel'perin, and A. M. Kagan. 773 320
A Nondestructive Method of Determining the Pu/U Ratio in Fast Reactor Fuel Elements, Based on X-Ray Spectrometry — A. V. Bushuev, V. I. Galkov, A. V. Zbonarev, A. F. Zolotov, A. A. Kutuzov, N. A. Mel'nichenko, V. N. Ozerkov, and V. V. Chachin 776 322
Calculation of Energy Liberation in the Loop Channels by the Monte Carlo Method — V. A. Antonov, F. M. Arinkin, G. A. Batyrbekov, A. A. Blyskavka, V. V. Sinyavskii, and Yu. A. Sobolev. 778 323
Investigation of the Structure of Kh18N10T Stainless Steel, Irradiated with Fast Neutrons at a Temperature of 300°C — Sh. Sh. Ibragimov, V. F. Reutov, S. P. Vagin, and B. D. Utkelbaev 781 324
New Class of Boundary Integral Equations of Neutron-Transport Theory — B. D. Abramov. 783 325
Influence of Radiation History on the Swelling of Steel — N. A. Demin and Yu. V. Konobeev. 785 327
Determining the Relaxation Length of a Flux of Moderated and Thermal Neutrons on the Basis of the P_2 Approximation — I. A. Kozachok and V. V. Kulik. 787 328
Accommodation Length of Helium in the Gap between the Fuel and the Shell — Yu. M. Golovchenko, V. M. Makhin, V. A. Neverov, B. V. Samsonov, A. P. Sych, V. A. Tsykanov, and V. P. Sheshunov. . . 791 330
A Scintillation Gamma Spectrometer for the Investigation of Ultra-Deep Boreholes — E. M. Arm, A. A. Il'inskii, B. É. Metzger, and V. I. Pyatakhin. 794 332
Remote Control Measurements of Ionizing Radiation Fields in Boreholes, Based on a Fiber-Optics Cable — V. A. Andronov, V. I. Balaev, E. M. Dianov, A. A. Il'inskii, E. V. Karus, O. L. Kuznetsov, E. V. Mishin, L. G. Petrosyan, A. M. Prokhorov, and V. I. Pyatakhin. 797 333
Applying Summator Operators to the Computer Solution of the Integrodifferential Equation of Radiation Transfer — V. I. Bilenko 800 335
Durability of ZTL Piezoceramic Under the Action of Reactor Radiation — V. M. Baranov, S. P. Martynenko, and A. I. Sharapa 803 337
Radioactive Aerosols in Ventilation Systems of the Chernobyl'sk Nuclear Power Plant — S. S. Chernyi and V. P. Grigorov 805 338

Volume 53, Number 6 December, 1982

Comparison of the Technicoeconomic Characteristics of Nuclear Power Stations with Modern Thermal and Fast Reactors — A. A. Rineiskii 807 360
Physical Characteristics of an RBMK Reactor in the Transitional Period — V. S. Romanenko and A. V. Krayushkin 816 367
Radiation Environment during the Commissioning and Power Runup in the Fifth Unit at the Novyi Voronezh Nuclear Power Station — N. A. Verkhovetskii, V. P. Ivannikov, V. F. Kozlov, V. P. Kruglov, L. M. Luzanova, A. T. Pocevin, P. D. Slavyagin, and L. P. Kham'yanov . . 825 373
A New Method of Monitoring Radioactive Aerosols from Nuclear Power Stations with RBMK Reactors — L. N. Moskvin, G. G. Leont'ev, S. N. Nekrest'yanov, A. P. Eperin, V. G. Shcherbina, and A. G. Mokhnachev 828 376

Gas Desorption during Irradiation of Metals with Molybdenum Ions — N. P. Katrich and V. N. Kanishchev 832 379
Simulation of Reactor Conditions in Investigations of Radiation Damage of the Surface of Materials — B. A. Kalin 837 382
Analysis and Estimate of Neutron Cross Sections of Curium Isotopes — T. S. Belanova 841 386
Neutron-Transmission Function for the Region of Unresolved Resonances — A. V. Komarov and A. A. Luk'yanov 849 392

LETTERS TO THE DITOR

Analysis of the Surface and Erosion of the Graphite Diaphragm of the T-3M Tokamak in the Tearing Mode — D. G. Baratov, G. V. Gordeeva, M. I. Guseva, V. N. Dem'yanenko, A. N. Mansurova, S. V. Mirnov, V. A. Stepanchikov, and V. P. Fokin 854 396
Photoneutrons from Thick D_2O, Be, and Pb Converters at E_{max} = 15 MeV — A. V. Drobinin, M. Leonard, and Yu. M. Tsipenyuk 858 398
Direct Charged-Particle Energy Conversion in a System Composed of a Magnetic Expander and Planar Collector — S. K. Dimitrov and A. V. Makhin 861 400
Currents Generated in Pyroelectrics by γ Irradiation — B. A. Levin 863 401
Reactor Tests of Two Thermoemission Electric Power Generating Elements in a Single Loop Channel — V. P. Baril'chenko, V. P. Berzhatyi, A. S. Karnaukhov, V. P. Kirienko, V. A. Maevskii, V. K. Morozov, A. V. Nikonov, N. N. Parkhomenko, V. S. Pastukhov, V. V. Sinyavskii, and Yu. A. Sobolev 866 402

MEASUREMENT TECHNIQUES
Izmeritel'naya Tekhnika
Vol. 25, 1982 (12 issues) $400

MECHANICS OF COMPOSITE MATERIALS
Mekhanika Kompozitnykh Materialov
Vol. 18, 1982 (6 issues) $330

METAL SCIENCE AND HEAT TREATMENT
Metallovedenie i Termicheskaya Obrabotka Metallov
Vol. 24, 1982 (12 issues) $420

METALLURGIST
Metallurg
Vol. 26, 1982 (12 issues) $435

PROBLEMS OF INFORMATION TRANSMISSION
Problemy Peredachi Informatsii
Vol. 18, 1982 (4 issues) $320

PROGRAMMING AND COMPUTER SOFTWARE
Programmirovanie
Vol. 8, 1982 (6 issues) $135

PROTECTION OF METALS
Zashchita Metallov
Vol. 18, 1982 (6 issues) $380

RADIOPHYSICS AND QUANTUM ELECTRONICS
Izvestiya Vysshikh Uchebnykh Zavedenii, Radiofizika
Vol. 25, 1982 (12 issues) $400

REFRACTORIES
Ogneupory
Vol. 23, 1982 (12 issues) $380

SIBERIAN MATHEMATICAL JOURNAL
Sibirskii Matematicheskii Zhurnal
Vol. 23, 1982 (6 issues) $495

SOIL MECHANICS AND FOUNDATION ENGINEERING
Osnovaniya, Fundamenty i Mekhanika Gruntov
Vol. 19, 1982 (6 issues) $380

SOLAR SYSTEM RESEARCH
Astronomicheskii Vestnik
Vol. 16, 1982 (4 issues) $275

SOVIET APPLIED MECHANICS
Prikladnaya Mekhanika
Vol. 18, 1982 (12 issues) $400

SOVIET ATOMIC ENERGY
Atomnaya Énergiya
Vols. 52–53 (12 issues) $440

SOVIET JOURNAL OF GLASS PHYSICS AND CHEMISTRY
Fizika i Khimiya Stekla
Vol. 8, 1982 (6 issues) $175

SOVIET JOURNAL OF NONDESTRUCTIVE TESTING
Defektoskopiya
Vol. 18, 1982 (12 issues) $485

SOVIET MATERIALS SCIENCE
Fiziko-khimicheskaya Mekhanika Materialov
Vol. 18, 1982 (6 issues) $345

SOVIET MICROELECTRONICS
Mikroélektronika
Vol. 11, 1982 (6 issues) $195

SOVIET MINING SCIENCE
Fiziko-tekhnicheskie Problemy Razrabotki Poleznykh Iskopaemykh
Vol. 18, 1982 (6 issues) $420

SOVIET PHYSICS JOURNAL
Izvestiya Vysshikh Uchebnykh Zavedenii, Fizika
Vol. 25, 1982 (12 issues) $400

SOVIET POWDER METALLURGY AND METAL CERAMICS
Poroshkovaya Metallurgiya
Vol. 21, 1982 (12 issues) $435

STRENGTH OF MATERIALS
Problemy Prochnosti
Vol. 14, 1982 (12 issues) $495

THEORETICAL AND MATHEMATICAL PHYSICS
Teoreticheskaya i Matematicheskaya Fizika
Vols. 50–53, 1982 (12 issues) $380

UKRAINIAN MATHEMATICAL JOURNAL
Ukrainskii Matematicheskii Zhurnal
Vol. 34, 1982 (6 issues) $380

Send for Your Free Examination Copy

Plenum Publishing Corporation, 233 Spring St., New York, N.Y. 10013
In United Kingdom: 88/90 Middlesex St., London E1 7EZ, England
Prices slightly higher outside the U.S. Prices subject to change without notice.

RUSSIAN JOURNALS IN THE PHYSICAL AND MATHEMATICAL SCIENCES

AVAILABLE IN ENGLISH TRANSLATION

ALGEBRA AND LOGIC
Algebra i Logika
Vol. 21, 1982 (6 issues) $270

ASTROPHYSICS
Astrofizika
Vol. 18, 1982 (4 issues) $320

AUTOMATION AND REMOTE CONTROL
Avtomatika i Telemekhanika
Vol. 43, 1982 (24 issues) issues) $495

COMBUSTION, EXPLOSION, AND SHOCK WAVES
Fizika Goreniya i Vzryva
Vol. 18, 1982 (6 issues) $345

COSMIC RESEARCH
Kosmicheskie Issledovaniya
Vol. 20, 1982 (6 issues) $425

CYBERNETICS
Kibernetika
Vol. 18, 1982 (6 issues) $345

DIFFERENTIAL EQUATIONS
Differentsial'nye Uravneniya
Vol. 18, 1982 (12 issues) $395

DOKLADY BIOPHYSICS
Doklady Akademii Nauk SSSR
Vols. 262–267, 1982 (2 issues) $145

FLUID DYNAMICS
Izvestiya Akademii Nauk SSSR, Mekhanika Zhidkosti i Gaza
Vol. 17, 1982 (6 issues) $380

FUNCTIONAL ANALYSIS AND ITS APPLICATIONS
Funktsional'nyi Analiz i Ego Prilozheniya
Vol. 16, 1982 (4 issues) $320

GLASS AND CERAMICS
Steklo i Keramika
Vol. 39, 1982 (6 issues) $460

HIGH TEMPERATURE
Teplofizika Vysokikh Temperatur
Vol. 20, 1982 (6 issues) $400

HYDROTECHNICAL CONSTRUCTION
Gidrotekhnicheskoe Stroitel'stvo
Vol. 16, 1982 (12 issues) $305

INDUSTRIAL LABORATORY
Zavodskaya Laboratoriya
Vol. 48, 1982 (12 issues) $400

INSTRUMENTS AND EXPERIMENTAL TECHNIQUES
Pribory i Tekhnika Eksperimenta
Vol. 25, 1982 (12 issues) $460

JOURNAL OF APPLIED MECHANICS AND TECHNICAL PHYSICS
Zhurnal Prikladnoi Mekhaniki i Tekhnicheskoi Fiziki
Vol. 23, 1982 (6 issues) $420

JOURNAL OF APPLIED SPECTROSCOPY
Zhurnal Prikladnoi Spektroskopii
Vols. 36–37 (12 issues) $420

JOURNAL OF ENGINEERING PHYSICS
Inzhenerno-fizicheskii Zhurnal
Vols. 42–43, 1982 (12 issues) $420

JOURNAL OF SOVIET LASER RESEARCH
A translation of articles based on the best Soviet research in the field of lasers
Vol. 3, 1982 (4 issues) $95

JOURNAL OF SOVIET MATHEMATICS
A translation of Itogi Nauki i Tekhniki and *Zapiski Nauchnykh Seminarov Leningradskogo Otdeleniya Matematicheskogo Instituta im. V. A. Steklova AN SSSR*
Vols. 18–20, 1982 (18 issues) $680

LITHOLOGY AND MINERAL RESOURCES
Litologiya i Poleznye Iskopaemye
Vol. 17, 1982 (6 issues) $420

LITHUANIAN MATHEMATICAL JOURNAL
Litovskii Matematicheskii Sbornik
Vol. 22, 1982 (4 issues) $205

MAGNETOHYDRODYNAMICS
Magnitnaya Gidrodinamika
Vol. 18, 1982 (4 issues) $325

MATHEMATICAL NOTES
Matematicheskie Zametki
Vols. 31–32, 1982 (12 issues) $400

continued on inside back cover